

**HARNESSING PALLIDAL CELL-TYPE DIVERSITY TO TREAT
NEUROLOGICAL DISORDERS**

by

Kevin Joseph Mastro

Bachelor of Science in Biological Sciences and Psychology, University of Connecticut, 2012

Submitted to the Graduate Faculty of
School of Medicine in partial fulfillment
of the requirements for the degree of
Doctor of Philosophy

University of Pittsburgh

2017

UNIVERSITY OF PITTSBURGH

School of Medicine

This dissertation was presented

by

Kevin Joseph Mastro

It was defended on

June 6, 2017

and approved by

Robert S. Turner, Ph.D., Professor, Department of Neurobiology

Susanne E. Ahmari, M.D., Ph. D., Assistant Professor, Department of Psychiatry

Bitá Moghaddam, Professor and Chair, Department of Behavioral Neuroscience, Oregon

Health and Science University

Peter L. Strick, Ph.D., Distinguished Professor and Chair, Department of Neurobiology,

Professor, Department of Psychiatry

Thomas Wichmann, MD, Professor, Department of Neurology

Dissertation Advisor: Aryn H. Gittis, Ph.D., Assistant Professor

Copyright © by Kevin Joseph Mastro

2017

HARNESSING PALLIDAL CELL-TYPE DIVERSITY TO TREAT NEUROLOGICAL DISORDERS

Kevin J Mastro, B.S

University of Pittsburgh, 2017

The identification of distinct cell-types within the basal ganglia has played a critical role in our understanding of basal ganglia function and the treatment of neurological disorders. As discussed in the introduction, the use of transgenic animals and bevy of emerging tools available to isolate, manipulate and control distinct populations of neurons have revolutionized neuroscience. We are gaining insight into the underlying structure of neural circuits that previously was inaccessible. Here, we defined cellular diversity within the globus pallidus externa (GPe), a nucleus within the motor-suppressing pathway of the basal ganglia, and investigated its contributions to circuit function in health and disease.

First, we defined two genetically distinct populations of GPe neurons using transgenic mouse lines. Utilizing a combination of anatomy and physiology, we found significant difference between the two populations of GPe neurons. Briefly, viral expression of EYFP revealed that Limhomeobox6 (Lhx6-) and Parvalbumin (PV-) GPe neurons differed in their axonal projection patterns as well as electrophysiological properties measured in slice recordings. These results provide a new set of tools to target molecularly, anatomically, and electrophysiologically distinct cell-types in the GPe which will enables studies of the organization and function of GPe circuits in health and disease.

Next, we demonstrate that optogenetic interventions that dissociate the activity of these two neuronal populations in the GPe – elevating the activity of PV-GPe neurons over that of Lhx6-GPe neurons – restores movement in dopamine depleted mice and attenuates pathological

activity of basal ganglia output neurons for hours beyond stimulation. These results establish the utility of cell-specific interventions in the GPe to target functionally distinct pathways, with the potential to induce long-lasting recovery of movement despite the continued absence of dopamine.

In the final chapter, we will discuss the evolving and often-controversial field of GPe cellular heterogeneity and the future of these neural cell-types. Secondly, we will provide potential mechanisms for which GPe cell-types exert profound therapeutic benefit during the disease state that could build on current treatments. Taken together, these results demonstrate the anatomic, physiological and functional differences that exist within the GPe cell-types and its potential to disrupt pathological activity and restore behavior during disease.

TABLE OF CONTENTS

PREFACE.....	XVI
1.0 INTRODUCTION.....	1
1.1 ADVANCEMENTS IN CELL-TYPE DEFINITIONS	2
1.1.1 Basal Ganglia Evolution: From Brain Areas to Boxes.....	2
1.1.2 Defining Basal Ganglia Cell-Types	4
1.1.3 Input-Output Relationships.....	7
1.2 HARNESSING CELL-TYPES TO TREAT NEUROLOGICAL DISORDERS.....	8
1.2.1 Parkinson’s Disease	8
1.2.1.1 Striatum	8
1.2.1.2 Subthalamic Nucleus (STN)	10
1.2.1.3 Globus Pallidus Externa (GPe).....	11
1.3 SUMMARY AND AIMS OF DISSERTATION	12
2.0 TRANSGENIC MOUSE LINES SUBDIVIDE EXTERNAL SEGMENT OF THE GLOBUS PALLIDUS (GPE) NEURONS AND REVEAL DISTINCT GPE OUTPUT.....	14
2.1 INTRODUCTION	15
2.2 MATERIALS AND METHODS.....	17
2.2.1 Mouse Lines and Tissue Processing.....	17

2.2.2	Animal Surgery and Viral Injections.....	18
2.2.3	Fluorescence Quantification	19
2.2.4	Three-Dimensional Sholl’s Analysis	21
2.2.5	Electrophysiological Recordings	21
2.3	RESULTS	23
2.3.1	Distinct Neuronal Subpopulations Identified in Lhx6 and PV Transgenic Mouse Lines	23
2.3.2	Lhx6- and PV-GPe Neurons Express Different Baseline Firing Rates.....	25
2.3.3	Lhx6- and PV-GPe Neurons Have Different Passive and Active Membrane Properties	27
2.3.4	Projections of Lhx6- and PV-GPe Neurons to the STN.....	31
2.3.5	Lhx6- and PV-GPe Neurons Differentially Innervate the Substantia Nigra Pars Compacta but Similarly Innervate GABAergic Output Nuclei of the Basal Ganglia	34
2.3.6	Lhx6-GPe Neurons Project More Densely to the Dorsolateral Striatum than PV-GPe Neurons	36
2.3.7	Distinct Projections of PV-GPe Neurons to the Parafascicular Nucleus of the Thalamus	39
2.4	DISCUSSION.....	41
2.4.1	Lhx6 and PV Transgenic Mouse Lines Subdivide GPe Neurons Into Two Groups.....	42
2.4.2	Lhx6 and PV Neurons Have Different Intrinsic Electrophysiological Properties	43

2.4.3	Implications of Genetically-Defined Output Pathways for Basal Ganglia Function	44
2.5	ACKNOWLEDGEMENTS	48
3.0	CELL-TYPE SPECIFIC PALLIDAL INTERVENTION INDUCES LONG-LASTING MOTOR RECOVERY IN DOPAMINE-DEPLETED MICE.....	49
3.1	INTRODUCTION	49
3.2	MATERIALS AND METHODS	51
3.2.1	Animals.....	51
3.2.2	Viral Transfection.....	52
3.2.3	Optogenetic Behavioral Implantation and Dopamine Depletion	53
3.2.4	Behavioral Paradigm.....	54
3.2.5	Implantation of Head-Fixation System.....	54
3.2.6	Head-Fixation Training and Recording	55
3.2.7	Optical Tagging Method	56
3.2.8	SNr Recordings	57
3.2.9	Tissue Processing	58
3.2.10	TH Quantification	58
3.2.11	Behavioral Analysis	59
3.2.12	Electrophysiology Analysis	59
3.2.13	Statistics.....	60
3.3	RESULTS	61
3.3.1	Global GPe Stimulation Does Not Restore Movement in DD Mice	61

3.3.2	Selective Activation of PV-GPe Neurons Restores Movement Persistently in DD Mice	64
3.3.3	Neuronal Responses In The GPe During PV-ChR2 Stimulation	67
3.3.4	Selective Inhibition of Lhx6-GPe Neurons Restores Movement Persistently in DD Mice	70
3.3.5	Persistent Behavioral Rescue Depends on the Ratio of Lhx6 and PV Activity	72
3.3.6	PV-ChR2 and Lhx6-Arch Reverse Pathological Burst Firing in SNr	74
3.4	DISCUSSION.....	78
3.4.1	Conclusions.....	80
3.5	ACKNOWLEDGEMENTS	81
4.0	SUMMARY AND CONCLUSIONS	82
4.1	SHIFTING CELLULAR LANDSCAPE OF THE GPE.....	84
4.1.1	Low-Frequency Discharge with Bursts: Arkypallidal Population	84
4.1.2	High-Frequency Discharge with Pause: Prototypic Population.....	85
4.1.3	Probing Diversity in Axonal Projections	87
4.1.4	Cellular Controversy	89
4.2	MECHANISMS FOR LONG-LASTING THERAPEUTIC INTERVENTION.....	91
4.2.1	State-Dependent Shifts	91
4.2.2	STN-Mediated Mechanisms.....	94
4.3	FINAL REMARKS	96
	APPENDIX A.....	98

APPENDIX B	105
BIBLIOGRAPHY	106

LIST OF TABLES

Table 1. Intrinsic Properties of GPe Neurons	31
--	----

LIST OF FIGURES

Figure 1-1 Basal Ganglia Circuit under Normal and Parkinsonian conditions	4
Figure 1-2 Molecular census of somatosensory S1 cortex and hippocampal CA1 by unbiased sampling and single-cell RNA-seq	6
Figure 2-1 Identification and distribution of Lhx6- and PV-GPe neurons in transgenic mice.....	24
Figure 2-2 Differences in baseline firing rates of Lhx6- and PV-GPe neurons.....	26
Figure 2-3 Differences in passive and active membrane properties of the Lhx6- and PV-GPe neurons in slice recordings.....	29
Figure 2-4 PV-GPe neurons project more strongly to the STN than Lhx6-GPe neurons.....	33
Figure 2-5 Lhx6- and PV-GPe projections to basal ganglia output nuclei.	35
Figure 2-6 Lhx6-GPe neurons project more strongly to the dorsolateral striatum than PV-GPe neurons.....	38
Figure 2-7 Lhx6- and PV-GPe projections to the thalamus.....	40
Figure 2-8 Summary of cell-type specific projection densities	45
Figure 3-1 Global GPe stimulation does not rescue movement in DD mice.....	62
Figure 3-2 Selective stimulation of PV-GPe rescues movement persistently in DD mice.....	65
Figure 3-3 Local response during PV-ChR2 stimulation directly inhibits other high-firing GPe neurons.....	69

Figure 3-4 Selective suppression of Lhx6-GPe rescues movement persistently in DD mice. 71

Figure 3-5 The induction of persistent behavioral rescue is cell-type specific..... 73

Figure 3-6 PV-ChR2 and Lhx6-Arch reverse pathological bursting activity persistently..... 76

Figure 4-1 Retrograde opsin or indicator expression..... 88

Figure 4-2 Stimulation setup for electrical stimulation. 93

LIST OF FIGURES: APPENDIX A

Figure A1 Behavioral and pathophysiological symptoms of bilateral DD are apparent within 3-5 d post-depletion.....	98
Figure A2 Histological verification of TH immunoreactivity, viral expression and fiber placements for behavioral optogenetics in global manipulations.	99
Figure A3 Histological verification of viral expression and fiber placements for behavioral optogenetics in cell-type manipulations.....	100
Figure A4 PV-ChR2 stimulation induces transient effects in partially and unilaterally depleted mice.....	101
Figure A5 Optical identification using ChR2 and Arch and their corresponding firing properties and waveforms.	102
Figure A6 PV and Lhx6 overlap partially in the Lhx6-Cre transgenic mouse.	103
Figure A7 SNr firing rate is unaltered after PV-ChR2 and Lhx6-Arch, but decreased after hSyn-ChR2 manipulation.	104

LIST OF FIGURES: APPENDIX B

Figure B1 Video 1: PV-ChR2 fast speed..... 105

Figure B2 Video 2: PV-ChR2 HD..... 105

Figure B3 Video 3:Lhx6-Arch fast speed..... 105

Figure B4 Video 4: Lhx6-Arch HD 105

PREFACE

I would like to acknowledge the many individuals who have supported and inspired me throughout this incredible process. First and foremost, I would like to thank Dr. Aryn Gittis for accepting me as her first graduate student and affording me the opportunity to lead, to learn, to fail and to succeed. It must have not been easy to start your lab and have me as your only option, but I am sure glad that you took the chance. It has been a journey with obstacles that together we were able to overcome and today, I am incredibly proud of our work and look forward to supporting you for the rest of our careers. Next, I would like to thank my committee for their advice and guidance: Drs Robert Turner (Chair), Susanne Ahmari, Bitu Moghaddam, and Peter Strick. You each have contributed in unique ways and I thank you for your time and commitment to my training. I wanted a committee that both supported and urged me to do better. You all have inspired me to be a better scientist, a more thoughtful thinker, and to never, never stop pushing forward.

There are so many individuals who I had the pleasure of working with and learning from over the last five years. The Great Hall of Brain Science of CMU Biological Sciences has been my home away from home. From the intellectually stimulating discussions with Drs. Alison Barth, Nathan Urban and Sandra Kuhlman to the intellectual growth with fellow GHBS graduate students, notably Nick Audette and Berquin Freese, it has been a strong training environment.

The Gittis lab contains a group of individuals who have come to shape my journey in more ways than they may know. Since starting the lab, Rachel Bouchard has been a vital member who works hard every single day while making life better for every member of the lab. My early success within the lab is in large part due to her support and encouragement; thank you for believing in me. I also would like to thank Kevin Zitelli for just being rock-solid. His ability to stay focused, on-task and constantly moving forward is a skill worth admiring and I am excited for your future and the impact you will continue to have on the field of neuroscience. To my undergraduates, especially Brandon Rogowski, Zachary Sachar and my favorite, Hiromi Holt (a legend), thank you for being active contributors who were able to learn and adapt as I was growing as a mentor and scientist. To the newest members of our community, Teresa Spix, Timothy Whalen, Katrina Nguyen, you each bring unique skill sets and vibrant personalities and it has been a joy to be a small part of your academic journey. I wish you all the best and

encourage you to continue pushing the bounds of what is possible here, you may be surprised at what you find.

Amanda Willard is my scientific partner. Thank you for always being there to lean on, to learn from and to grow with. This journey was not always easy, but it was more enjoyable having you by my side as we pushed down every new obstacle, together. I may be moving on, but I will continue to be your biggest fan and support you every step of the way. Special thanks to Jess Thomas and Kate Sadler who continue to inspire me to go after whatever will make me happy.

Thanks to my fellow graduate students, faculty and administrators of the Center for Neuroscience at the University of Pittsburgh (CNUP). A special thank you to Patti Argenzio who provided boundless support and laughter; thank you for everything. Within this community, I have formed life-long friendships with strong, intelligent, independent thinkers and scientists who never stopped supporting me. Special thanks to my science soulmate, Dr. Laura Rupprecht, Dr. Annie Liu, Dr. Elizabeth Manning and future Drs. Victoria Corbit, Patrick Beukema, Lindsey Snyder, Sean Piantadosi, Meredyth Wegener. To you all, my growth both personally and scientifically is linked to and because of each one of you. Thank you for never ceasing to inspire me and to challenge me and I am so excited to see where life takes each of us next. Regardless, I am glad that we will do this together.

Lastly, of course, is my family and friends. I have always been extremely fortunate to have a family who has supported and loved me unconditionally; this chapter is no different. Special thanks to my mother, Kim A. Mastro, and father, James V. Mastro, both of who seem to really think I can succeed. To my brother James W. Mastro and my best friends Marissa Dunn, Celeste Dupont, and Seth Nadeau, thank you for keeping up with my wild antics.

For my friends outside of neuroscience, thank you for giving me a reason to leave lab. Special thanks go to Ryan Rathman, Simi Lofti, and Drs. Shuchi Talati and Kristen Schell; I am incredibly fortunate to have had the opportunity to call each of you my friend. To Dr. Long Lam, thank you for giving me a reason to explore the world and to fight to be a better person. To Dr. Sophy Perdomo, thank you for inspiring me each and every day and showing by example how to overcome the impossible, to make your dreams possible.

Here, in reflection, is five years of growth that could not have been accomplished without the love, compassion and support of an incredible network of friends and family. Thank you.

1.0 INTRODUCTION

Neural circuits are made up of functionally specialized cell-types whose diversity allow for the generation of simple to complex behaviors. With the goal of understanding circuit function for the development of novel treatments for disease, the National Institute of Health declared the identification of neural cell-types as the leading BRAIN initiative (Jorgenson et al., 2015). Over the last decade, the emergence of new technologies has spurred innovative approaches to define and manipulate cell-types in the brain. These tools will be featured throughout the dissertation while shifting the attention from the identification and manipulation of cell-types (see Reviews by (Tye and Deisseroth, 2012, Lerner et al., 2016, Rajasethupathy et al., 2016) to the development of cell-type specific therapeutic interventions during disease.

Here, we will first utilize the basal ganglia as an exemplary circuit that has been revolutionized by the identification of neural cell-types and the emerging opportunities to harness this diversity to treat neurological disorders. In doing so, we will highlight the use of these advanced technologies and the refinement and development of future treatments. Over the last 15 years, neuronal cellular resolution has been resolved at an awe-inspiring rate and today we stand at the precipice of a most exciting future; to translate basic findings to the development of novel, innovative and impactful therapeutic interventions.

1.1 ADVANCEMENTS IN CELL-TYPE DEFINITIONS

At the turn of the 20th century, Santiago Ramon y Cajal and his students produced artistic renderings of brain cells that exemplified the diversity in structure of individual cells throughout the brain. Utilizing a microscope and the newest staining method (Golgi Stain), they were able to visualize individual cells from a host of brain areas. Cajal (Cajal, 1888) postulated that the brain is made up of individual cells whose shape, size and overall structure depend greatly on their overall location (brain area) and their functional specialization (Yuste, 2015). This relationship between structure and function have come to form the fundamental tenants of modern neuroscience (Lopez-Munoz et al., 2006); cellular heterogeneity, or cell-types, are the building blocks of neural circuits that provide the diversity necessary to produce simple to complex behavior. Therefore, major advancements in systems neuroscience are intimately linked to the identification of neural cell-types that contribute to function.

1.1.1 Basal Ganglia Evolution: From Brain Areas to Boxes

The basal ganglia is a prime example of how advancements in cell-type identification has revolutionized the way we understand its function in health and disease. Historically, the large striated tissue that sits deep in the brain has drawn an incredible amount of interest for both its anatomical differences from cortex and thalamus and its functional implications. Thomas Willis was the first to describe the corpus striatum, later termed the basal ganglia, within his *Cerebre Anatomii* (1664) (Willis, 1973), but it was not until the 20th century when the functional and anatomical contributions of basal ganglia became clearer (DeLong, 1983, Penney and Young, 1983, Albin et al., 1989, DeLong, 1990).

During the golden age of basal ganglia research (1960-1990s), there was a proliferation of physiology and anatomy studies seeking to understand how information flow navigated this subcortical space. Utilizing available neuronal tracing methods and single cell electrophysiology, scientists sought to define neuronal populations based on their projections to other nuclei and their physiological responses to initiation, maintenance and termination of movements. In a set of seminal reviews, the field coalesced on a model of normal and disease states that provided a framework to test hypotheses and would go on to dominate the field for decades to come (DeLong, 1983, Penney and Young, 1983, Albin et al., 1989, DeLong, 1990).

As shown in figure 1-1, the striatum is the canonical basal ganglia input structure and receives massive inputs from both cortex and thalamus. These excitatory inputs are topographically organized and segregated based on their functions (Alexander et al., 1986, Smith and Parent, 1986, Ragsdale and Graybiel, 1991, Nelson and Kreitzer, 2014). The striatum then funnels this information through two parallel pathways, the direct and indirect. The direct pathway represents the projections to the output nuclei of the basal ganglia, globus pallidus interna (GPi) and substantia nigra pars reticulata (SNr). The indirect pathway represents the polysynaptic route through the globus pallidus externa (GPe) and onward to the subthalamic nucleus (STN) before terminating in these same output nuclei. Though obvious anatomical and physiological differences existed within many of the basal ganglia nuclei, it was not until the advent of transgenic animals and viral manipulations that we gained access to tools that allow for delineation of the function of these pathways in health and disease.

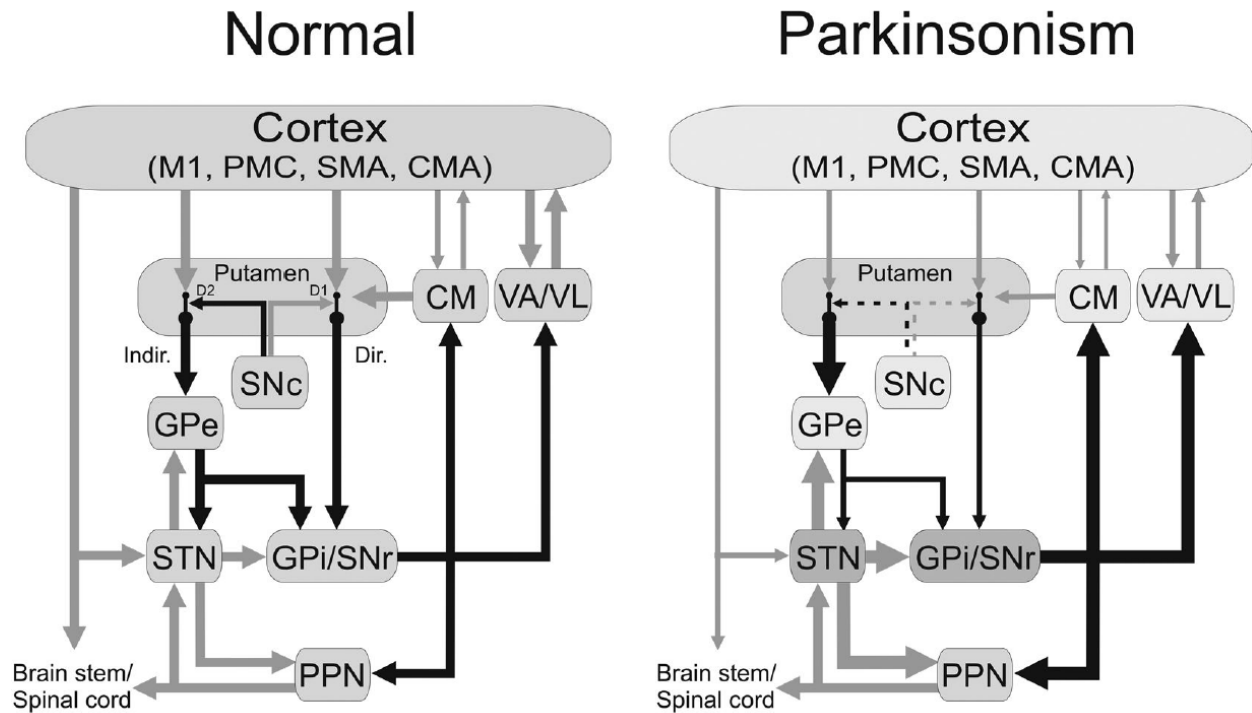


Figure 1-1 Basal Ganglia Circuit under Normal and Parkinsonian conditions

Weight of black (inhibitory) and grey (excitatory) arrows indicate the presumed activity of each connection. CM, centromedian nucleus of thalamus; CMA, cingulate motor area; Dir., direct pathway; D1, D2, dopamine receptor subtypes; GPe, external segment of the globus pallidus; GPi, internal segment of the globus pallidus; Indir., indirect pathway; M1, primary motor cortex; Pf, parafascicular nucleus of the thalamus; PMC, premotor cortex; PPN, pedunculopontine nucleus; SMA, supplementary motor area; SNc, substantia nigra pars compacta; SNr, substantia nigra pars reticulata; STN, subthalamic nucleus; VA, ventral anterior nucleus of thalamus; VL, ventrolateral nucleus of thalamus. From Galvan et al. (2016), with permission.

1.1.2 Defining Basal Ganglia Cell-Types

Major advancements within the field of basal ganglia neuroscience is linked to the identification of neural cell-types associated with their differences in gene and protein expression. The first major breakthrough occurred within the two striatal projection pathways which are associated with distinct molecular markers and receptor expression (Brownstein et al., 1977, Mroz et al., 1977, Beckstead, 1988, Gerfen et al., 1990). The development of BAC transgenic mice that selectively expressed *cre*-recombinase in either D1- or D2 - dopamine receptor expressing neurons associated with the direct and indirect pathway, respectively, provided distinguishable

populations of neurons within the striatum for further investigation (Gerfen et al., 1990). For example, optogenetic excitation of the direct pathway produced a robust increase in movement. In contrast, the indirect pathway activation led to a Parkinsonian-like state, characterized by an increase in freezing and slowness of movement (Kravitz et al., 2010, Kravitz and Kreitzer, 2011). In addition to the gross behavioral contributions, there has been tremendous progress in analyzing differences in morphology (Day et al., 2008, Gertler et al., 2008), plasticity (Kreitzer and Malenka, 2007, Shen et al., 2008) and their physiological activity during behavior (Cui et al., 2013) (for thorough review of D1/D2 contributions, see review (Calabresi et al., 2014)).

Cell-types exist throughout the basal ganglia, The GPe, a nuclei within the motor-suppressing indirect pathway, has benefited greatly from expression-based analysis of neurons. A set of seminal work identified a population of GPe neurons by their expression of parvalbumin (PV) and delineated the anatomical contributions that extended well outside of the canonical representation (Bevan et al., 1998, Kita et al., 1999). In Chapter 2, we utilize transgenic mouse lines to subdivide the GPe based on the expression of PV or Lim homeobox 6 (Lhx6) that uncover differences in their anatomical and physiological properties. Subsequent studies have defined the GPe population using additional transgenic animals (Hernandez et al., 2015, Oh et al., 2016a) and molecular markers (Mallet et al., 2012, Abdi et al., 2015, Dodson et al., 2015). Together, these studies provide definitive evidence for widespread connections of the GPe to multiple brain areas both within and outside of the basal ganglia and identifies markers for the physiologically distinct populations observed *in vivo* decades earlier (DeLong, 1971). In addition, there has been progress on defining the role of neurons during behavior (Abdi et al., 2015, Mallet et al., 2016) and decoding their physiology during movement (Dodson et al., 2015).

An obvious limitation for the transgenic or gene expression subdivision is that it lacks a direct correlate to the functional output of the given neuronal population. Though optical activation of the direct and indirect pathway led to opposing behavioral output (Kravitz et al., 2010, Kravitz and Kreitzer, 2011), the intricacies of action selection are much more complex (Cui et al., 2013). This suggests that further delineations may be necessary. To gain greater insight into the diversity that may contribute to the functional complexity, groups are utilizing genome-wide expression profiling of individual cells (Macosko et al., 2015). As seen within the cortex (Figure 1-2) (Zeisel et al., 2015, He et al., 2017), basal ganglia (Wallace et al., 2017) and brainstem (Kodama et al., 2012), these expression profiles can be plotted and used to find common clusters across high dimensional space and aid in the identification of unique genetic markers.

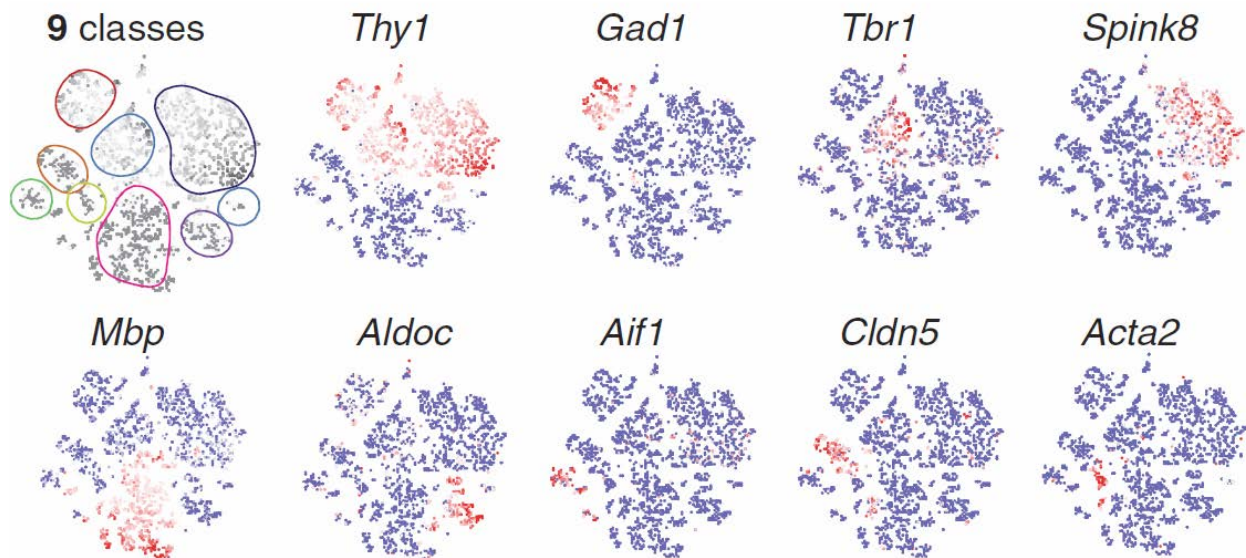


Figure 1-2 Molecular census of somatosensory S1 cortex and hippocampal CA1 by unbiased sampling and single-cell RNA-seq

Visualization of nine major classes of cells using t-distributed stochastic neighbor embedding. Each dot is a single cell, and cells are laid out to show similarities. Adapted from (Zeisel et al., 2015) Zeisel et al. (2015), with permission.

To understand neural circuits, we must understand the types of cells that are within them. These unbiased sampling methods can be applied across brain areas and provide a database of expression profiles for future investigation.

1.1.3 Input-Output Relationships

From the earliest investigations of neural circuits, the goal has been to understand the relationship of one element to the next. For any given node, we sought to define brain areas based on their connectivity within and outside of its local circuit. As discussed in Lerner et al. (2016), this provides profound insights into the organization of neural circuits and uncovers functionally related sets of neurons. Due to the advancement of retrograde and anterograde transported viruses, we have the ability to define these elements for classes of neurons within a brain area.

Many brain areas receive a diverse but distinct set of inputs and the extent to which these inputs synapse on individual neurons has often been technically inaccessible, until now. Take for example, the renaissance that has occurred recently within the dopamine field. Dopamine neurons are a critical component of the basal ganglia circuit and have been shown to be instrumental in reward prediction (Schultz, 1998) and often homogenous in their information processing (Eshel et al., 2016). Though a massive deal of research has focused on these neurons' role in a wide range of behaviors, there was a significant movement to understand how individual dopamine neurons wire into circuits at large. Multiple groups published dissections of dopaminergic hubs (Substantia nigra pars compacta and ventral tegmental area) that were based on evaluating the input and/or output relationship of single neurons and utilizing these

distinctions to understand their function during behavior (Lammel et al., 2011, Watabe-Uchida et al., 2012, Beier et al., 2015, Lerner et al., 2015, Menegas et al., 2015).

Together, these emerging tools that allow for the identification, manipulation and analysis of distinct populations of neurons based on expression profiles and connectivity will provide invaluable access to cellular diversity. In doing so, we are continuing to break open the black box that transform neural signal to simple and complex behaviors. These same neural cell-types can then be harnessed to treat neurological disorders and probe the underlying mechanisms for symptoms of a wide range of neurological and psychiatric disorders.

1.2 HARNESSING CELL-TYPES TO TREAT NEUROLOGICAL DISORDERS

The ultimate goal of defining cell-types is to delineate their functional contributions in health and disease. These advancements that will be highlighted within the basal ganglia circuit have provided a great opportunity to develop treatments for neurological disorders, including Parkinson's disease (PD). Each of the following sections will highlight the most promising cell-types in the disease pathology and development of therapeutic interventions.

1.2.1 Parkinson's Disease

1.2.1.1 Striatum

PD is characterized by a progressive loss of dopamine within the basal ganglia that leads to devastating motor and cognitive deficits. Under healthy conditions, dopamine regulates the two pathways by having opposing functions on their excitability mediated by their differential

expression of dopamine receptors (Cepeda et al., 2008). In models of basal ganglia dysfunction during PD, the loss of dopamine leads to an imbalance in these striatal pathways and ultimately the overactivity of the motor-suppressing indirect pathway and underactivity of motor-facilitating direct pathway activity (DeLong, 1983, Penney and Young, 1983, Albin et al., 1989, DeLong, 1990). Therefore, the prediction from the classic rate model is that activation of the motor-facilitating direct pathway should restore motor function.

In an animal model of PD, optogenetic activation of the direct pathway, mediated by the expression of channelrhodopsin within the D1 dopamine receptor-expressing striatal neurons, rescued motor function (Kravitz et al., 2010). These findings provided the first evidence for the utility of direct pathway manipulation as a therapeutic intervention. Currently, the administration of L-aromatic amino acid decarboxylase (L-DOPA), a dopamine precursor, capable of crossing the blood brain barrier, has provided a substantial therapeutic benefit. Though effective, dopamine replacement therapies are non-specific and prolonged usage leads to L-DOPA induced dyskinesia (LID; involuntary movements) in over 80% of Parkinson's patients. LID are believed to be caused by the over-inhibition of indirect pathway projection neurons that leads to decreased output of the basal ganglia and a loss of motor control (Obeso et al., 2000). Future treatments can capitalize on the distinct population of direct pathway projection neurons by identifying unique targets for drug application. By either altering intrinsic properties or increasing specificity of drug delivery, the new treatment would rescue motor function while avoiding the negative side effects of prolonged dopamine-replacement therapies.

1.2.1.2 Subthalamic Nucleus (STN)

The STN contains glutamatergic neurons that project to the output nuclei, SNr and GPi, and sends a reciprocal connection to the GPe. The STN receives massive cortical innervation that is topographically organized (Parent and Hazrati, 1995). Under healthy conditions, STN neurons are high-firing and tonically active where changes in their activity can be related to movement (Wichmann et al., 1994, Jaeger et al., 1995, Bergman et al., 1998). In PD, the STN is implicated in the onset and propagation of harmful synchrony and forms a detrimental relationship with the reciprocally connected and largely GABAergic, GPe (Wichmann and DeLong, 1996, Bevan et al., 2002).

The STN is one of the major targets for deep brain stimulation (DBS) which includes the surgical implantation of electrodes where high frequency (~130 Hz) electrical stimulation restores motor function. Similar to the dopamine replacement therapies, DBS struggles with a lack of neuronal and pathway specificity and often increase the appearance of other motor, sensory and cognitive deficits. Though the cellular mechanisms of DBS are still unclear, there has been work to localize optimal STN placement and alternatives to probing its activity. Baron et al. (2002) found that focal inactivation of the STN or GPi were sufficient for amelioration of Parkinsonian motor deficits. Moreover, the targeting of DBS electrodes is most effective within the sensorimotor region of either the STN or GPe (Wichmann and DeLong, 2016). Interestingly, optical activation of afferents to the STN provided a strong amelioration of PD deficits that was not observed upon direct activation of the STN neurons (Gradinaru et al., 2009). Together, these data indicate that modulation of the sensorimotor pathway, irrespective of STN neuronal activation, is sufficient to rescue motor function in animal models of PD. Future treatments may work to selectively alter the activity within this region of the STN by improving targeting of

DBS electrodes or by way of transcranial magnetic stimulation (TMS) of cortex. Recently, Udupa et al. (2016) paired TMS of the motor cortex (M1) and DBS of the STN and showed an increase in the cortical plasticity at the M1-STN node. Therefore, this study provided the proof of principle for the development of protocols that would exploit the LTP-like effects of TMS on M1-STN connection while paired with DBS. By doing so, it would reduce the amount of time necessary for DBS stimulation which must remain on to gain the therapeutic benefits.

1.2.1.3 Globus Pallidus Externa (GPe)

The GPe is in the motor-suppressing indirect pathway and has widespread connections within and outside of the basal ganglia. The striatum and STN constitute two of the greatest sources of inputs. The GPe and STN are implicated in PD pathological activity and the disruptions of which corresponds to motor recovery. In PD, the activity of the GPe is severely diminished (Nini et al., 1995, Plenz and Kital, 1999, Raz et al., 2000, Bevan et al., 2002, Levy et al., 2002, Terman et al., 2002). Like the STN, the GPe is a possible target for successful DBS (Johnson et al., 2012, Vitek et al., 2012), but experimental attempts to restore the activity of the GPe, globally, did not provide a therapeutic benefit (Chan et al., 2011, Mastro et al., 2017).

In Chapter 3, we harness cell-types within the GPe to disrupt pathological activity and restore motor function (Mastro et al., 2017). Briefly, upon activation of PV-GPe or the inhibition of Lhx6-GPe neurons in a dopamine-depleted animal, there is the induction of a persistent and long-lasting recovery in motor function. Moreover, these successful manipulations attenuate pathological activity in the output nucleus of the basal ganglia that persists for hours and hours after stimulation. In Chapter 4, there will a discussion focused on the potential mechanism for

the long-lasting recovery. Including a review of a new DBS protocol that has been shown to destabilize the BG network and provide relief for hours to days after treatment.

Overall, these results suggest that the development of future treatments to persistently disrupt pathological activity is first, possible and second, may hinge on preferentially increasing the activity of PV-GPe neurons relative to other GPe neurons. Current work is focused on highlighting the differences between the two populations that may be used to dissociate their activity. For example, PV- and Lhx6-GPe neurons project differently to the STN (Mastro et al., 2014) and may provide an opportunity through targeting of the DBS electrodes for a greater relief of motor dysfunction. Due to the similar proportion of PV-GPe neurons in humans to that in mice (Hardman and Halliday, 1999), directly targeting this population of neurons represents another translational approach. Here, we could capitalize on the electrophysiological differences that exist between PV-GPe neurons and other populations (Mastro et al., 2014, Abdi et al., 2015, Glajch et al., 2016) that would increase the excitability and restore the activity of these neurons. Together, these results support the development of potential treatments that utilize cell-type specific GPe interventions that can persistently disrupt pathological activity and restore motor function.

1.3 SUMMARY AND AIMS OF DISSERTATION

In summary, the identification of neural cell-types has revolutionized neuroscience and provides new opportunities to harness these differences and treat neurological disorders. The basal ganglia represent a circuit that is constantly evolving and has benefited greatly from the identification of neural cell-types. This dissertation represents the steps taken to break open one critical node

within the basal ganglia, the GPe. In the following chapters, we will highlight the transgenic animals that provided unparalleled access to two partially-overlapping populations of GPe neurons. This study establishes the differences that exist between PV- and Lhx6-GPe neurons along a range of factors: topography, physiological properties (*ex vivo*) and axonal projections. Secondly, we will demonstrate the utility of cell-type specific interventions in a dopamine depleted mouse and its ability to restore motor function and disrupt pathological activity in the basal ganglia circuit. Lastly, we will explore the two major themes within this document; GPe cellular heterogeneity and the potential mechanisms underlying cell-type specific rescue of motor function during disease.

2.0 TRANSGENIC MOUSE LINES SUBDIVIDE EXTERNAL SEGMENT OF THE GLOBUS PALLIDUS (GPe) NEURONS AND REVEAL DISTINCT GPe OUTPUT

Cell-type diversity in the brain enables the assembly of complex neural circuits, whose organization and patterns of activity give rise to brain function. However, the identification of distinct neuronal populations within a given brain region is often complicated by a lack of objective criteria to distinguish one neuronal population from another. In the external segment of the globus pallidus (GPe), neuronal populations have been defined using molecular, anatomical, and electrophysiological criteria, but these classification schemes are often not generalizable across preparations, and lack consistency even within the same preparation. Here, we present a novel use of existing transgenic mouse lines, Lhx6-Cre and PV-Cre, to define genetically distinct cell populations in the GPe that differ molecularly, anatomically, and electrophysiologically. Lhx6-GPe neurons, which do not express PV, are concentrated in the medial portion of the GPe. They have lower spontaneous firing rates, narrower dynamic ranges, and make stronger projections to the striatum, and SNc compared to PV-GPe neurons. In contrast, PV-GPe neurons are more concentrated in the lateral portions of the GPe. They have narrower action potentials, deeper AHPs, and make stronger projections to the STN and parafascicular nucleus of the thalamus. These electrophysiological and anatomical differences suggest that Lhx6- and PV-GPe neurons participate in different circuits with the potential to contribute to different aspects of motor function and dysfunction in disease.

2.1 INTRODUCTION

The basal ganglia are a set of subcortical nuclei that play an important role in facilitating voluntary movement in health and disease (Albin et al., 1989, DeLong, 1990). The basal ganglia are thought to control movement through the coordinated activity of the direct and indirect pathways that have opposite effects on movement (Alexander and Crutcher, 1990, Smith et al., 1998a, Kravitz et al., 2010). The external segment of the globus pallidus (GPe) is a central nucleus in the motor-suppressing indirect pathway, which receives inputs from the striatum, subthalamic nucleus (STN) and parafascicular nucleus of the thalamus (pf) (Robledo and Feger, 1990, Kincaid et al., 1991, Kita and Kitai, 1991, Parent and Hazrati, 1995). In vivo recordings have shown that GPe neurons fire independently (Nini et al., 1995), with firing rates that are characterized by complex temporal patterns and low correlation during movement (DeLong et al., 1985, Wichmann et al., 1994, Jaeger et al., 1995, Bergman et al., 1998).

Overall, the specific contributions of the GPe to basal ganglia function are not well defined, but the GPe has been strongly implicated in the onset and maintenance of motor dysfunction in movement disorders such as dystonia and Parkinson's disease (Lozano et al., 2000, Kita, 2007, Obeso et al., 2008). Most notably, the activity of GPe neurons in patients suffering from Parkinson's disease is reduced and the synchronization of GPe neurons is thought to contribute to pathological oscillations (Nini et al., 1995, Plenz and Kital, 1999, Raz et al., 2000, Bevan et al., 2002, Levy et al., 2002, Terman et al., 2002). Consistent with the hypothesis that oscillations contribute to motor dysfunction, deep brain stimulation of the GPe has been shown to relieve Parkinsonian motor symptoms in humans (Vitek et al., 1998, Yelnik et al., 2000, Vitek et al., 2004, Vitek et al., 2012).

Progress in linking activity of GPe neurons to behavior has been complicated by the fact that the GPe contains a heterogeneous population of neurons that likely contribute differentially to motor function in healthy and diseased individuals. Anatomical studies have shown that GPe neurons project to a number of brain areas, but most of these projections are given little consideration in models of basal ganglia function (Parent et al., 1983, Smith and Bolam, 1989, Kita and Kitai, 1994, Smith et al., 1998b, Sato et al., 2000). For example, the identification of pallidostriatal neurons using tracing techniques in rodents and primates suggests a complexity of neural circuit organization in the GPe that has long been underappreciated (Kita and Kitai, 1994, Bevan et al., 1998, Kita et al., 1999, Sato et al., 2000, Mallet et al., 2012). Attempts have been made to classify cell-types in the GPe, but these criteria are often difficult to generalize across preparations (Nambu and Llinas, 1994, Cooper and Stanford, 2000, Kita, 2007, Deister et al., 2013), rely on postmortem cell-type identification (Hoover and Marshall, 1999, Sato et al., 2000, Hoover and Marshall, 2002), or rely on activity in disease states (Mallet et al., 2012).

Here, we utilize transgenic mouse lines to define two genetically distinct, non-overlapping populations of GPe neurons in healthy rodents. Viral expression of EYFP revealed that Lhx6- and PV-GPe neurons differed in their axonal projection patterns as well as electrophysiological properties measured in slice recordings. These results provide a new set of tools to target molecularly, anatomically, and electrophysiologically distinct cell-types in the GPe which will enable studies of the organization and function of GPe circuits in health and disease.

2.2 MATERIALS AND METHODS

2.2.1 Mouse Lines and Tissue Processing

All procedures were carried out in accordance with the guidelines from the NIH and with approval of the CMU IACUC. Male and female heterozygous 4-8 week-old mice on a C57BL/6J background were used for experiments. Lhx6-GPe neurons were targeted using Lhx6-GFP (GENSAT, www.gensat.org) or Lhx6-Cre (Fogarty et al., 2007) mouse lines. PV-GPe neurons were targeted using a Pvalb-2A-Cre mouse line (Madisen et al., 2010).

For immunohistochemistry, mice were perfused transcardially with phosphate buffered saline (PBS), followed by 4% paraformaldehyde in PBS. Brains were removed and drop-fixed with the same fixative at 4°C for 24 h. After rinsing with PBS, brains were transferred to 30% sucrose in PBS and stored at 4°C for at least 24 h before sectioning. Tissue was sectioned in 30 μ m sections, blocked with 10% normal donkey serum and permeabilized with 0.5% Triton X-100 for 1 h. Primary antibody incubations were performed at 4°C for 24 h, using either rabbit anti-GFP (1:500, Millipore), chicken anti-GFP (1:1000, Aves), mouse anti-NeuN (1:1000, Millipore), rabbit anti-TH (1:1000), or at 4°C for 48 h when using rabbit anti-PV (1:1000, Swant). Primary antibodies were detected with Alexa Fluor 488-conjugated goat anti-chicken (1:500, Vector Laboratories), Alexa Fluor 488-conjugated goat anti-rabbit (1:500, Vector Laboratories), Alexa Fluor 568-conjugated donkey anti-rabbit (1:500, Vector Laboratories), Alexa Fluor 568-conjugated donkey anti-mouse (1:500, Vector Laboratories), Alexa Fluor 647-conjugated donkey anti-rabbit (1:500, Vector Laboratories), or Alexa Fluor 647-conjugated donkey anti-mouse (1:500, Vector Laboratories), incubated for 2 h at room temperature.

For processing of Fluoro-Gold (FG) labeling, primary antibody incubations were performed at 4°C for 48 h using rabbit anti-FG (1:3000, Fluorochrome). Primary antibody was detected using Alexa Fluor 647-conjugated donkey anti-rabbit (1:500, Vector Laboratories) for 3 h at room temperature.

2.2.2 Animal Surgery and Viral Injections

Injections of AAV2-DIO-EYFP or AAV5-DIO-ChR2-EYFP (used for electrophysiology), produced at the University of North Carolina (Vector Core Facility) were made in 4-5 week-old PV-Cre or Lhx6-Cre transgenic mice. Anesthesia was induced using 50 mg/mL ketamine / 15 mg/mL xylazine and maintained throughout surgery using 2% isoflurane. Mice were placed in a stereotaxic frame (Kopf Instruments), the scalp was opened and bilateral holes were drilled in the skull (0.27-0.30 mm anterior, 2.1-2.2 mm lateral from Bregma). 150 – 200 nL of virus was injected with a Nanoject (Drummond Scientific) through a pulled glass pipet (tip diameter ~30 μ m) whose tip was positioned 3.70 mm below the top of the skull. To prevent backflow of virus, the pipet was left in the brain for 5 min after completion of the injection. Animals were housed for at least 2 weeks following injection to allow time for viral expression.

Injections of Fluoro-Gold were done using the same surgical procedures, but bilateral holes were drilled over the striatum (1.0 mm anterior, 2.3 mm lateral from Bregma) and 1 μ L of Fluoro-Gold (0.5% in saline, Fluorochrome) was injected 3.7 mm below the surface of the skull using a syringe pump (0.2 μ L/min; Genietouch). Mice were perfused two weeks following injections and tissue was prepared as described above.

2.2.3 Fluorescence Quantification

Quantification of axonal projection patterns of Lhx6- and PV-GPe neurons was carried out in sagittal sections from hemispheres where GPe injections met the following criteria: viral expression within the GPe was strongest within the central plane of analysis (Lateral 1.56 mm, Figure 114 (Paxinos, 2004), and labeled cell bodies were observed throughout the full rostral-caudal, dorsal-ventral, and medial-lateral extent of the structure. Analyses were carried out in 7 sagittal planes: (Lateral from bregma, mm) 3.12, 2.76, 2.04, 1.56, 1.20, 0.84, and 0.48 (Paxinos, 2004). Hemispheres in which there was significant spillover of virus and EYFP expression in neighboring structures, such as the reticular thalamic nucleus, ventral palladium, and striatum were excluded from analysis. To aid in visualization of axonal projections from the GPe, EYFP signal was enhanced with an immunostain against GFP. Epifluorescent images were taken at 25x magnification in seven sagittal slices of each brain and the same sectional planes across animals were used for analyses. To control for differences in viral expression or antibody retrieval, data from each animal was normalized to the fluorescence intensity in the GPe during analysis. Images were analyzed offline utilizing the pixel intensity-measuring tool on ImageJ. Data were quantified by averaging the pixel intensity within and across each brain structure. On average, three 100 px x 100 px (75 μ m x 75 μ m: Area = 5625 μ m²) squares were quantified in each of the images. The mean of all pixel intensities designated as within a single structure was found and normalized to GPe expression of each animal. For example, dorsolateral striatum was identified in three planes of section (Lateral from Bregma, mm: 3.12, 2.76, and 2.04). Three measures of pixel intensity were taken by randomly placing the 75 x 75 μ m square throughout the image. The mean of each image was taken and then averaged across the three planes of section to identify the average pixel intensity of dorsolateral striatum. Finally, the average was normalized to the

brightest GPe expression found within the animal, which was located in the central plane of analysis (Lateral 1.56 mm, Figure 114). Striatum, RT, GPi, BLA, PSTh and pf were analyzed using the method described above.

Due to the irregular shape of the STN and the ease at which the STN borders could be identified at 25x magnification, ImageJ hand draw tool was used to measure average pixel intensity of the entire structure. Similar to other structures, the STN was identified in more than one plane of section, and the pixel intensity from each plane was averaged and then normalized to GPe expression.

In the case of the substantia nigra, a tyrosine hydroxylase (TH) stain was used to define the borders between dopamine neurons of the pars compacta and the non-dopaminergic (GABAergic) neurons of the pars reticulata. GFP and TH expression was sequentially imaged in the GPe and SN using the epifluorescent microscope at 10x-magnification. For ImageJ analysis, zones were clearly defined using TH expression as a marker for the pars compacta and utilizing the hand draw tool described above. These zones were then overlaid on the images showing GFP expression and the average pixel intensity was found. The average across sections was taken and normalized to GPe expression. Differences in normalized fluorescence intensities were compared using a t-test.

Results of Fluoro-Gold retrograde labeling were analyzed in 2-4 sections each from three PV mice (PV-Cre x Ai3 or PV-Cre x Ai9) and three Lhx6 mice (Lhx6-GFP). GPe sections were magnified to 63X on an epifluorescent microscope. The number of FG+ neurons in an 225 μm x 175 μm square of tissue were counted and scored as Lhx6+, PV+, or neither. Populations of FG+ neurons that were either Lhx6 or PV were compared using a Fisher's Exact Test.

2.2.4 Three-Dimensional Sholl's Analysis

To quantify the selective innervation of striatal fast-spiking striatal interneurons (FSIs) by Lhx6- and PV-GPe neurons, a three-dimensional Sholl's analysis was performed as described previously (Chattopadhyaya et al., 2004). Briefly, tissue from mice expressing EYFP in Lhx6- or PV-GPe neurons was immunostained for PV and NeuN to identify FSIs and medium spiny neurons in the striatum, respectively. Although NeuN does not selectively stain MSNs, MSNs make up 95% of neurons in the striatum, so for the purposes of this analysis, we assumed that NeuN+/PV- neurons were most likely MSNs. Confocal z-stack images of presumed striatal FSIs and MSNs were taken at 63x-magnification and channels were sequentially imaged to avoid bleedthrough. Stacked images were merged using ImageJ and concentric circles of increasing diameter (2 μ m) were drawn from the center of each identified neuron. Innervation was quantified as the number of axonal varicosities counted in each circle.

2.2.5 Electrophysiological Recordings

Parasagittal sections (300 μ m thickness) containing the GPe or parafascicular nucleus were prepared from brains of 5-8 week-old mice. Lhx6-GPe neurons were targeted in slices from Lhx6-GFP mice, Lhx6-Cre mice injected in the GPe with AAV2-DIO-EYFP, or Lhx6-Cre mice crossed to the reporter strains Ai9 (red) or Ai3 (green) (Jackson Laboratories). PV-GPe neurons were targeted in slices from PV-Cre mice injected in the GPe with AAV2-DIO-EYFP or PV-Cre crossed to Ai9 or Ai3 reporter strains.

Slices were prepared on a Leica VT1200 vibratome in an ice-cold Hepes cutting solution (in mM): 92 NaCl, 2.5 KCl, 1.2 NaH₂PO₄, 30 NaHCO₃, 20 Hepes, 25 glucose, 5 sodium ascorbate,

2 thiourea, 3 sodium pyruvate, 10 MgCl₂, and 0.5 CaCl₂. Slices were allowed to recover for 15 min at 33°C in a chamber filled with NMDG-Hepes recovery solution (in mM): 93 NMDG, 2.5 KCl, 1.2 NaH₂PO₄, 30 NaHCO₃, 20 Hepes, 25 glucose, 10 MgSO₄, 0.5 CaCl₂, 5 sodium ascorbate, 2 thiourea, 3 sodium pyruvate. After 15 min, slices were held at room temperature for at least 1 h before recording in a holding solution that was similar to the Hepes cutting solution but with 1 mM MgCl₂ and 2 mM CaCl₂. Recordings were made at 33°C in carbogenated ACSF (in mM): 125 NaCl, 26 NaHCO₃, 1.25 NaH₂PO₄, 2.5 KCl, 12.5 glucose, 1 MgCl₂, and 2 CaCl₂. For recordings of intrinsic excitability, 50 μM picrotoxin and 5 μM DNQX were included in the bath to block fast inhibitory and excitatory transmission, respectively.

Data were collected with a MultiClamp 700B amplifier (Molecular Devices) and ITC-18 A/D board (HEKA) using Igor Pro software (Wavemetrics) and custom acquisition routines (Recording Artist, Richard C. Gerkin). Current-clamp recordings were filtered at 10 kHz and digitized at 40 kHz; voltage clamp recordings were filtered at 2 kHz and digitized at 10 kHz. Electrodes were made from borosilicate glass (pipette resistance, 2 – 4 M). The internal solution for current clamp recordings consisted of (in mM): 130 KMeSO₃, 10 NaCl, 2 MgCl₂, 0.16 CaCl₂, 0.5 EGTA, 10 Hepes, 2 Mg-ATP, 0.3 Na-GTP and the internal for voltage clamp recordings consisted of (in mM): 120 CsMeSO₃, 15 CsCl, 8 NaCl, 0.5 EGTA, 10 Hepes, 2 Mg-ATP, 0.3 Na-GTP, 5 QX-314.

Differences in electrophysiological parameters were compared using a Wilcoxon non-parametric test. Action potential half-width was calculated as the width of the action potential, measured at a point halfway between threshold and AP peak. AP threshold was defined as the voltage at which the acceleration in voltage exceeded 3×10^5 V/s/s. Maximum firing rate was measured as the average maximum firing rate over a 1 s step that could be sustained without

entering depolarization block. Input resistance was calculated in voltage clamp as the deviation from the holding current caused by a 5 mV hyperpolarizing step. The change in current was calculated as the difference between baseline holding current and the average current during the last 10 ms of the 40 ms hyperpolarizing voltage step. Whole-cell capacitance was calculated by integrating the area under the transient following a 5 mV hyperpolarizing voltage step from the holding potential, -80 mV. The holding current was subtracted before integrating.

2.3 RESULTS

2.3.1 Distinct Neuronal Subpopulations Identified in Lhx6 and PV Transgenic Mouse

Lines

Transgenic mouse lines were used to identify two distinct subpopulations of neurons in the GPe. In the first transgenic line, Pvalb-2a-Cre (PV-Cre) (Madisen et al., 2010), gene expression was driven under the promoter for parvalbumin (PV), a calcium binding protein found in GABAergic neurons in the CNS. In the second transgenic line, Lhx6-Cre (Fogarty et al., 2007) or Lhx6-GFP (Gensat), gene expression was driven under the promoter for Lhx6, a homeobox protein found in a subset of GABAergic neurons in the brain (Marin et al., 2000, Cobos et al., 2006). An immunostain against PV in tissue from an Lhx6-GFP mouse revealed non-overlapping populations of neurons in the GPe (Fig. 2-1A). Lhx6- and PV-GPe neurons each accounted for about 1/3 of NeuN⁺ neurons in the GPe. Lhx6-GPe neurons made up 34% (1030/3517) of NeuN⁺ GPe neurons while PV-GPe neurons made up 29% (1149/3517), with only 2% (54/3517)

of NeuN+ GPe neurons expressing both (Fig. 2-1B). Neurons were scored as positive for Lhx6 or PV if pixel intensity was >10x background.

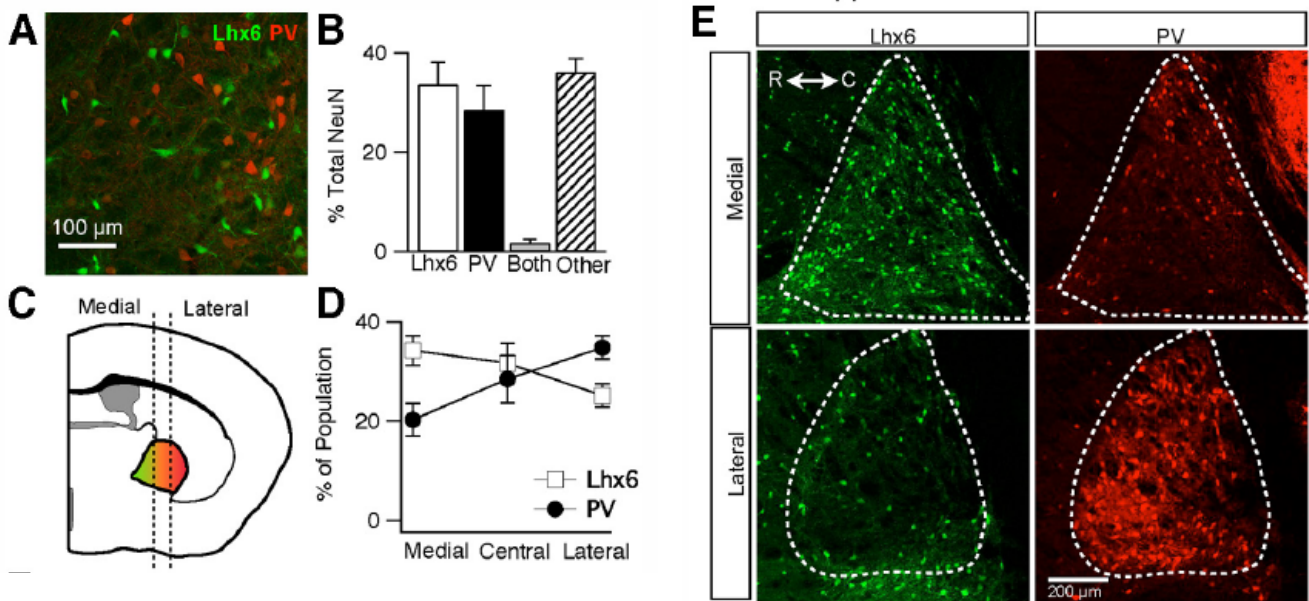


Figure 2-1 Identification and distribution of Lhx6- and PV-GPe neurons in transgenic mice.

A. Epifluorescent image from the GPe of an Lhx6-GFP mouse immunostained for PV showing two distinct populations of Lhx6+/PV- (green) and Lhx6-/PV+ (red) neurons. B. Graph showing the percentage of neurons that are Lhx6+/PV-, Lhx6-/PV+, both, or other throughout the GPe. Error bars are SEM. C. Schematic depiction of cell-type gradient found along the medial-lateral axis. Dotted lines divide the GPe into the three zones used for analysis of the medial-lateral axis. Lhx6 population (green) is found primarily in the medial portion while PV population (red) is found more laterally. D. Graph of the percentage of each cell population located within the three divisions along the medial-lateral axis. Error bars are SEM. E. Epifluorescent images of medial and lateral sections of the GPe showing Lhx6-GFP (green) or PV immunofluorescence (red). Scale bar, 200 μ m.

Because the fraction of PV-GPe neurons observed with immunostaining was lower than what has been reported in other species, we utilized a second, genetic approach to quantify the fraction of PV-GPe neurons. PV-Cre mice were crossed to fluorescent reporter mice (Ai3) and fixed sections from these animals were immunostained with NeuN and PV. Consistent with our immunohistochemistry data, genetically-identified PV-GPe neurons were less than half of all GPe neurons (41%, 235/571), and 78% (1226 / 1544) of genetically-defined PV-GPe neurons were immunopositive for PV.

To quantify the spatial distribution of Lhx6 and PV neurons within the GPe, cells were counted along medial-lateral, dorsal-ventral, and rostral-caudal axes. No gradients were observed along the rostral-caudal and dorsal-ventral axes, but opposing gradients were observed along the medial-lateral axis (Fig. 2-1C-E). Lhx6-GPe neurons were most concentrated in the medial portions of the GPe and decreased in concentration from medial to lateral, while PV-GPe neurons were most concentrated in the lateral and less concentrated in the more medial portions of the GPe.

2.3.2 Lhx6- and PV-GPe Neurons Express Different Baseline Firing Rates

To determine whether Lhx6- and PV-GPe neurons correspond to electrophysiologically distinct subpopulations, neurons of each cell-type were targeted for recording in acute slices from 5-8 week-old Lhx6 or PV transgenic mice. To determine the rates of intrinsic pacemaking in each cell-type, 50 μ M picrotoxin and 5 μ M DNQX were bath applied to block fast inhibitory and excitatory transmission, respectively. In the cell attached configuration, both cell-types fired tonically with low inter-spike variability ($CV_{Lhx6} = 0.31 \pm 0.39$, $n = 25$ vs. $CV_{PV} = 0.22 \pm 0.25$, $n = 20$; $p = 0.1$) (Fig. 2-2A). On average, PV-GPe neurons exhibited faster extracellular firing rates than Lhx6-GPe neurons (Lhx6 = 34.2 ± 33.2 Hz, range 1.3 - 142 Hz vs. PV = 64.4 ± 34.3 Hz, range 9.2 - 131 Hz; $p = 0.001$) (Fig. 2-2B). To ensure that extracellular firing rates were not influenced by the voltage clamp recording configuration or the gigaohm seal, we recorded extracellular firing rates in a second population of neurons using loose patch in cell attached recording mode. Once again, PV-GPe neurons were found to have significantly higher extracellular firing rates than Lhx6-GPe neurons (Lhx6 = 28.9 ± 17.7 Hz, range 3.9 - 55.2 Hz, $n = 20$ vs. PV = 66.1 ± 39.0 Hz, range 14.8 - 140 Hz, $n = 17$; $p < 0.0001$). In the whole cell-

recording configuration, spontaneous firing persisted in 20/27 PV-GPe neurons but in only 18/38 Lhx6-GPe neurons (Fig. 2-2C). Spontaneous firing rates were measured within 5 minutes of break-in because spontaneous firing rates tended to run down over the duration of a recording. Spontaneous firing rates recorded in whole cell configuration were also significantly faster in PV-GPe neurons compared to Lhx6-GPe neurons (Lhx6 = 7.8 ± 14.2 Hz, n = 38 vs. PV = 28.4 ± 24.9 Hz, n = 27; p = 0.0003) (Fig. 2-2D).

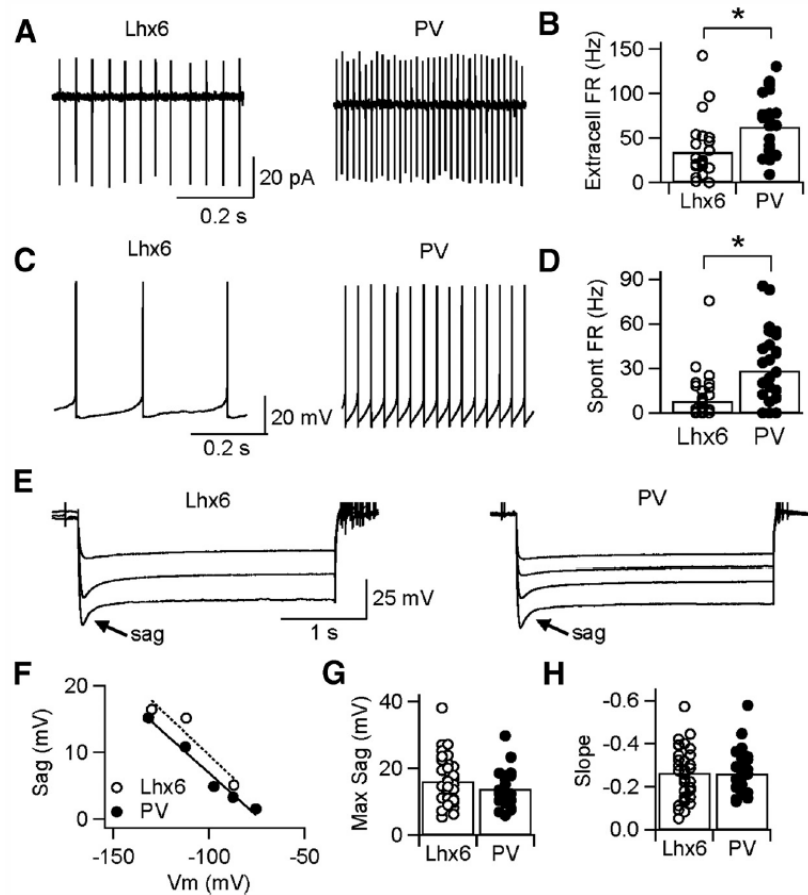


Figure 2-2 Differences in baseline firing rates of Lhx6- and PV-GPe neurons

A. Representative traces of cell attached recordings from Lhx6 (*left*) and PV (*right*) neurons, showing tonic firing with low inter-spike variability. B. Extracellular firing rates recorded for the population of PV-GPe neurons were significantly faster than those for Lhx6-GPe neurons. C. Representative traces of spontaneous firing in whole cell recording configuration for Lhx6 (*left*) and PV (*right*) neurons. D. Spontaneous firing rates recorded for the population of PV-GPe neurons were significantly faster than those for Lhx6-GPe neurons. E. Responses of representative Lhx6 (*left*) and PV (*right*) neurons to 3 s hyperpolarizing steps in current clamp. F. Amplitude of sag current plotted as a function of Vm reached immediately following the hyperpolarizing step for neurons in E. G-H. Maximum amplitude of the sag current (G) and its linear relationship to Vm (H), recorded for the population of Lhx6- and PV-GPe neurons.

Because autonomous pacemaking in GPe neurons relies in part on hyperpolarization-activated, cyclic nucleotide-gated cation (HCN) channels (Chan et al., 2004), we hypothesized that differences in intrinsic firing rates between Lhx6- and PV-GPe neurons might arise from differences in hyperpolarization-activated currents (I_h). To measure I_h, Lhx6- and PV-GPe neurons were given 3 s hyperpolarizing current injections of increasing magnitude (Fig. 2-2E). In the current clamp recording configuration, hyperpolarization resulted in an I_h-mediated rectification of the membrane potential, often referred to as a membrane potential “sag”, which increased monotonically as a function of membrane potential (Fig. 2-2F). Surprisingly, we observed no difference in the maximum sag recorded in Lhx6- and PV-GPe neurons (Lhx6 = 16.1 ± 7.0 mV, n = 35 vs. PV = 13.8 ± 5.5 mV, n = 22; p = 0.22) (Fig. 2-2G) and no difference in the slope of the monotonic relationship between sag and membrane potential (Lhx6 = -0.264 ± 0.14 vs. PV = -0.259 ± 0.13 ; p = 0.77) (Fig. 2-2H). These results suggest that differences in I_h expression are unlikely to account for differences in intrinsic firing rates of Lhx6- and PV-GPe neurons, but do not rule out this possibility entirely.

2.3.3 Lhx6- and PV-GPe Neurons Have Different Passive and Active Membrane

Properties

Variability in a number of passive and active membrane properties has been reported across GPe neurons, including resting membrane potential, firing rate adaptation, and action potential shape (Nambu and Llinas, 1994, Cooper and Stanford, 2000). To determine whether passive membrane properties vary systematically between Lhx6- and PV-GPe neurons, neurons were held in voltage clamp (-80 mV) and given brief hyperpolarizing steps (-5 mV, 100 ms). Figure 3A shows the response of a representative Lhx6-GPe neuron and a representative PV-GPe neuron.

Input resistance, calculated from the current flowing during the hyperpolarizing step, was significantly greater in Lhx6- relative to PV-GPe neurons ($300.6 \pm 168 \text{ M}\Omega$, $n = 38$ vs. $170 \pm 88 \text{ M}\Omega$, $n = 28$; $p = 0.0007$) (Fig. 2-3B). Whole cell capacitance, calculated as the integral under the transient (Fig. 2-3A, inset), was significantly greater in PV-GPe relative to Lhx6-GPe neurons ($241 \pm 113 \text{ pF}$, $n = 28$ vs. $164 \pm 65 \text{ pF}$, $n = 38$; $p = 0.002$) (Fig. 2-3C). Because capacitance is proportional to the surface area of a neuron, these results suggest that PV-GPe neurons are larger, or have more extensive dendritic arborizations than Lhx6-GPe neurons.

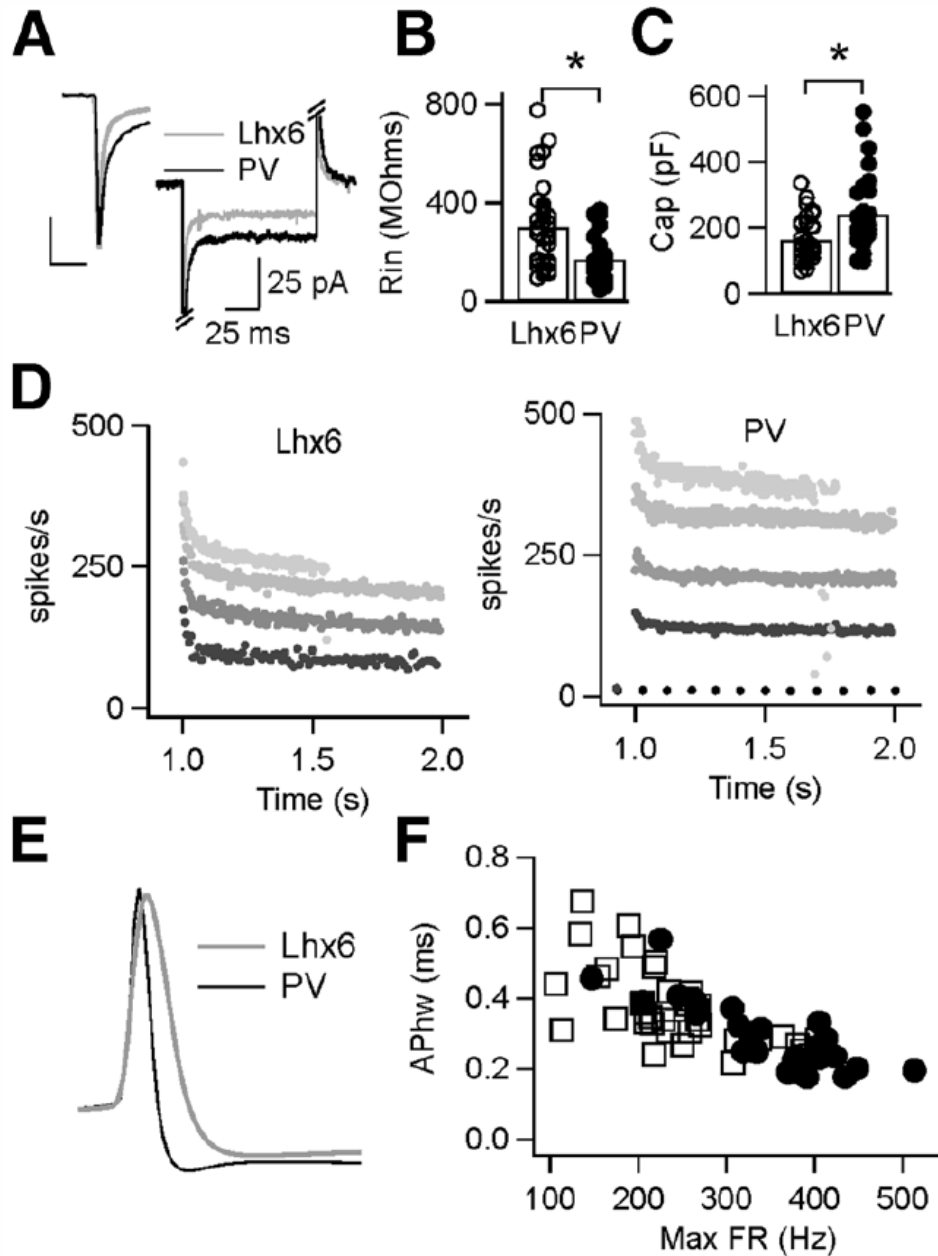


Figure 2-3 Differences in passive and active membrane properties of the Lhx6- and PV-GPe neurons in slice recordings.

A. Voltage clamp recordings ($V_{\text{hold}} = -80$ mV) showing the response of representative Lhx6- and PV-GPe neurons after a brief hyperpolarizing step (-5 mV, 100 ms). Inset shows the difference in membrane time constant (τ). Scale bar, 100 pA, 2 ms. B-C. Population data showing significant differences in input resistance (B) and whole cell capacitance (C) between Lhx6- and PV-GPe neurons. D. Instantaneous firing rates from representative Lhx6 (*left*) and PV (*right*) neurons in response to 1 s depolarizing current injections of increasing amplitude until neurons entered depolarization block. For Lhx6-GPe neuron, firing rates are shown in response to injections of 0 pA (no spikes), 200 pA, 400 pA, 800 pA, 1400 pA. For PV-GPe neuron, firing rates are shown in response to injections of 0 pA, 400 pA, 800 pA, 1200 pA, 2700 pA. E. Average spike waveforms of representative Lhx6- and PV-GPe neurons firing at 5-10 Hz. F. Scatter plot of action potential width vs. maximum firing rate for the population of Lhx6- and PV-GPe neurons. These parameters varied continuously across the population, but were significantly different between Lhx6- and PV-GPe neurons.

To compare active membrane properties of Lhx6- and PV-GPe neurons, the recording configuration was switched to current clamp and neurons were driven to fire with 1 s depolarizing current steps. The amplitude of injected current was increased incrementally until a neuron reached its maximum firing rate, defined as the average firing rate sustained over the 1 s step without entering depolarization block (Fig. 2-3D). The maximum firing rate of PV-GPe neurons was significantly greater than that of Lhx6-GPe neurons (347 ± 80 Hz, $n = 38$ vs. 248 ± 80 Hz, $n = 27$; $p < 0.0001$). Maximum firing rate was well correlated with action potential width (Fig. 2-3F), and PV-GPe neurons had narrower action potentials than Lhx6-GPe neurons (0.28 ± 0.09 ms, $n = 27$ vs. 0.37 ± 0.11 ms, $n = 38$; $p = 0.003$) (Fig. 2-3E). Although action potential widths and maximum firing rates varied continuously across the population of GPe neurons, Lhx6-GPe neurons clustered more at one end of the distribution while PV-GPe neurons clustered more at the other end of the distribution (Fig. 2-3F). Using maximum firing rate as the sole criteria enabled Lhx6- and PV-GPe neurons to be distinguished with ~75% accuracy (78% of PV-GPe neurons had maximum firing rates > 300 Hz and 72% of Lhx6-GPe neurons had maximum firing rates < 300 Hz). This degree of overlap emphasizes the importance of utilizing genetic markers to segregate cell-types in the GPe. A list of additional parameters quantifying the firing properties of Lhx6- and PV-GPe neurons is provided in Table 1.

Table 1. Intrinsic Properties of GPe Neurons

	Lhx6	PV
<i>n</i>	40	30
Input resistance (M Ω)	301 \pm 168	170 \pm 16**
Capacitance (pF)	164 \pm 65	241 \pm 113**
V_m rest (mV)	-71.7 \pm 7.2	-68.9 \pm 5.5
AP threshold (mV)	-55.4 \pm 14.1	-55.7 \pm 4.4
AP half-width (ms)	0.37 \pm 0.11	0.28 \pm 0.09**
Afterhyperpolarization (mV)	19.3 \pm 4.0	21.9 \pm 4.7*
Maximum firing rate (Hz)	249 \pm 80	347 \pm 80**
Adaptation ratio (Hz)	0.80 \pm 0.11	0.81 \pm 0.03
Linear slope (Hz/nA)	491 \pm 164	494 \pm 287
Cell-attached firing rate (Hz)	34 \pm 33	62 \pm 34**
Cell-attached CV	0.31 \pm 0.39	0.22 \pm 0.25
Whole-cell firing rate (Hz)	7.8 \pm 14.2	28 \pm 25**
Sag (mV)	16.1 \pm 7.0	13.8 \pm 5.5

Summary of intrinsic parameters recorded in Lhx6-GPe and PV-GPe neurons. ** $p < 0.01$; * $p < 0.05$. Values for AP threshold and V_m rest were corrected for liquid junction potential (12 mV). Values are mean \pm SD.

2.3.4 Projections of Lhx6- and PV-GPe Neurons to the STN

To study the axonal projection patterns of Lhx6- and PV-GPe neurons, we utilized a Cre-dependent adenoassociated virus (AAV2) to express EYFP selectively in one neuronal population or the other. Virus was stereotaxically injected into the GPe of PV-Cre and Lhx6-Cre transgenic mice and tissue was processed and analyzed two weeks later. To control for variations in viral expression or immunolabeling across mice, fluorescence intensities in target brain regions were normalized to fluorescence intensity in the GPe of the same animal (see methods). Fluorescence intensities measured in the GPe ranged from 146-249 a.u. but were not significantly different between Lhx6 and PV mice (Lhx6 = 216 \pm 27 a.u., $n = 4$ vs. PV = 202 \pm 51 a.u., $n = 4$; $p = 0.6$) (Fig. 2-4C). To confirm that fluorescence intensity varied similarly as a function of axonal density in both mouse lines, we measured the fluorescence intensity of a small region of tissue (143 μm^2) and manually counted the number of axonal varicosities present. In

both mouse lines, a linear relationship was observed between fluorescence intensity and number of boutons, quantified in brain areas receiving low (striatum), medium (SNr), and high (STN) amounts of axonal projections (Fig. 2-4D). Therefore, we were able to use the normalized fluorescence intensity to compare the density and pattern of axonal projections from Lhx6- and PV-GPe neurons to many different brain regions.

The first brain region investigated was the subthalamic nucleus (STN), the canonical target of the GPe (Fig. 2-4A). Both Lhx6 and PV-GPe neurons densely innervated the STN, but innervation from PV-GPe neurons was significantly greater than innervation from Lhx6-GPe neurons (Lhx6 = 59.9 ± 13.6 a.u., $n = 4$ vs. PV = 96.2 ± 11.3 a.u., $n = 4$; $p = 0.0063$) (Fig. 2-4B). This difference in innervation density was largely due to the unique patterning of Lhx6 projections to the STN. Unlike PV-GPe projections, which were evenly distributed throughout the extent of the nucleus, Lhx6-GPe projections were clustered around the periphery of the STN and did not target the central portion of the nucleus (Fig. 2-4E).

To examine the topographical organization of projections from the GPe to the STN, viral injections were targeted to rostral and caudal portions of the GPe (Fig. 2-4F). No differences in axonal projection patterns to the STN were observed in the Lhx6-Cre line from different regions of the GPe. In contrast, axonal projection patterns to the STN were topographically organized in the PV-Cre line. The rostral-ventral region projected to the central portion of the STN and rarely showed expression in the periphery (Fig 2-4G, left). In contrast, the caudal region of the GPe projected to the periphery of the STN, similar to what was observed in the Lhx6 population (Fig. 2-4G, right). These results suggest a topographic organization of PV projections to distinct zones within the STN.

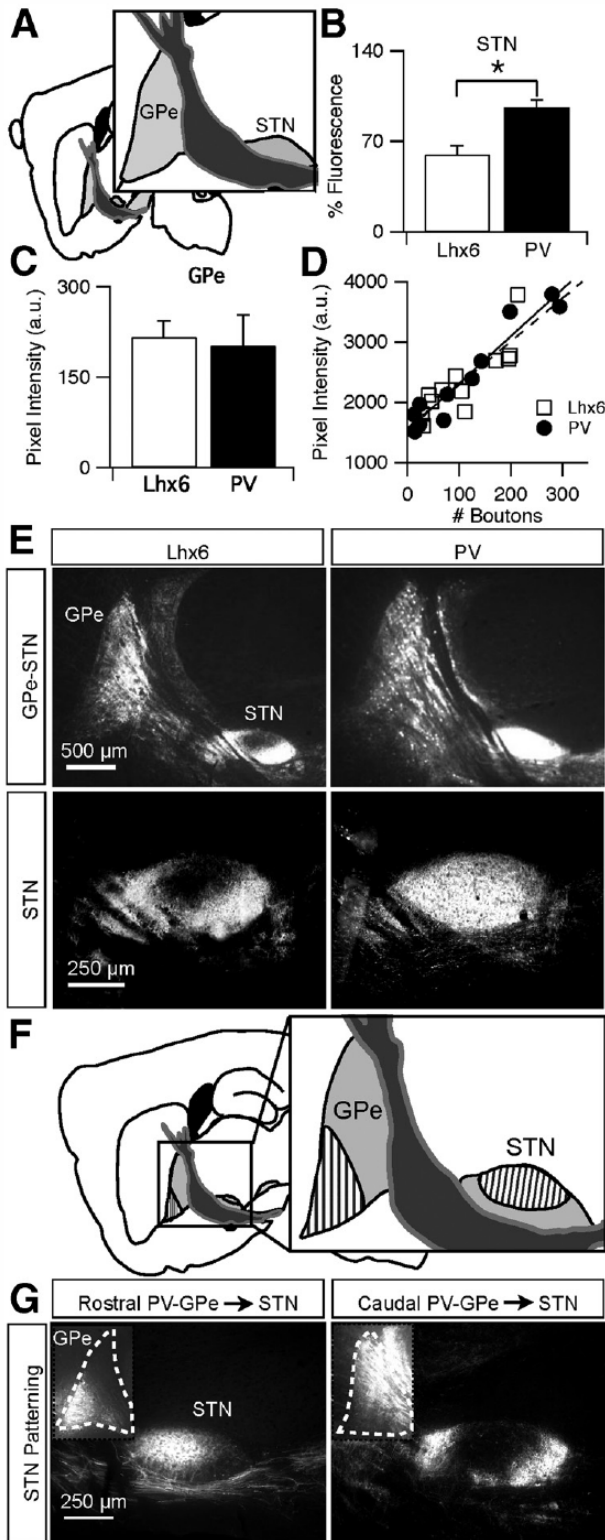


Figure 2-4 PV-GPe neurons project more strongly to the STN than Lhx6-GPe neurons.

A. Schematic of central sagittal plane used for analysis. B. Normalized fluorescence intensity of axons from Lhx6- and PV-GPe neurons in the STN. Error bars are SEM. C. Fluorescence intensities measured in the GPe of Lhx6 and PV-Cre mice 2 weeks after viral injections. Error bars are s.d. D. Scatter plot showing similar, linear relationship between pixel intensity and bouton number within a 143 μm^2 area of tissue, analyzed in brain areas receiving low, medium, and high densities of axonal innervation. E. EYFP fluorescence in Lhx6-Cre (left) and PV-Cre (right) mice, two weeks after viral injections. (top) 2.5x-epifluorescent images displaying typical expression in the GPe and STN. (bottom) 10x-epifluorescent images from the central plane of analysis displaying fluorescence in the STN. F. Schematic of topographic organization of PV-GPe projections from rostral (striped) and caudal (solid) GPe to the STN. G. Representative examples of viral injections in the rostral (left) or caudal (right) GPe and their resulting projections onto the STN.

2.3.5 Lhx6- and PV-GPe Neurons Differentially Innervate the Substantia Nigra Pars Compacta but Similarly Innervate GABAergic Output Nuclei of the Basal Ganglia

The substantia nigra is subdivided into two regions that subserve distinct purposes in basal ganglia function (Fig. 2-5A). The pars reticulata (SNr) is made up of GABAergic neurons that act as a major output of the basal ganglia. The pars compacta (SNc) is a region that lies dorsal to the SNr and contains a dense collection of dopaminergic neurons that innervate the striatum and many other structures (Bjorklund and Dunnett, 2007). GPe projections have been shown to innervate both the SNr and SNc in rats but these connections are still poorly understood (Paladini et al., 1999). In the SNr, there was no significant difference in density of axons arising from Lhx6- vs. PV-GPe neurons (Lhx6 = 15.3 ± 3.85 a.u., n = 4 vs. PV = 22.8 ± 14.7 a.u., n = 3; p = 0.3) (Fig. 2-5B). Both populations of neurons projected to the SNr diffusely with no clear topographical organization (Fig. 2-5C, top & middle).

A markedly different scenario was observed in the SNc. As seen in Figure 5C, the distinct clustering of axons was observed in the dorsal region of the substantia nigra. To resolve the borders of the SNc and SNr, tissue was stained with antibodies against tyrosine hydroxylase (TH) to label dopamine neurons. Axonal projections to the SNc were more concentrated than those to the SNr, and the majority of SNc projections arose from Lhx6-GPe neurons (Lhx6 = 41.0 ± 9.40 a.u., n = 4 vs. PV = 21.4 ± 6.05 a.u., n = 3; p = 0.03) (Fig. 2-5C).

The internal segment of the globus pallidus (GPi), one of the major output structures of the basal ganglia, is nested in the internal capsule fibers between the GPe and STN (Fig. 2-5D). Both Lhx6- and PV-GPe neurons projected to the GPi in equal amounts (Lhx6 = 37.5 ± 25.7 a.u.,

n = 4 vs. PV = 45.8 ± 11.1 a.u., n = 4; p = 0.57) (Fig 2-5E). As expected, axonal projections from the both populations of GPe neurons formed basket synapses onto the neurons of the GPi (Fig. 2-5F). Viral expression was not observed in GPi neurons.

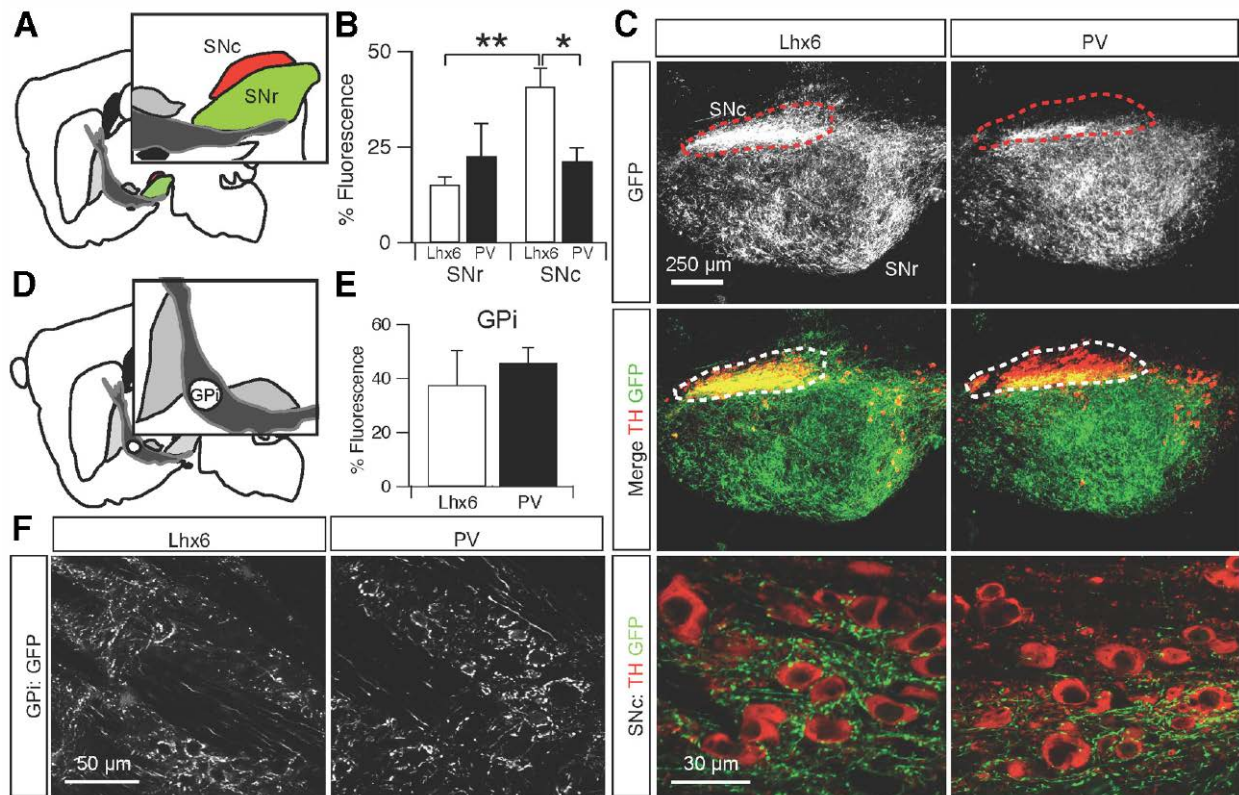


Figure 2-5 Lhx6- and PV-GPe projections to basal ganglia output nuclei.

A. Schematic of central sagittal plane used for analysis and reference to the distinct areas of the substantia nigra: pars compacta (SNc, red) and pars reticulata (SNr, green). B. Normalized fluorescence intensity of axons from Lhx6- and PV-GPe neurons in the SNr and SNc. Lhx6-GPe neurons projected more densely to the SNc than PV-GPe neurons and Lhx6 projections to the SNc were denser than those to the SNr. Error bars are SEM. C. (*top*) Epifluorescent images of axons from Lhx6- and PV-GPe neurons in the SNr and SNc (outlined with dotted line). (*middle*) Overlay of GPe axons (green) and TH immunofluorescence (red). (*bottom*) Confocal images of Lhx6- and PV-GPe axons (green) in the SNc; TH+ dopamine neurons are red. D. Schematic of GPi location within the internal capsule. E. Normalized fluorescence intensity of axons from Lhx6- and PV-GPe neurons in the GPi. Error bars are SEM. F. Confocal images of Lhx6- and PV-GPe axons in the GPi. Note the GPi neurons did not express EYFP.

2.3.6 Lhx6-GPe Neurons Project More Densely to the Dorsolateral Striatum than PV-GPe Neurons

The densities of axons from Lhx6- or PV-GPe neurons innervating the striatum were quantified within three functionally distinct striatal zones: dorsolateral, dorsomedial, and ventral. The dorsolateral region of the striatum is important for sensorimotor processing while ventral striatum deals with appetitive and rewarding aspects of behavior (Packard and Knowlton, 2002, Kelley, 2004, O'doherty et al., 2004). The dorsomedial region is important for instrumental conditioning and behavioral flexibility and is considered the associative territory of striatum (Ragozzino et al., 2002, Yin et al., 2005). GPe neurons sent sparse projections to striatum and formed a gradient of high to low density along the dorsal-ventral axis and the lateral-medial axis (Fig 2-6B-C).

In the dorsolateral region of the striatum, where GPe projections were most dense, axonal projections from Lhx6-GPe neurons were significantly more dense than axonal projections from PV-GPe neurons (DL StrLhx6 = 3.80 ± 1.38 a.u., n = 4 vs. DL StrPV = 1.14 ± 0.27 a.u., n = 4, p = 0.009) (Fig. 2-6B-C). In contrast, axonal projections to the medial striatum, an associative territory of the striatum, were less dense for both cell-types and the density did not differ significantly between Lhx6- and PV-GPe neurons (DM StrLhx6 = 0.79 ± 1.32 a.u., n = 4 vs. DM StrPV = 0.32 ± 0.29 a.u., n = 4, p = 0.5) (Fig. 2-6B). Similarly, the ventral striatum showed little to no axonal projections from both populations of neurons (V StrLhx6 = 0.34 ± 0.23 a.u., n = 4; V StrPV = 0.19 ± 0.31 a.u., n = 4, p = 0.48).

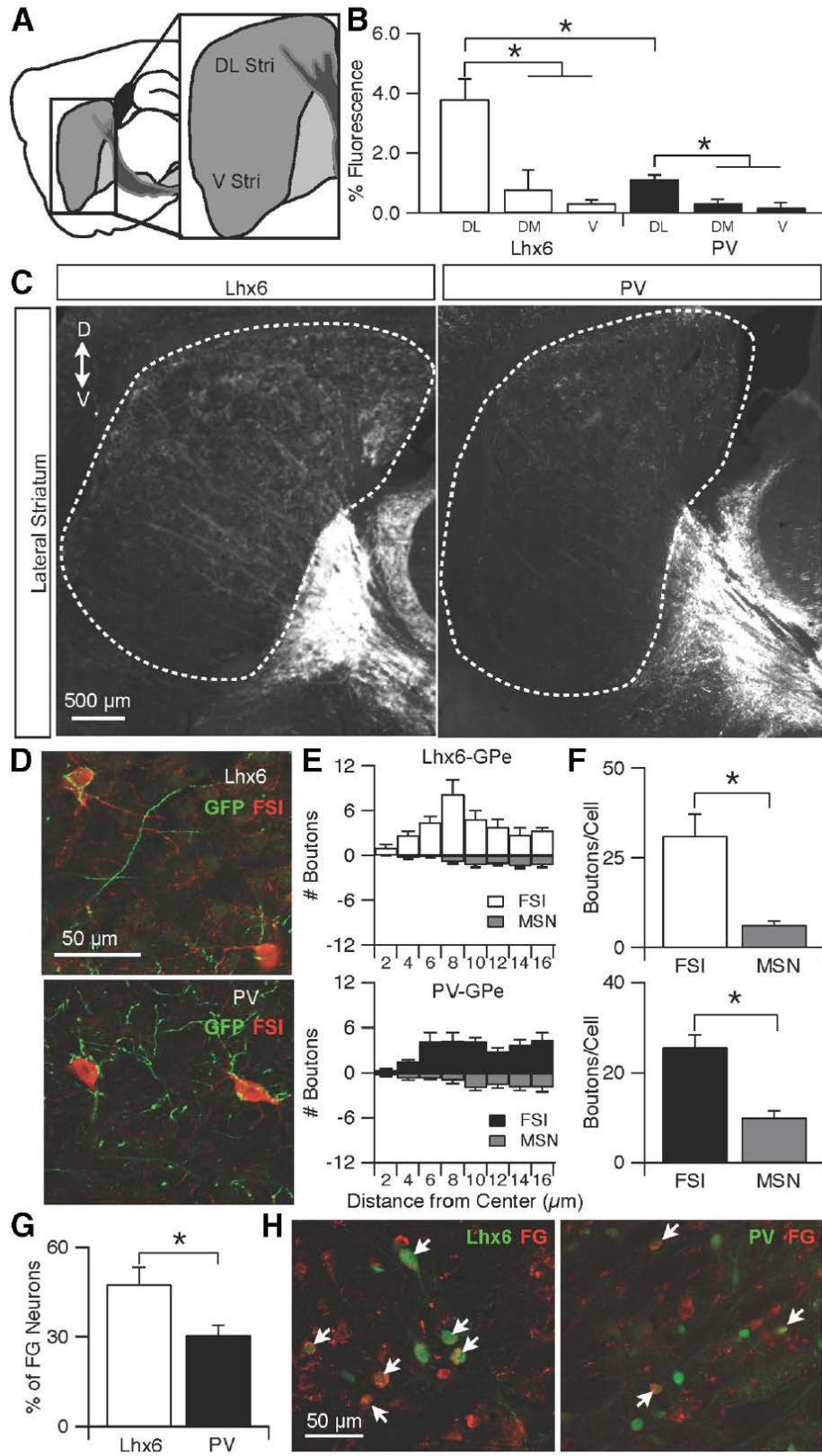


Figure 2-6 Lhx6-GPe neurons project more strongly to the dorsolateral striatum than PV-GPe neurons.

A. Schematic of sagittal plane used for analysis. DL = dorsolateral striatum; V = ventral striatum. B. Normalized fluorescence intensity of axons from Lhx6- and PV-GPe neurons to the dorsolateral striatum (DL), dorsomedial striatum (DM), and ventral striatum (V). Striatal projections from both cell-types were significantly denser to the dorsolateral region than to the dorsomedial or ventral regions (Lhx6: DL vs. DM, $p = 0.020$; DL vs. V, $p = 0.003$; PV: DL vs DM $p = 0.006$; DL vs V, $p = 0.004$); dorsolateral projections from Lhx6-GPe neurons were significantly denser than dorsolateral projections from PV-GPe neurons. Error bars are SEM. C. Epifluorescent images of axons from Lhx6- and PV-GPe neurons in the striatum. D. Confocal images showing the selective innervation of Lhx6-GPe axons (*top*, green) or PV-GPe axons (*bottom*, green) onto striatal FSIs (red). E. Results of Sholl analysis. Number of boutons from Lhx6-GPe (*top*) or PV-GPe (*bottom*) neurons were counted in concentric circles of increasing diameter (2 μm) around striatal FSIs or MSNs. F. Bar graphs comparing total number of boutons onto FSIs or MSNs from Lhx6-GPe (*top*) or PV-GPe (*bottom*) neurons. G. Bar graph showing the percentage of Fluoro-Gold-labeled neurons that were either Lhx6+ or PV+. Significantly more Fluoro-Gold neurons were Lhx6+ than were PV+. H. Confocal images of the GPe in tissue from an Lhx6-GFP mouse, stained for PV and antibodies against Fluoro-Gold. The Lhx6- (Left) and PV-GPe (Right) neurons (green) showed colocalization with the retrograde tracer, FG (red). Arrows indicate double labeled neurons.

Consistent with previous work, axonal projections from both Lhx6- and PV-GPe neurons appeared to target GABAergic interneurons in the striatum (Bevan et al., 1998), as indicated by axonal varicosities which were clustered around PV+ interneurons, corresponding to fast-spiking interneurons (FSIs) (Fig. 2-6D). To quantify the selectivity of GPe innervation for striatal FSIs compared to MSNs, we counted the number of boutons surrounding each cell-type using a Sholl analysis (Chattopadhyaya et al., 2004). Striatal FSIs received significantly more innervation from the GPe than MSNs (Fig. 2-6E-F).

Our quantification of axon densities suggest that Lhx6-GPe neurons give rise to a greater proportion of striatal projections than do PV-GPe neurons. To confirm this result, we injected the retrograde tracer, Fluoro-Gold, into the dorsolateral striatum of Lhx6-GFP or PV-Cre x Ai9 mice (Fig. 2-6G-H). After two weeks, tissue was processed and analyzed to determine what percentage of retrogradely-labeled neurons in the GPe were either Lhx6 or PV. As shown in Fig. 2-6G, Fluoro-Gold labeled significantly more Lhx6-GPe neurons than PV-GPe neurons (Lhx6 = $47.5 \pm 18.4\%$, $n = 84/177$ vs. PV = $30.5 \pm 11.0\%$, $n = 59/182$; $p = 0.003$, Fisher's Exact Test). Together, these data suggest that a greater proportion of GPe projections to the striatum arise

form Lhx6-GPe neurons and the focus of these projections is interneurons in the sensorimotor input region of the striatum.

2.3.7 Distinct Projections of PV-GPe Neurons to the Parafascicular Nucleus of the Thalamus

GPe projections to the thalamus have been previously described (Hazrati and Parent, 1991, Chattopadhyaya et al., 2004), but are typically restricted to reticular nucleus of the thalamus, which is located rostral to the GPe and extends further medially in the brain (Fig. 2-7A). The reticular nucleus is a specialized thalamic nucleus containing mostly GABAergic neurons that inhibit numerous thalamic nuclei and have no direct cortical projections (Houser et al., 1980, Ohara, 1988, Pinault and Deschenes, 1998). Consistent with previous studies, axonal projections from both populations of neurons were found in the reticular nucleus with no significant difference in density (Lhx6 = 28.0 ± 6.71 a.u., n = 4 vs. PV = 24.4 ± 14.0 a.u., n = 4; p = 0.6) (Fig. 2-7B-C).

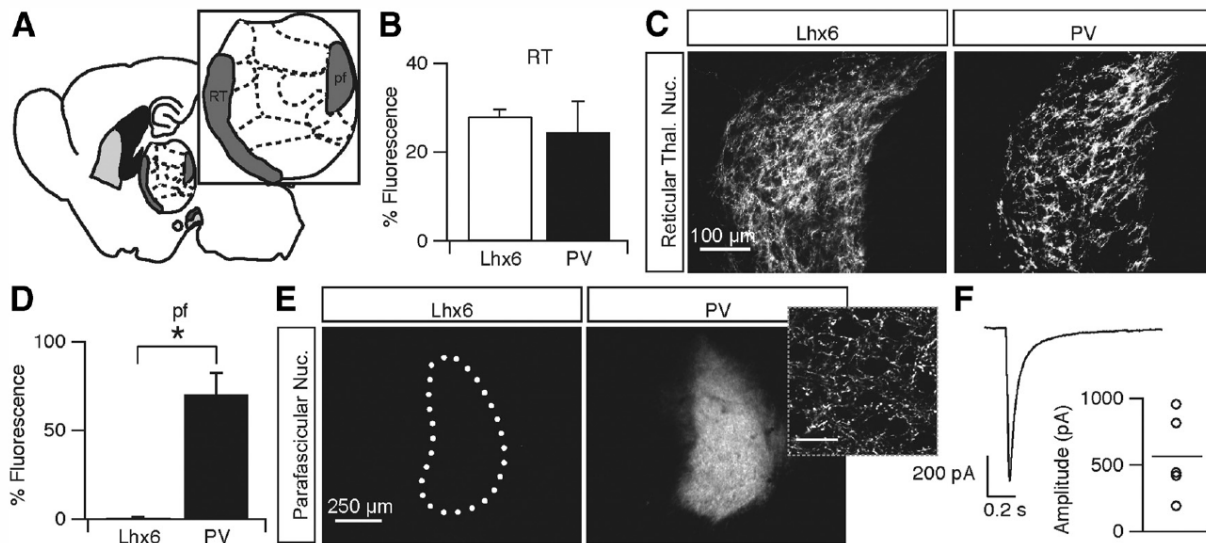


Figure 2-7 Lhx6- and PV-GPe projections to the thalamus.

A. Schematic of thalamic nuclei locations in a medial sagittal slice. RT = reticular nucleus; pf = parafascicular nucleus. B. Normalized fluorescence intensity of axons from Lhx6- and PV-GPe neurons to the RT. There was no significant difference between the two populations. Error bars are SEM. C. Epifluorescent images of axons from Lhx6- and PV-GPe neurons in the RT. D. Normalized fluorescence intensity of axons from Lhx6- and PV-GPe neurons in the pf. Axons from Lhx6-GPe neurons were not observed in the pf. Error bars are SEM. E. Epifluorescent images of axons from Lhx6- and PV-GPe neurons in the pf. (*inset*) Confocal image of dense axonal innervation in the pf from PV-GPe neurons. Scale bar, 25 μ m. F. IPSC recorded in a pf neuron in response to optical stimulation (1 ms) of ChR2-expressing PV-GPe axons. Graph shows IPSC amplitudes recorded from five pf neurons and the population average.

In contrast to projections to the reticular nucleus, Lhx6- and PV-GPe neurons differed substantially in their projections to the parafascicular nucleus. The Lhx6-GPe population exhibited virtually no axonal projections to the parafascicular nucleus while PV-GPe neurons projected densely, covering the full extent of nucleus (Lhx6 = 0.83 ± 1.3 a.u., $n = 4$ vs. PV = 69.0 ± 19.9 a.u., $n = 4$; $p = 0.0005$) (Fig 7D-E). As seen in Figure 7E, the nuclei surrounding the parafascicular nucleus showed no axonal projections, which would be expected if axons arose from spillover labeling of neurons in the reticular nucleus. Furthermore, there was a topographic organization of projections from the GPe to the parafascicular nucleus. Upon targeted injections of rostral and caudal portions of the GPe, we found that the parafascicular nucleus was only

targeted by caudal PV-GPe neurons but not by rostral PV-GPe neurons (data not shown). Injections in the rostral portion of the GPe show little to no expression within the parafascicular nucleus. To ensure that PV-GPe axonal projections to the parafascicular nucleus were functionally active and not just fibers of passage, a virus containing ChR2-EYFP was injected into the GPe of PV-Cre mice. Optically evoked inhibitory synaptic currents (IPSCs) from a holding potential of -70 mV were observed in 5/5 pf neurons (565.04 ± 312.3 pA, $n = 5$) (Fig. 2-7F), confirming that PV-GPe neurons form functional inhibitory synapses onto parafascicular nucleus neurons. These results suggest the presence of a previously undescribed output projection from the GPe to the parafascicular nucleus.

2.4 DISCUSSION

Here, we establish the use of Lhx6 and PV transgenic mouse lines to identify genetically distinct classes of GPe neurons that differ molecularly, anatomically, and electrophysiologically. Viral-mediated expression of EYFP revealed that both Lhx6- and PV-GPe neurons differed in their axonal innervation of a number of brain regions, including the striatum, SNc, STN, and the parafascicular nucleus. These results reveal cell-type specific segregation of GPe output and establish genetic tools for elucidating the role of distinct GPe output pathways in behavior and disease.

2.4.1 Lhx6 and PV Transgenic Mouse Lines Subdivide GPe Neurons Into Two Groups

Approximately two-thirds of GPe neurons were labeled in Lhx6 (1/3) or PV (1/3) transgenic mouse lines. The remaining 1/3 of GPe neurons could represent a third, as yet unidentified neuronal population in the GPe, or could represent incomplete labeling of Lhx6 and PV populations. Although the fraction of PV-GPe neurons in mice (1/3) was lower than that reported in rats (2/3) (Kita, 2007), we observed a similarly low number of PV neurons using both immunohistochemical and genetic techniques. These results suggest that the number of PV-GPe neurons is lower in mice than in other species such as rats and primates.

Lhx6 is a homeobox protein expressed in the medial ganglionic eminence (MGE) during development. The MGE is the origin of most forebrain GABAergic interneurons (Marin et al., 2000, Cobos et al., 2006) as well as GPe neurons (Flandin et al., 2010, Nobrega-Pereira et al., 2010). It remains unclear why only a subset of GPe neurons are labeled in Lhx6 transgenic mice, but one possibility is that Lhx6-GPe neurons correspond to a fraction of MGE neurons in which Nkx2.1 expression is downregulated during embryonic stages (Nobrega-Pereira et al., 2010). Whereas PV has been previously used to identify a subset of GPe neurons (Kita, 1994, Kita, 2007, Mallet et al., 2012), our results show for the first time that Lhx6 can be used to identify a second, non-overlapping subset of GPe neurons.

Lhx6- and PV-GPe neurons were differentially distributed along the lateral-medial axis of the GPe. PV-GPe neurons were more densely distributed in the lateral portion of the GPe, the sensorimotor territory of the nucleus (Alexander and Crutcher, 1990, Matsumura et al., 1995, Haber et al., 2000, Francois et al., 2004), where pharmacological activation produces dyskinetic movements in primates (Matsumura et al., 1995, Grabli et al., 2004). In contrast, Lhx6-GPe neurons, were more densely distributed in the medial portion of the GPe, the limbic and

associative territories of the nucleus (Alexander and Crutcher, 1990, Haber et al., 2000, Francois et al., 2004), where pharmacological activation produces stereotypies and hyperactivity (Grabli et al., 2004).

2.4.2 Lhx6 and PV Neurons Have Different Intrinsic Electrophysiological Properties

Differences in the electrophysiological properties of GPe neurons have been described both in vivo (Kelland et al., 1995, Mallet et al., 2008, Benhamou et al., 2012, Mallet et al., 2012) and in slice preparations (Nambu and Llinas, 1994, Cooper and Stanford, 2000, Kita, 2007, Deister et al., 2013), but a rigorous classification scheme has not been established. Furthermore, there is some controversy about whether or not intrinsic properties can even be used to define groups of GPe neurons because these properties vary continuously across the population and can change during the course of an experiment (Gunay et al., 2008, Deister et al., 2013).

Because Lhx6- and PV-GPe neurons are genetically defined, this establishes a rigorous classification scheme with which to determine how intrinsic firing properties vary across cell-types in the GPe. Intracellular recordings from Lhx6- and PV-GPe neurons revealed that intrinsic parameters varied continuously across the population, but a number of parameters differed significantly between these two cell-types. PV-GPe neurons had narrower action potentials and could sustain higher maximum firing rates than Lhx6-GPe neurons, suggesting PV-GPe neurons are better tuned to reliably respond to rapid, high frequency inputs than Lhx6-GPe neurons. In addition, PV-GPe neurons had lower input resistances and higher whole cell capacitances than Lhx6-GPe neurons, suggesting that PV-GPe neurons are larger.

Lhx6- and PV-GPe neurons also differed with respect to spontaneous firing rates, which were higher in PV-GPe neurons. Spontaneous firing in GPe neurons is mediated by a

combination of Ih and persistent Na⁺ currents (Chan et al., 2004, Mercer et al., 2007, Chan et al., 2011). Our results that sag currents were similar between Lhx6- and PV-GPe neurons suggests that additional currents besides Ih may contribute to the different firing rates between these two cell populations, including persistent Na⁺ currents, or Ca²⁺-sensitive K⁺ currents which have also been shown to regulate firing rates in GPe neurons (Deister et al., 2009, Schultheiss et al., 2010).

2.4.3 Implications of Genetically-Defined Output Pathways for Basal Ganglia Function

Historically, one of the most robust classification schemes for GPe neurons has been based on their axonal projection patterns (Bevan et al., 1998, Hoover and Marshall, 1999, Kita et al., 1999, Sato et al., 2000, Hoover and Marshall, 2002, Kita, 2007, Mallet et al., 2012). Although both Lhx6- and PV-GPe neurons projected to many of the same brain regions, the density of these projections differed significantly in a number of areas, including the striatum and SNc, which were more densely innervated by Lhx6-GPe neurons, and the STN and parafascicular nucleus, which were more densely innervated by PV-GPe neurons (Fig. 2-8). Both cell-types made similarly dense projections to a number of additional brain regions, both within and outside the basal ganglia, including the GPi, SNr, reticular nucleus of the thalamus, basolateral amygdala, and paraventricular nucleus (Fig. 2-8). We also observed that both cell-types made projections to the cortex, but the diffuse nature of these projections made quantification difficult.

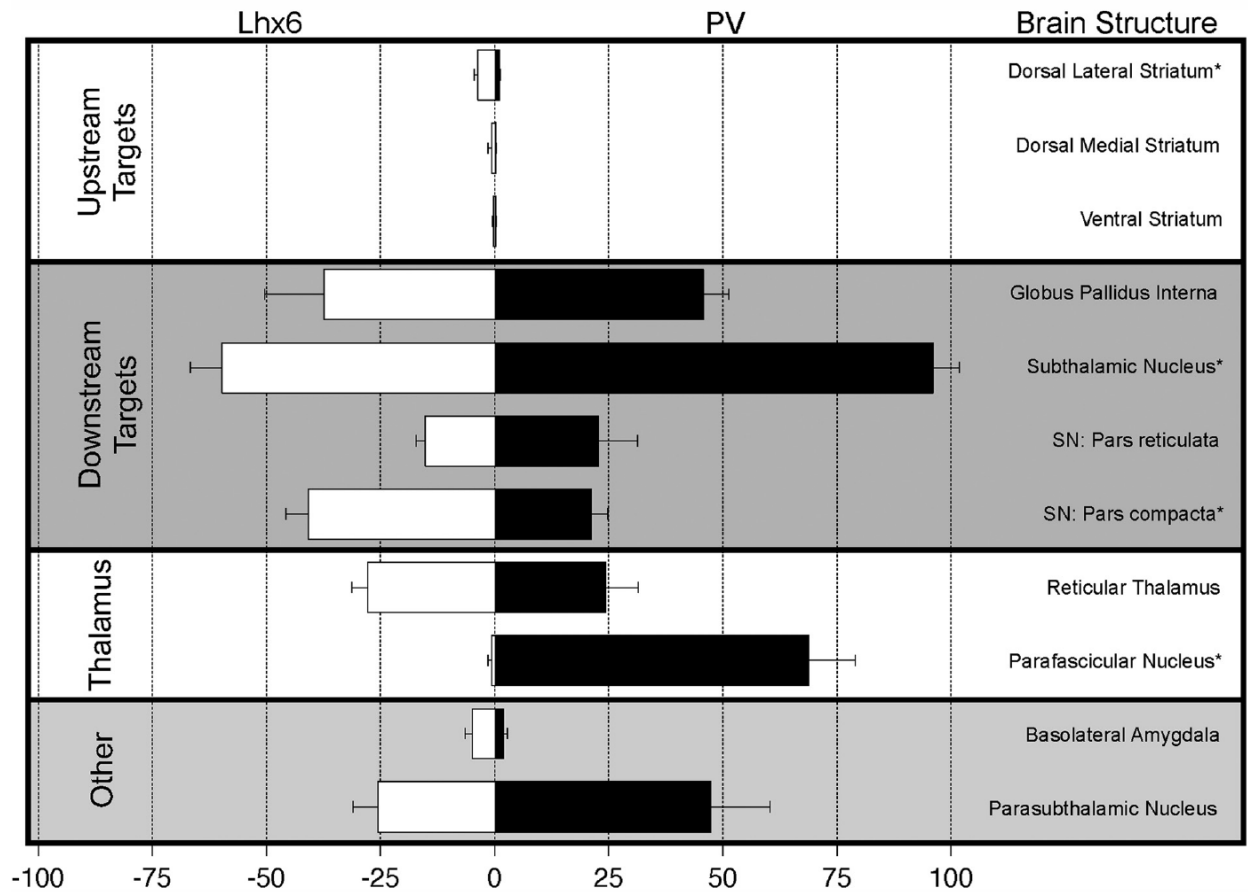


Figure 2-8 Summary of cell-type specific projection densities

Summary of normalized fluorescence intensity of axons from Lhx6- (white) and PV-GPe (black) neurons to identified brain structures. Error bars are SEM. Asterisks denote significance between cell-types.

Based on axonal density and retrograde labeling, we found that Lhx6-GPe neurons made up a greater portion of GPe projections to the striatum than PV-GPe neurons. This is consistent with previous studies in which most striatal-projecting neurons lack PV expression (Hoover and Marshall, 1999, Kita et al., 1999, Hoover and Marshall, 2002, Mallet et al., 2012). Our results suggests that Lhx6 labels a greater proportion of ‘pallidostratial neurons’ previously described in monkeys and rats (Bevan et al., 1998, Sato et al., 2000). Axons of pallidostratial neurons target GABAergic interneurons in the striatum (Bevan et al., 1998), and this projection may play an

important and underappreciated role in regulating striatal activity (Wilson, 2009, Gage et al., 2010).

Lhx6-GPe neurons also make stronger projections to the SNc than PV-GPe neurons. The SNc contains the majority of dopamine neurons that innervate the dorsal striatum as well as the GPe (Parent and Smith, 1987, Lavoie et al., 1989, Rommelfanger and Wichmann, 2010). Dopamine release from the SNc is critically involved in motor aspects of basal ganglia function (Gerfen et al., 1990, Bjorklund and Dunnett, 2007, Kreitzer and Malenka, 2008, Gerfen and Surmeier, 2011, Surmeier et al., 2011), therefore, projections from Lhx6-GPe neurons may play an underappreciated yet influential role in movement (Hausser and Yung, 1994, Paladini et al., 1999).

The axonal projections of PV-GPe neurons were significantly stronger to the STN than those of Lhx6-GPe neurons. The difference in STN innervation by PV- and Lhx6-GPe neurons was most apparent in an inner region of the nucleus, largely devoid of innervation from Lhx6-GPe neurons but strongly innervated by PV-GPe neurons located in the rostral portion of the nucleus. This result confirms the presence of a topographical projection from the GPe to the STN that has been observed in primates (Francois et al., 2004), but the functional role of the medial portions of the STN in rodents is not known. The GPe and STN form a reciprocally connected network that has received much attention for its role in pathological oscillations in Parkinson's disease (Bergman et al., 1994, Nini et al., 1995, Plenz and Kital, 1999, Magill et al., 2001, Bevan et al., 2002, Terman et al., 2002, Mallet et al., 2008, Holgado et al., 2010, Fan et al., 2012). Although both Lhx6- and PV-GPe neurons project strongly to the STN, changes in the denser PV-GPe projections may play a more prominent role in the development or maintenance of pathological oscillations in Parkinson's disease.

The most striking difference in the projection patterns of Lhx6- and PV-GPe neurons observed was in the parafascicular nucleus, which received dense innervation from PV-GPe neurons but not Lhx6-GPe neurons. The parafascicular nucleus plays a role in attention and behavioral flexibility and its projections to the striatum are particularly important for the control of cholinergic interneurons (Matsumoto et al., 2001, Minamimoto and Kimura, 2002, Smith et al., 2004, Smith et al., 2011). The dense projections of PV-GPe neurons to the parafascicular nucleus suggest that they are an important component of non-motor output pathways of the GPe. The parafascicular nucleus may play a role in motor control as well, based on results that deep brain stimulation in the parafascicular nucleus is particularly effective at alleviating tremors in patients with movement disorders (Krauss et al., 2002, Goff et al., 2009, Stefani et al., 2009).

In summary, we have shown that Lhx6 and PV transgenic mice can be used as tools to identify genetically-distinct circuits within the GPe with the potential to subserve different roles in basal ganglia function. By virtue of their projections to striatal interneurons and SNc dopamine neurons, Lhx6-GPe neurons are well positioned to regulate striatal output and influence the balance of direct and indirect pathway activity to determine overall levels of motor output. In contrast, PV-GPe neurons make stronger projections to the STN and parafascicular nucleus, brain areas with both motor and non-motor functions, and areas that have been implicated specifically in the generation of pathological oscillations and tremor in Parkinson's disease, suggesting a role of PV-GPe neurons in these aspects of disease pathophysiology.

2.5 ACKNOWLEDGEMENTS

The authors would like to thank Richard C. Gerkin for specialized IGOR analysis and acquisition routines. We thank Nicoletta Kessaris for providing Lhx6-Cre mice and Hongkui Zeng for providing PV-Cre mice. We thank Haibeng Teng of the Molecular Biosensor and Imaging Center for assistance with the confocal microscopy. This work was supported by NIH grant R00 NS076524.

3.0 CELL-TYPE SPECIFIC PALLIDAL INTERVENTION INDUCES LONG-LASTING MOTOR RECOVERY IN DOPAMINE-DEPLETED MICE

The identification of distinct cell-types within the basal ganglia has played a critical role in our understanding of basal ganglia function and the treatment of neurological disorders. The external globus pallidus (GPe) is a key contributor to motor suppressing pathways in the basal ganglia, yet its neuronal heterogeneity has remained an untapped resource for therapeutic interventions. Here, we demonstrate that optogenetic interventions that dissociate the activity of two neuronal populations in the GPe – elevating the activity of PV-GPe neurons over that of Lhx6-GPe neurons – restores movement in dopamine depleted mice and attenuates pathological activity of basal ganglia output neurons for hours beyond stimulation. These results establish the utility of cell-specific interventions in the GPe to target functionally distinct pathways, with the potential to induce long-lasting recovery of movement despite the continued absence of dopamine.

3.1 INTRODUCTION

Cell-types in neural circuits provide a functional diversity that can be harnessed to treat neurological disorders. The identification of distinct cell-types within the basal ganglia has played a critical role in our understanding of basal ganglia function and the treatment of neurological disorders, particularly Parkinson's disease (PD). However, a major limitation of PD

treatments is that they provide only transient relief of symptoms, which rapidly return if a drug dose is missed or deep brain stimulation (DBS) is discontinued.

The external globus pallidus (GPe) is a key contributor to motor suppressing pathways in the basal ganglia, yet its neuronal heterogeneity has remained an untapped resource for therapeutic interventions. It extends projections to all nuclei within the basal ganglia as well as the thalamus, amygdala, brainstem, and cortex(Kita, 2007, Mastro et al., 2014, Saunders et al., 2015), and has been implicated as a critical node in the generation and amplification of pathological activity in the dopamine depleted (DD) state(Bergman et al., 1998, Bevan et al., 2002, Mallet et al., 2008). Recently, molecular and genetic strategies have been developed to subdivide GPe neurons into different subpopulations that vary in physiological and anatomical projections(Mallet et al., 2012, Mastro et al., 2014, Abdi et al., 2015, Dodson et al., 2015, Hernandez et al., 2015, Saunders et al., 2015). Two major subdivisions are ‘prototypical’ and ‘arkypallidal’ neurons(Mallet et al., 2012, Dodson et al., 2015, Hegeman et al., 2016). Approximately 75-80% of GPe neurons are prototypical, meaning they have high, regular firing rates in vivo and project strongly to downstream basal ganglia nuclei(Dodson et al., 2015, Hernandez et al., 2015). Within the prototypical population, neurons can be further subdivided based on expression of parvalbumin (PV-GPe) and lim homeobox 6 (Lhx6-GPe)(Mastro et al., 2014, Oh et al., 2016b). Although expression of these markers is partially overlapping(Abdi et al., 2015, Dodson et al., 2015, Hernandez et al., 2015, Oh et al., 2016b), as a whole, PV and Lhx6 populations differ in their intrinsic physiology and projection densities to downstream nuclei(Mastro et al., 2014). To date, however, the behavioral significance of these neuronal subdivisions has not been directly demonstrated.

Here, we demonstrate that in DD mice, transiently dissociating the activity of PV-GPe and Lhx6-GPe subpopulations induces long-lasting recovery of movement and reversal of pathological activity in the basal ganglia circuit that persists for hours beyond stimulation. These prokinetic effects are only engaged by restricting manipulations to particular neuronal subsets, and not by manipulations that modulate all GPe neurons simultaneously. These results establish the behavioral relevance of functionally distinct neuronal subpopulations in the GPe and suggests their potential as therapeutic nodes for the long-term restoration of movement in PD.

3.2 MATERIALS AND METHODS

3.2.1 Animals

Experimental procedures were approved by the Carnegie Mellon University Committee for the Use and Care of Animals and in accordance to the guidelines set forth by the National Institute of Health and Society for Neuroscience Use of Animals in Neuroscience Research. Male and female heterozygous 8-15 week-old mice on a C57BL/6J background were used for all experiments. D1-SPNs were targeted using the D1-cre mouse line(Gong et al., 2007). PV-GPe neurons were targeted using a Pvalb-2A-Cre mouse line(Madisen et al., 2010). Lhx6-GPe neurons were targeted using Lhx6-iCre mouse line(Fogarty et al., 2007). To ensure health of the animals undergoing the dopamine depletion, weights were closely monitored and every animal weighed greater than 20 g prior to initial surgery. Animals were group housed (2-8 per group) in a 12hr-12hr light dark cycle until the time of second surgery (as noted below) and all experiments were completed during the light cycle.

3.2.2 Viral Transfection

Injections of purified double-floxed AAV2-DIO-EYFP (controls), AAV2-DIO-ChR2-EYFP (cell-specific activation), AAV2-DIO-ArchT-tdTomato (cell-specific inhibition), AAV2-hsyn-hChR2(H132R)-tdTomato (non-specific activation) or AAV2-CAG-ArchT-tdTomato (non-specific inhibition) produced at the University of North Carolina (Vector Core Facility) were made in 8-12 week-old D1-cre, PV-Cre or Lhx6-iCre transgenic mice. Littermates were randomly assigned to either the rhodopsin-positive or control groups. Injections into the dorsomedial striatum(Kravitz et al., 2010) or GPe(Mastro et al., 2014) were completed in accordance to methods previously described. Briefly, anesthesia was induced using 0.2 μ L ketamine/xylazine (0.2cc/ 5 mg/ml) and maintained throughout surgery using 1.5% isoflurane. Mice were placed in a stereotaxic frame (Kopf Instruments) where the scalp was opened and bilateral holes were drilled in the skull (Striatum: 0.5mm anterior, 1.5mm lateral, GPe: 0.27-0.30 mm anterior, 2.1-2.2 mm lateral from bregma). 200–250 nL of virus was injected with a Nanoject (Drummond Scientific) through a pulled glass pipet (tip diameter \sim 30 μ m) whose tip was positioned below the top of the skull (Striatum: 2.80 mm, GPe: 3.65 mm). To prevent backflow of virus, the pipet was left in the brain for 5 min after completion of the injection. All experiments were performed at least 2 weeks following injection to allow time for full viral expression. At which point, mice underwent a second surgery for either behavioral optogenetics or physiology, where experimenters were blind to the experimental condition. Sample sizes for each experiment are in line with previous published studies(Gradinaru et al., 2009, Kravitz et al., 2010).

3.2.3 Optogenetic Behavioral Implantation and Dopamine Depletion

For behavioral optogenetic experiments in freely moving mice, a second surgery was performed at least 10 days after viral injections to deplete dopamine and insert optical fibers. For the second surgery, mice were anesthetized, placed on the stereotaxic frame and holes were re-drilled from the previous viral injection. In addition, bilateral holes were drilled over the medial forebrain bundle (-0.45 mm posterior, +/-1.15 mm lateral from bregma) for 6-OHDA injections. A 33-gauge cannula (Plastics One, Roanoke, VA, USA) attached to a syringe pump, was slowly lowered down into place (MFB: 4.95mm from top of the skull) and allowed to settle for five minutes. At this point, 1 μ L of 6-OHDA (5 μ g/ μ L in 0.9% NaCl), saline (0.9% NaCl) for unilateral depletions or lipopolysachairide (LPS, Sigma-Aldrich) for inflammatory induction was slowly injected into the MFB at a rate of 0.1 μ L/min. The injection cannula was left in place for five additional minutes.

After the bilateral injections, a custom-made plastic button containing 2 polished ferrules was placed over the holes previously used for viral injections. The fibers were slowly advanced to the top of the viral expression (Striatum: 2.60 mm, GPe: 3.45 mm). Dental cement was used to secure the button to the top of the skull. After all dopamine depletions, mice were individually housed and placed into a recovery station. The station consisted of a new cage, soft food, trail mix, shallow water dish and half of the cage was placed on a heating pad. In addition, a daily injection of saline (0.9% NaCl; intraperitoneally) was used to curb dehydration, and weight was closely monitored to ensure the greatest level of health for each animal.

3.2.4 Behavioral Paradigm

Three to five days following fiber implantation, mice were connected to bilateral fibers and subsequently placed in the center of a 1600 cm² square open field. Fibers were adjusted to ensure 1 mW of power at the tip of the previously implanted ferrule. Activity was monitored from overhead and the side of the arena and the center-point was tracked utilizing Noldus Ethovision software. After collecting 10 minutes of ‘baseline’ activity, the LED delivered a 30 second pulse of light that was repeated 10 times and separated by 3 minute intervals. Following the final stimulation bout, 10 minutes of ‘post-stim’ activity was collecting. In a subset of conditions, mice were observed for an additional three hours to capture the persistence of behavioral intervention.

For the food-retrieval task, mice were placed in a new cage (30 x 20 cm) following the completion of the behavioral paradigm. Mice were placed in the opposing corner of the cage from two small dishes of food and water. Mice were tracked overhead using Noldus Ethovision. Successful trials were when mice reached the food or water dishes within 5 min.

3.2.5 Implantation of Head-Fixation System

A subset of virally injected mice were utilized for head-fixed *in vivo* physiology. Two weeks following viral expression, mice followed the same dopamine depletion protocol described above. After the bilateral injection of 6-OHDA, bilateral craniotomies were created over the GPe (-0.45-0.45 mm anterior, 1.75-2.35 mm lateral to bregma) or SNr (-2.75-3.25 mm anterior, 1.15-2.00 mm lateral to bregma). For SNr recordings, holes were drilled over the site of viral injections into the GPe and fibers (transmittanceoutput = 1 mW measured at the end of the fiber)

were implanted for direct optical stimulation during recordings. After which, all animals were implanted with a copper headpost fixed to the posterior portion of the skull (approximately -3.5 mm posterior to bregma) utilizing a combination of glue and dental cement. The dental cement fixation was extended to surround the entirety of both craniotomies. The subsequent well that was formed was filled with a silicon elastomer (Kwik-sil, WPI) that prevented infection and damage to the brain tissue. During recording, this well was filled with saline and used as a ground reference.

3.2.6 Head-Fixation Training and Recording

Mice were placed atop a running wheel and allowed to run freely for 60 minutes the day before recording. Movement was tracked for the full period of recordings using an inverted optical mouse and custom MATLAB script. Craniotomies were cleaned, prepared for recordings the following day and silicone elastomer was replaced.

GPe Recordings: On the day of recording, mice were fixed to the top of the wheel and allowed 15 minutes to acclimate to the head fixed position. After removal of the silicon elastomer and clearing of the craniotomy, a linear 16-channel silicone optrode with sites spaced 50 μm apart (Neuronexus) and a 100 μm fiber terminating 50 μm above the uppermost site was attached to the micromanipulator and centered on bregma. Transmittance through the optical fiber was measured prior to recording to ensure ~ 0.5 mW in both the blue and green light conditions. The probe was slowly advanced (5-7 $\mu\text{m}/\text{sec}$) until the top of the GPe (~ 3.20 mm from top of the skull) was found. GPe activity was distinguished based on a combination of physiological features: presence of high-firing neurons, presence of low firing, irregular neurons, lack of spindle-like activity (thalamic) and responsiveness to light activation or inhibition. Post-mortem

tissue analysis for viral hit and craniotomy placements were further evidence for proper targeting.

The probe was left in place for approximately 15 min before neuronal activity was measured. During this time, a drop of saline was placed in the well that surrounds the craniotomy and a reference ground electrode was placed in contact with the saline. Extracellular recordings and local field potentials were acquired using the omniplex system (Plexon Inc) and stored for offline analysis.

3.2.7 Optical Tagging Method

In the cell-type manipulations, single units could be isolated and an optical tagging strategy was employed to distinguish a neuron's activity as positive or negative for rhodopsin expression. For ChR2 conditions, brief pulses (pulse width = 5 ms, 10 Hz, 120 pulses) were administered at the start and end of each recording session before advancing the probe to the next location. For Arch conditions, a set of longer pulses (pulse width = 1 sec, 0.5 Hz, 10-20 pulses) was administered to clearly denote neurons that were directly inhibited by the light. After the optical tag, activity of the neurons was measured in response to a thirty second period of light. In a subset of neurons, stability of recording was great enough to allow for the application of the full optogenetic paradigm (pulse width = 30 sec, interpulse interval = 3 min, 10 pulses). After the recording period, mice were sacrificed and tissue was utilized to verify placement of the craniotomy and documentation of probe entrance and placement.

For analysis, we utilized the previously published identification tool to classify neurons based on responsiveness to brief pulses (5 ms)(Kravitz et al., 2013). Briefly, baseline activity (-110 to -10 ms) for each pulse was compared to the number of significant bins within 0-10 ms of

light onset. As seen in Fig. A5a, the first significant bin (yellow) denotes the latency to spike due to direct ChR2-activation. For the Arch tagging, peri-event histograms (bin size = 10 - 50 ms) were produced centered on the start of each of the 10-20 pulses and a student's t test ($p < 0.005$) was performed to compare the baseline firing rate (-510 ms to -10 ms from light onset) to the firing rate during light onset (0 ms to 200 ms). 30 sec Pulse Analysis: Neurons were binned based on the average firing rate changes during stimulation compared to 20 seconds prior to stimulation.

3.2.8 SNr Recordings

Following the acclimation protocol described earlier, mice were fixed atop the wheel and the appropriate light source was attached to the optical fibers (transmittance = 1 mW, tested prior to implantation). After removal of the silicon elastomer and clearing of the craniotomy, a linear 16-channel silicone probe with sites spaced 50 μm apart (Neuronexus) was centered on lambda. The probe was slowly advanced (5-7 $\mu\text{m}/\text{sec}$) until the top of the SNr (~4.75 mm from top of the skull) was found. SNr activity was distinguished based on a combination of physiological features: presence of putative dopamine neurons, presence of putative GABAergic neurons, lack of spindle-like activity (thalamic) and responsiveness to light activation or inhibition. Post-mortem tissue analysis for viral hit and craniotomy placements were further evidence for proper targeting.

During the pre- and post-stimulation period, the probe was advanced to record a new set of neurons every 30-40 mins. Due to the scale of our craniotomy, when the probe was advanced to the bottom of the SNr (~5.00 mm), the probe was taken out of the brain and reinserted. This allowed for sampling across the SNr. During the full optical stimulation, the probe was left at the

same recording site for the full duration, including an additional 10 minutes before and after stimulation. In a subset of the recordings, the signal to noise ratio and the subsequent population clusters were sufficiently isolated to track a set of neurons throughout the recording.

3.2.9 Tissue Processing

Shortly after the behavioral or electrophysiology experiments, mice were sacrificed and perfused transcardially with phosphate buffered saline (PBS), followed by 4% paraformaldehyde (PFA) in PBS. Brains were retrieved, fixed in 4% PFA for 24 hr before being placed in a 30% sucrose solution. Brains were sliced at 30 μ m thickness and prepared for the appropriate incubations, as described previously⁵⁰. Primary antibody included rabbit anti-GFP (1:1000, Millipore 06-896), Mouse anti-HuC/D (1:200, Molecular Probes A21271), mouse anti-NeuN (1:100, Millipore MAB377), rabbit anti-TH (1:1000, Pel-Freez P40101-0), at room temperature for 24 hours or at 4°C for 48 h when using rabbit anti-PV (1:1000, Swant PV 27). Secondary antibodies included Alexa Fluor 488-conjugated goat anti-chicken (1:500, Life Technologies), Alexa Fluor 488-conjugated goat anti-rabbit (1:500, Life Technologies), Alexa Fluor 568-conjugated donkey anti-rabbit (1:500, Life Technologies), Alexa Fluor 568-conjugated donkey anti-mouse (1:500, Life Technologies), Alexa Fluor 647-conjugated donkey anti-rabbit (1:500, Life Technologies), or Alexa Fluor 647-conjugated donkey anti-mouse (1:500, Life Technologies).

3.2.10 TH Quantification

Quantification of tyrosine hydroxylase staining was used as a measure of dopamine lesion on both hemispheres. As described previously⁵⁰, slices containing the dorsal striatum were imaged

using an epifluorescent scope at 10x magnification. To analyze the fluorescent intensity, the pixel intensity-measuring tool in ImageJ was used. A 100 x 100 μm square from each hemisphere was measured and normalized to the pixel intensities of a healthy control tissue that was processed and imaged in parallel. Unless noted, all mice had <20% TH remaining on both sides for all behavioral and physiology experiments to limit behavioral variability.

3.2.11 Behavioral Analysis

Videos collected during the behavioral paradigm were analyzed using the Noldus Ethovision. Immobility was quantified as the period of time where there was less than 1.2% change in pixels corresponding to the body segment. Center point detection was utilized to calculate movement velocities during movement bouts (velocity > 1 cm/s for at least 1 sec). For quantification of behavioral patterns, the behavior of a subset of randomly selected animals in the dopamine intact control, PV-ChR2, and Lhx6-Arch conditions was manually scored using Observer software to denote start and stop times that mice engaged in walking, rearing, grooming, and fine movements (scratching, sniffing, looking around). Periods of time not engaged in any of these movements were classified as ‘immobile’ in behavioral pattern analyses.

3.2.12 Electrophysiology Analysis

Data was filtered at 150-8000 Hz for spiking activity and 0.7-300 Hz for local field potentials. Spike detection was completed using the Plexon offline sorter where principal component analysis was used to delineate single and multi-units. To be classified as a single unit, the following criteria was utilized: (a) PCA clusters were significantly different ($p < 0.001$); (b) J3-

statistic was greater than 1; (c) percent of ISI violations ($< 2\text{ms}$) was less than 0.15%; (d) Davies-Bouldin test statistic was less than 0.5; (e) manual verification that optical stimulation did not occlude the ability to delineate single units from noise.

Following spike sorting, data was processed in Neuroexplorer and with custom scripts in MATLAB. Rest Period Analysis: Periods of rest were analyzed to identify the firing rates (FR) and coefficient of variation of the interspike intervals (CVISI) in the naive vs dopamine depleted state (Fig. A1c-e). Burst Analysis: Utilizing the surprise algorithm (surprise = 2), bursts were identified in the single unit SNr activity (FR > 5 Hz) and calculated across a two minute period, referred to as number of bursts (Fig. 3-6). For Fig. 3-6k-l, the number of bursts were calculated for thirty second time bins. Each unit was then normalized to baseline (Pre) and then averaged across all stably recorded units. Fractional Analysis: The fraction of highly ‘bursty’ neurons were identified by calculating the number of units that exceeded 1 MAD of the median in the distribution across all conditions, prior to optogenetic manipulation (Bursty threshold: 70).

3.2.13 Statistics

Statistical analysis were completed using SPSS software or GraphPad Prism 7 (GraphPad Software). All data was tested for normality and equal variance. Behavioral data were analyzed using two-sided, paired or unpaired Student’s t-tests for normally distributed data. In all other cases, a Mann Whitney U or a Chi-squared test was applied. For the analysis of behavioral persistence, behavioral conditions were tested using two-way repeated measures (RM) ANOVA and reported in the appropriate figure legend. As noted in the main text, comparisons made within or across conditions utilized Tukey’s or Sidak post hoc test, respectively. Results are reported as mean \pm S.D.

Physiology data was first tested for normality and equal variance. Then, the appropriate parametric (two sided, paired or unpaired Student's t-test) or non-parametric (Mann Whitney U or Kruskal-Wallis H test) tests were applied. Cumulative distributions were compared using the Kolmogorov-Smirnov two sample test (K-S two sample test). Fractional burst analysis applied a chi-squared statistic to measure if there was a change in the population burst firing before and after optogenetic intervention. Physiology results were reported as mean \pm SEM. The data that support the findings of this study are available from the corresponding author upon reasonable request.

3.3 RESULTS

3.3.1 Global GPe Stimulation Does Not Restore Movement in DD Mice

A prediction of the classic model of basal ganglia function under dopamine depleted (DD) conditions is that increasing firing rates of GPe neurons should improve movement (Albin et al., 1989, DeLong, 1990). To test this hypothesis, we expressed channelrhodopsin (ChR2) in all GPe neurons under control of the hSyn promoter (hSyn-ChR2) (Fig. 3-1a) and measured the efficacy of global GPe stimulation to rescue immobility and bradykinesia in bilaterally DD mice (see methods, Fig. A1a-b, and A2a-c).

Even though GPe neurons exhibited the expected decrease in firing rate (Naive: 44.3 ± 2.6 Hz, $n = 73$ neurons across 4 animals vs. bilateral DD: 24.6 ± 1.6 Hz, $n = 62$ neurons across 3 animals, $p < 0.0001$, Kruskal-Wallis H test) and increase in irregularity after dopamine depletion (CVNaive: 0.63 ± 0.03 vs CVDD: 0.80 ± 0.03 ; $p < 0.0001$, Kruskal-Wallis H test) (Fig. A1c-e),

hSyn-ChR2 did not rescue movement (Fig. 3-1b-c), nor did it reduce bradykinesia (normalized to dopamine intact control: Pre: 0.27 ± 0.23 vs. Post10min: 0.29 ± 0.25 , $n = 4$, $p = 0.683$, paired t -test) (Fig. 3-1d).

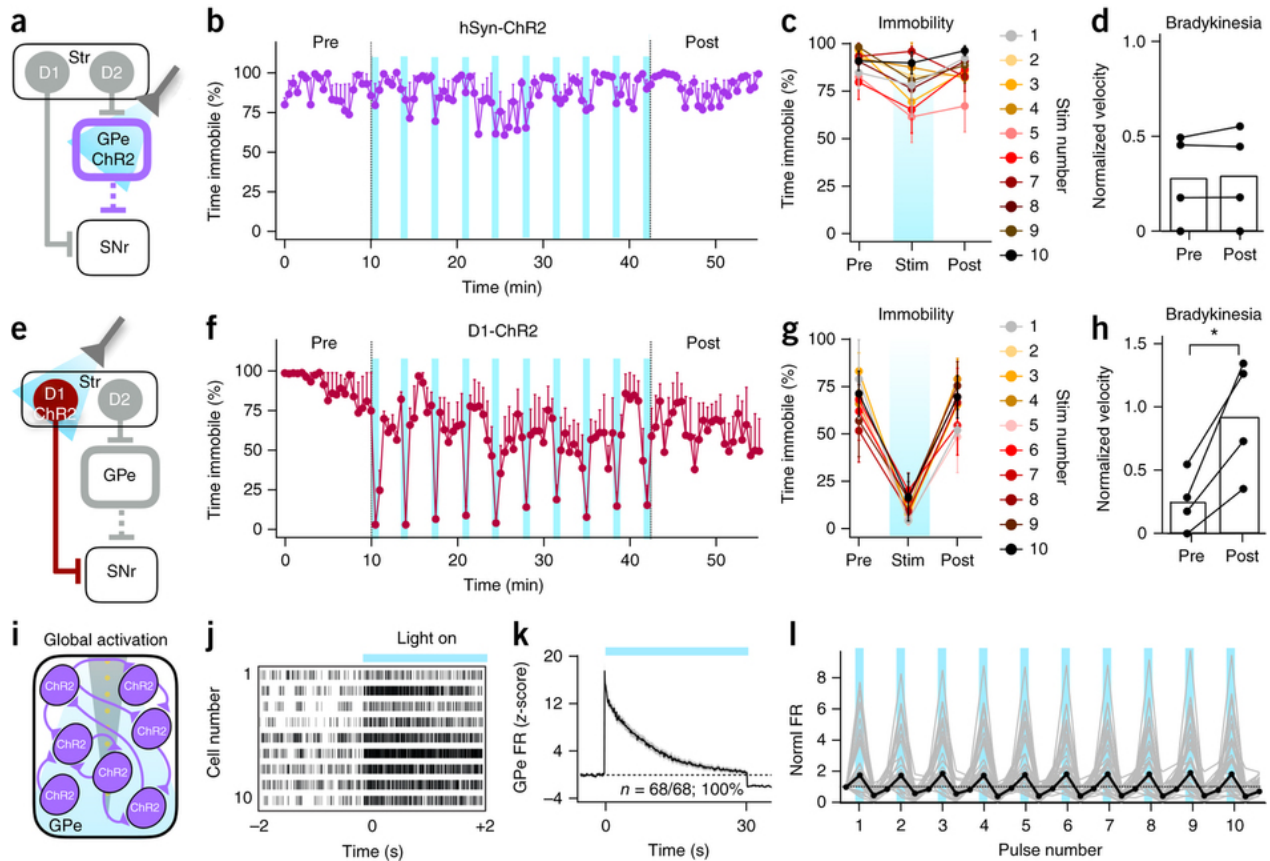


Figure 3-1 Global GPe stimulation does not rescue movement in DD mice.

(a) Schematic of global optogenetic stimulation in the GPe. GPe projections to the SNr are represented as a dashed line to indicate omission of the subthalamic nucleus. Str, striatum; D1 and D2, populations expressing D1 and D2 dopamine receptors. (b) Percentage of time spent in the immobile state before (Pre), during and after (Post) stimulation ($n = 4$). Stimulation epochs are indicated with vertical blue lines. (c) Overlay of immobility immediately before, during (Stim) and after each light pulse. (d) Movement velocities, normalized to those in dopamine-intact controls, before and after stimulation in b ($t(3) = -0.450$, $P = 0.683$, paired t -test). Bars denote population averages; connected circles show data for individual mice. (e) Schematic of direct-pathway stimulation with D1-ChR2. (f) Percentage of time spent in the immobile state before, during and after stimulation ($n = 4$). (g) Overlay of immobility immediately before, during and after each light pulse. (h) Movement velocities, normalized to dopamine-intact controls, before and after stimulation in f ($t(3) = 4.441$, $P = 0.02$, paired t -test). (i) Schematic of GPe network recording during global stimulation. (j) Light-evoked responses of ten example GPe multiunits. (k) Average multiunit responses ($n = 68$ across 3 animals) over the course of a 30-s optical stimulus, displayed as z-score ($t(67) = 1.6679$, $P = 0.0495$, one-tailed t test). Shaded area, s.e.m. FR, firing rate. (l) Average firing rates (normalized to baseline) of units ($n = 34$ across 3 animals) held across all ten stimulations. Each bin denotes firing in 30-s bins immediately before and after each stimulation (blue). Error bars, s.e.m.

This inability to rescue movement with global GPe stimulation could challenge predictions of the classic basal ganglia model (Albin et al., 1989, DeLong, 1990), but at least two other interpretations are possible. The first is that bilaterally DD mice are so impaired that they are no longer capable of robust movement. To address this possibility, we increased direct pathway activity by driving ChR2 expression in D1-spiny projection neurons (D1-ChR2) (Fig. 3-1e, A2d-e). Consistent with previous results (Kravitz et al., 2010), D1-ChR2 relieved immobility in a predominantly light-locked manner (Fig. 3-1f-g). Some movement persisted after the 10th light pulse, but this effect was not significant (Pre: $82 \pm 24\%$ vs. Post10min: $63 \pm 21\%$, $n = 4$, $p = 0.15$, paired t-test). When movement bouts did occur, velocities were significantly greater than before stimulation (normalized to dopamine intact controls: Pre: 0.25 ± 0.22 vs. Post10min: 0.91 ± 0.46 , $n = 4$, $p = 0.02$, paired t-test) (Fig. 3-1h). These results demonstrate that bilaterally DD mice are still capable of robust movement, so this cannot account for the inability of global GPe stimulation to rescue movement.

A second possibility is that our optogenetic stimulation does not effectively drive firing of GPe neurons. To test this, we recorded the responses of GPe neurons in vivo during optical stimulation with hSyn-ChR2 (see methods, Fig. 3-1i). Due to the large numbers of neurons responding, single unit activity could not be well isolated during stimulation, so these data reflect multiunit activity. On average, all units ($n = 68/68$ units across 3 animals) significantly increased in firing rate ($z\text{-score}_{100\text{ ms}} = 17.6 \pm 1.2$; $z = 1.65$, $p < 0.05$, one-tailed z-test) and achieved peak activation within ~ 1 sec (range: 0.1-9.7 s) (Fig. 3-1j-k). In a subset of recordings, we verified that neural responses in the GPe were stable across each of the 10 repeated stimulations ($n = 34$ units across 3 animals) (Fig. 3-1l). These results confirm that hSyn-ChR2 was effective at increasing firing rates of GPe neurons, yet this did not rescue movement in DD mice.

3.3.2 Selective Activation of PV-GPe Neurons Restores Movement Persistently in DD

Mice

The finding that movement can be rescued during D1-ChR2 stimulation, but not by global GPe stimulation, challenges the classic rate-based basal ganglia model and motivated a more in-depth analysis of GPe circuitry. The GPe contains a heterogeneous population of neurons (Gittis et al., 2014, Hegeman et al., 2016). Since these populations have different anatomical and physiological properties, we reasoned that they might make different contributions to behavior. As such, cell-specific interventions might be more effective than global ones. To test this hypothesis, we first restricted ChR2 expression to PV-containing GPe neurons (Fig. 3-2a, A3a-b).

Ten days to 2 weeks after viral injections, mice were bilaterally depleted and the prokinetic effects of PV-ChR2 stimulation were measured 3-5 days later. In contrast to global GPe stimulation, selective stimulation of PV-GPe neurons provided robust relief of immobility and bradykinesia (Fig. 3-2b-d, Video B1-2). In mice expressing a control fluorescent construct (DIO-EYFP), immobility was not reduced (Fig. 3-2b). Initial responses to PV-ChR2 were highly light-locked, but as stimulation progressed, continuous movement gradually accumulated between light pulses (Fig. 3-2b-c). By the 10th light pulse, PV-ChR2 had reduced immobility to the same degree as D1-ChR2 (10th Stim: PV-ChR2: $21 \pm 20\%$, $n = 10$ vs. D1-ChR2: $17 \pm 23\%$, $n = 4$, $p = 0.995$, Sidak's post hoc test). While the effects of D1-ChR2 decayed shortly after stim, the effects of PV-ChR2 persisted significantly after the 10th stimulation (Pre: $81 \pm 21\%$ vs. Post10min: $28 \pm 16\%$, $n = 10$, $p < 0.0001$, paired t-test). Movement velocities were also significantly increased (normalized to dopamine intact controls: Pre: 0.26 ± 0.10 vs. Post10min: 1.04 ± 0.67 , $n = 10$, $p < 0.0001$, paired t-test) (Fig. 3-2d).

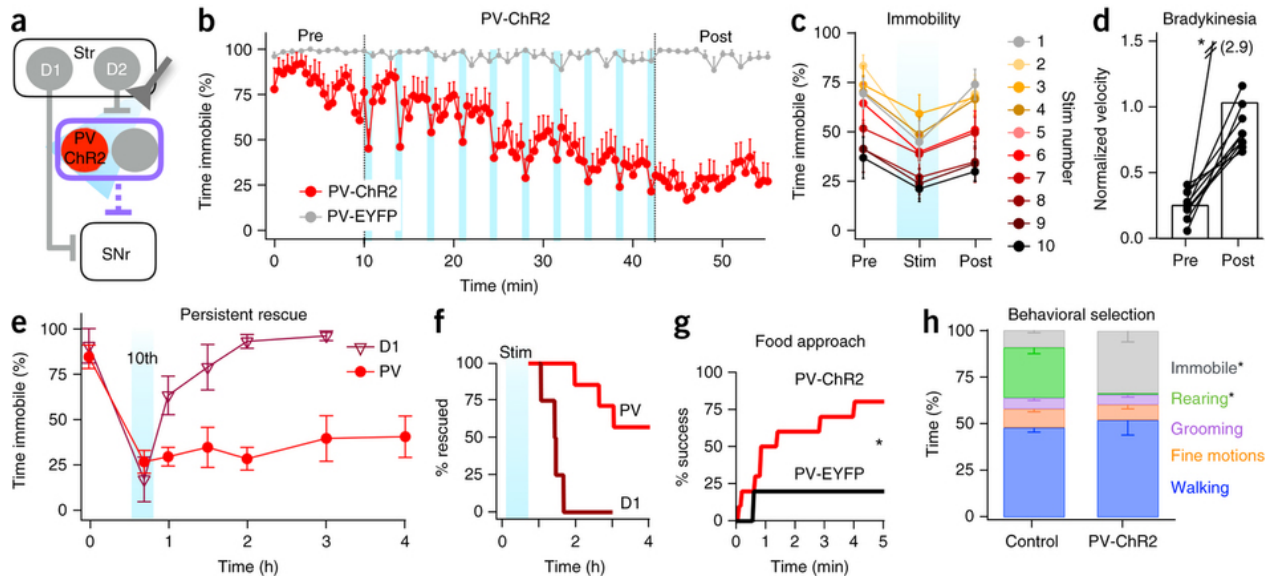


Figure 3-2 Selective stimulation of PV-GPe rescues movement persistently in DD mice.

(a) Schematic of optogenetic stimulation of PV-ChR2. Str, striatum. (b) Percentage of time spent in the immobile state before (Pre), during and after (Post) stimulation (PV-ChR2: $n = 10$, PV-EYFP: $n = 8$). (c) Overlay of immobility immediately before, during (Stim) and after each light pulse. (d) Movement velocities, normalized to those in dopamine-intact controls, before and after stimulation in b ($t(9) = 6.757$, $*P = 0.00008$, paired t -test). Bars denote population averages; connected circles show data for individual mice. (e) Duration of prokinetic effects of PV-ChR2 ($n = 10$) and D1-ChR2 ($n = 4$) stimulation (main effect_{time}: $F(6,54) = 7.672$, $P < 0.0001$; main effect_{condition}: $F(1,9) = 10.04$, $P = 0.0114$; interaction effect_{time \times condition}: $F(6,54) = 6.793$, $P < 0.0001$; two-way repeated-measures ANOVA). (f) Percentage of animals significantly more mobile than baseline (rescued) after D1-ChR2 or PV-ChR2 over the post-stimulation period. Blue bar (Stim) represents full optogenetic manipulation. (g) Cumulative success rate over the 5-min trial for PV-ChR2 ($n = 8$ of 10) and PV-EYFP ($n = 1$ of 5) mice to reach food dish at far end of cage ($\chi^2(1) = 5.000$, $P = 0.0253$, chi-squared test). (h) Comparison of behavioral patterns expressed by PV-ChR2 mice ($n = 10$) during the Post period in b compared to dopamine-intact controls ($n = 7$). The average time engaged in each behavior is expressed as a percentage of total time. Only immobility ($*P = 0.003$, Mann-Whitney U) and rearing ($*P = 0.0001$, Mann-Whitney U) were significantly different between conditions. Error bars, s.e.m.

To test the duration of the prokinetic effects of PV-ChR2, a subset of mice were left in the open field for 3 hrs after stimulation ($n = 7$) (Fig. 3-2e-f); 4 out of 7 mice remained highly mobile for the duration of the test (Fig. 3-2f) and immobility (averaged across all mice, $n = 7$) was significantly reduced for the entire 3 hrs (Fig. 3-2e). When mice were returned to their home cage after stimulation, locomotion ramped down within minutes. However, when mice were placed at one end of a 30 x 20 cm cage with food and water positioned at the other end, 8 out of 10 PV-ChR2 mice reached the food within 5 min (range: 0.08 – 3.9 min) whereas only 1 out of 5 PV-EYFP mice reached the food (latency = 0.58 min) ($p = 0.03$, Chi-squared test) (Fig. 3-2g).

Combined, these results demonstrate that the prokinetic effects of PV-ChR2 stimulation are long lasting and persist for hours after stimulation.

To characterize the behavioral patterns expressed by PV-ChR2 mice, open field behaviors were manually scored during the 10 min post stimulation period. Overall, behavioral patterns were remarkably similar between PV-ChR2 mice and dopamine intact controls (Fig. 3-2h). Control (n = 7) and PV-ChR2 (n = 10) mice spent similar percentages of time walking (Control: $48 \pm 6\%$ vs. PV: $52 \pm 25\%$; $p = 0.6$, Mann Whitney U), grooming (Control: $6 \pm 4\%$ vs. PV: $5 \pm 4\%$; $p = 0.734$, Mann Whitney U) and performing fine movements (Control: $10 \pm 4\%$ vs. PV: $8 \pm 7\%$; $p = 0.270$, Mann Whitney U). On average, walking bouts were longer in PV-ChR2 mice (6.8 ± 4.9 sec) compared to controls (3.1 ± 0.48 sec, $p = 0.043$, Mann Whitney U). Rearing was not rescued by stimulation (Control: $27 \pm 9\%$ vs. PV: $0.6 \pm 1\%$; $p = 0.0001$, Mann Whitney U) and PV-ChR2 mice spent more time immobile compared to controls (Control: $9 \pm 4\%$ vs. PV: $33 \pm 19\%$; $p = 0.003$, Mann Whitney U). Furthermore, PV-ChR2 mice retained a hunched posture and irregular gait (Video B2), suggesting that stimulation is more effective at alleviating bradykinesia/immobility than postural/gait symptoms.

Because the severity of motor symptoms induced by bilateral DD restricted our experimental time window to 3-5 days after depletion, we performed a number of control experiments to ensure that behavioral rescue was specific for symptoms related to dopamine loss, and not symptoms induced by other factors such as acute inflammation. First, to control for the effects of inflammation, dopamine-intact mice were injected with lipopolysaccharide (LPS), an inflammatory agent, in the MFB (Herrera et al., 2000). Five days after injections of LPS, mice exhibited no locomotor deficits in the open field and PV-ChR2 stimulation had no effects on immobility (Fig. A4a). Second, we observed that the persistent component of behavioral rescue

could not be induced in mice with partial dopamine depletions (mice with >20% striatal TH left on either side) (Fig. A4b-f), suggesting the long-lasting prokinetic effects of PV-ChR2 are specific to the dopamine depleted state of the mouse and not other factors associated with our depletion protocol. Third, consistent with data from partially DD mice, PV-ChR2 stimulation in unilaterally DD mice (14 days post depletion) did not alter their behavior persistently (Fig. A4g-i). Combined, these results demonstrate that the long-lasting prokinetic effects of PV-ChR2 are specifically induced only under conditions of advanced dopamine loss.

3.3.3 Neuronal Responses In The GPe During PV-ChR2 Stimulation

Our behavioral results demonstrate that movement is restored when PV-GPe neurons are stimulated selectively, but not when they are stimulated with all other GPe neurons (hSyn-ChR2). To investigate how PV-ChR2 stimulation differs at the network level from hSyn-ChR2 stimulation, we recorded responses of neurons in vivo during PV-ChR2 stimulation (Fig. 3-3a). To identify putative PV-GPe neurons, neurons were first classified as ChR2+ or ChR2- on the basis of their short-latency responses to brief (5 ms) optical pulses (see methods, Fig. A5a). Characteristic firing patterns and waveform distributions of ChR2+ and ChR2- neurons are summarized in Fig. A5b-c. Because the average firing rate of our putative PV-GPe population (24 ± 4 Hz, $n = 18$ across 3 animals) was lower than what has been reported by other groups (Dodson et al., 2015, Mallet et al., 2016), we validated our optical identification strategy in dopamine intact mice (Fig. A5d). In dopamine intact control mice, the average firing rate of the PV-GPe population was 46 ± 2 Hz, consistent with results from previous studies (48 ± 3 Hz (Dodson et al., 2015), and 47 ± 6 Hz (Mallet et al., 2016)). These results suggest that the

lower firing rates of putative PV-GPe neurons in our study are due to changes in population activity induced by dopamine loss, and not errors in neuronal classification.

In DD mice, 18 out of 18 ChR2+ neurons (putative PV-GPe) responded to 30 sec optical pulses with sustained increases in firing rates (Fig. 3-3b-c), averaging 24 ± 4 Hz before stimulation and 52 ± 8 Hz during stimulation ($p < 0.0002$, paired t-test) (Fig. 3-3d). A subset of recordings that were stable enough to track single units across a 10-pulse stimulation paradigm ($n = 7$ across 3 animals) revealed that responses were consistent across all 10 pulses (Fig. 3-3e). In contrast, most (14/21) ChR2- neurons were inhibited during optical pulses (Fig. 3-3b-c), averaging 30 ± 3 Hz before stimulation and 18 ± 2 Hz during stimulation ($p < 0.0004$, paired t-test) (Fig. 3d). Firing rates of the remaining (7/21) ChR2- neurons were not significantly modulated (data not shown). A subset of recordings that were stable enough to track inhibited units across a 10-pulse stimulation paradigm ($n = 4$ across 2 animals) revealed that inhibitory responses were consistent across all 10 pulses (Fig. 3-3e).

These data reveal a key difference between the effect of PV-ChR2 vs. hSyn-ChR2 on population dynamics within the GPe. PV-ChR2 produces a bidirectional response that transiently elevates the firing of PV-GPe neurons but suppresses the firing of other GPe neurons, a dissociation that is occluded during global stimulation with hSyn-ChR2. To test whether this dissociation is critical for the induction of behavioral rescue, we sought to mimic this effect by inhibiting a subset of neurons directly with archaerhodopsin (Arch). Because the firing rates and waveforms of ChR2- neurons were highly overlapping with those of ChR2+ neurons (Fig. A5b-c), we reasoned that both subtypes are part of the prototypical population (Dodson et al., 2015, Mallet et al., 2016). PV-GPe neurons constitute a major fraction of this population, but neurons

expressing Lhx6 represent a second, partially non-overlapping fraction (Mastro et al., 2014, Hernandez et al., 2015, Oh et al., 2016b) (Fig. A6a-b).

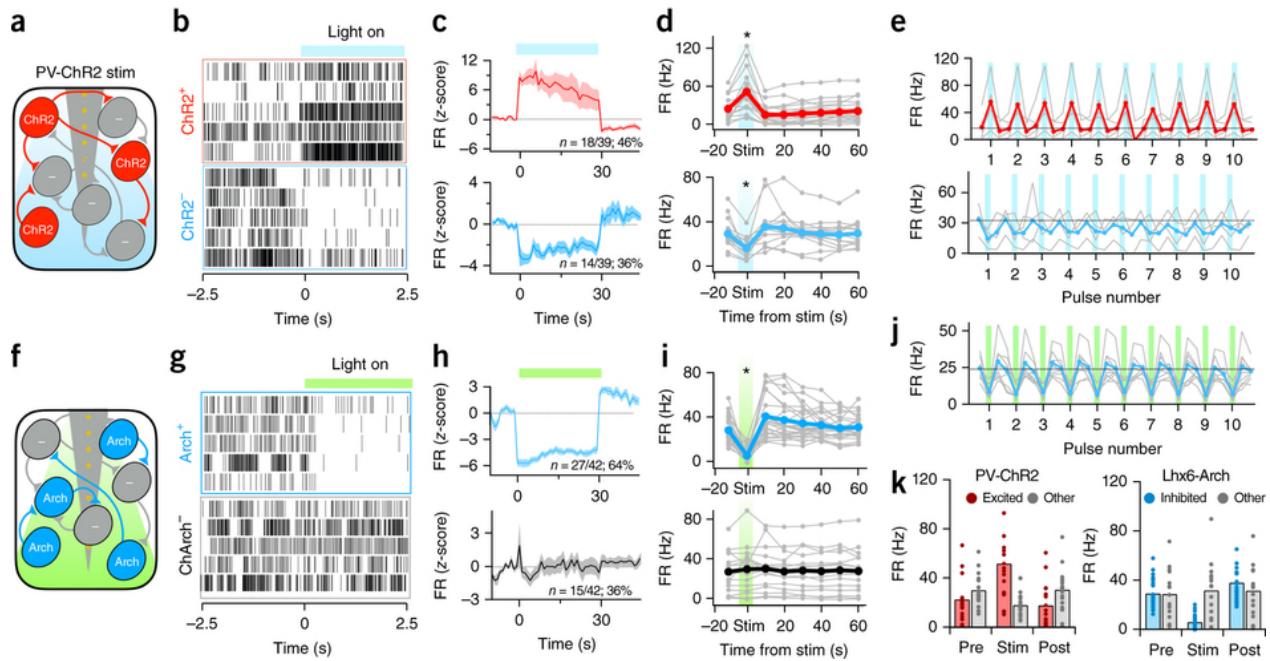


Figure 3-3 Local response during PV-ChR2 stimulation directly inhibits other high-firing GPe neurons.

(a) Schematic of GPe network recording during PV-ChR2 stimulation. (b) Light-evoked responses of ten single units during onset of a 30-s pulse. (c) Average z-score of excited (red, $n = 18$ of 39 across 3 animals) and inhibited (blue, $n = 14$ of 39) neurons during a 30-s optical pulse. Shaded area, s.e.m. FR, firing rate. (d) Firing rates of individual neurons before, during (time 0) and in 10-s bins after a 30-s light pulse (excited: $t(17) = -4.913$, $*P < 0.0001$, paired t -test, inhibited: $t(13) = 4.789$, $*P < 0.0001$, paired t -test). Population averages are shown as thick, colored lines. (e) Average firing rates of units across all ten 30-s pulses for excited (top, $n = 5$ across 3 animals) and inhibited units (bottom, $n = 4$ across 2 animals). Shaded bars (blue) indicate periods of stimulation and each point represents 30-s bins immediately before, during and after the stimulation. Error bars, s.e.m. (f) Schematic of GPe network during Lhx6-Arch stimulation. (g) Light-evoked responses of ten single units during onset of a 30-s pulse. (h) Average z-score of inhibited (blue, $n = 27$ of 42 across 3 animals) and unchanged (gray, $n = 15$ of 42) neurons during a 30-s optical pulse. Shaded area, s.e.m. (i) Firing rates of individual neurons before, during (time 0) and in 10-s bins after a 30-s light pulse (inhibited: $t(26) = 9.888$, $*P < 0.0001$, paired t -test, no change: $t(14) = -1.126$, $P = 0.279$, paired t -test). Population averages are shown as thick colored lines. (j) Average firing rates of inhibited units held across all ten 30-s pulses ($n = 11$ across 3 animals). Shaded bars (green) indicate periods of stimulation and each point represents 30-s bins immediately before, during and after the stimulation. Error bars, s.e.m. (k) Summary of average firing rates before, during and after 30-s stimulations of PV-ChR2 and Lhx6-Arch.

To measure the impact of inhibiting Lhx6-GPe neurons on population activity in the GPe, we performed in vivo recordings in Lhx6-Cre mice two weeks after viral-mediated expression of Flex-Arch (Fig. 3-3f). Neurons were classified as Arch+ or Arch- based on their response to 1 sec optical pulses of green light (see methods, Fig. A5e). Characteristic firing patterns and

waveform distributions of Arch+ and Arch- neurons were highly overlapping and are summarized in Fig. A5f-g.

In response to 30 sec optical pulses, 27 out of 27 Arch+ neurons responded with sustained decreases in firing rates (Fig. 3-3g-h), averaging 29 ± 3 Hz before stimulation and 6 ± 2 Hz during stimulation ($p = 2.68 \times 10^{-10}$, paired t-test) (Fig. 3-3i). A subset of recordings that were stable enough to track single units across a 10-pulse stimulation paradigm ($n = 11$ across 3 animals) revealed that responses were consistent across all 10 pulses (Fig. 3-3j). The remaining 15 out of 15 neurons were Arch- and showed no net change in firing rate during optical stimulation (Fig. 3-3g-i). Although some neurons exhibited sharp firing rate increases at the onset of a light pulse, this effect was transient, and often did not persist for >100 ms (Fig. 3-3h). These results demonstrate that Lhx6-Arch, like PV-ChR2, transiently dissociates population activity in the GPe, but with different effects on absolute firing rate (Fig. 3-3k).

3.3.4 Selective Inhibition of Lhx6-GPe Neurons Restores Movement Persistently in DD Mice

To test whether the transient dissociation of GPe activity produced by Lhx6-Arch was also sufficient to induce behavioral rescue, we assessed its effects on immobility and bradykinesia of DD mice in the open field (Fig. 3-4a-d, A3c). Initially, mice were highly immobile (Pre: $86 \pm 11\%$, $n = 9$), but over the course of 10 stimulations, Lhx6-Arch reduced immobility to a similar degree as PV-ChR2 (10th pulse: Lhx6-Arch: $28 \pm 38\%$, $n = 9$ vs. PV-ChR2: $21 \pm 20\%$, $n = 10$, $p = 0.80$, Tukey's post hoc test) (Fig. 3-4b,f, Video B3). Immobility was not reduced in mice expressing a control fluorescent construct (DIO-EYFP) (Fig. 3-4b), nor was it induced by globally inhibiting all GPe neurons with CAG-Arch (Fig. 3-4h-j, A3d).

Intriguingly, Lhx6-Arch induced the gradual, persistent component of behavioral recovery but not the early, light-locked component present in PV-ChR2 mice. Bradykinesia was also greatly reduced (Pre: 0.22 ± 0.08 vs. Post10min: 0.85 ± 0.45 , $n = 9$, $p = 0.002$, paired t -test) (Fig. 3-4d). Ten minutes after the last stimulation, Lhx6-Arch mice remained highly mobile, spending only $34 \pm 21\%$ (vs. Pre: $86 \pm 11\%$, $n = 9$, $p = 0.012$, Tukey's post hoc test) of their time in the immobile state. Similar to the long-lasting effects of PV-ChR2, immobility in Lhx6-Arch mice remained significantly reduced for hours after stimulation (Post3hr: Lhx6-Arch: $45 \pm 11\%$, $n = 5$ vs. PV-ChR2: $41 \pm 36\%$, $n = 7$, $p = 0.990$, Tukey's post hoc test) (Fig. 3-4f-g) and 3 out of 5 Lhx6-Arch mice remained highly mobile for the duration of the test (Fig. 3-4g).

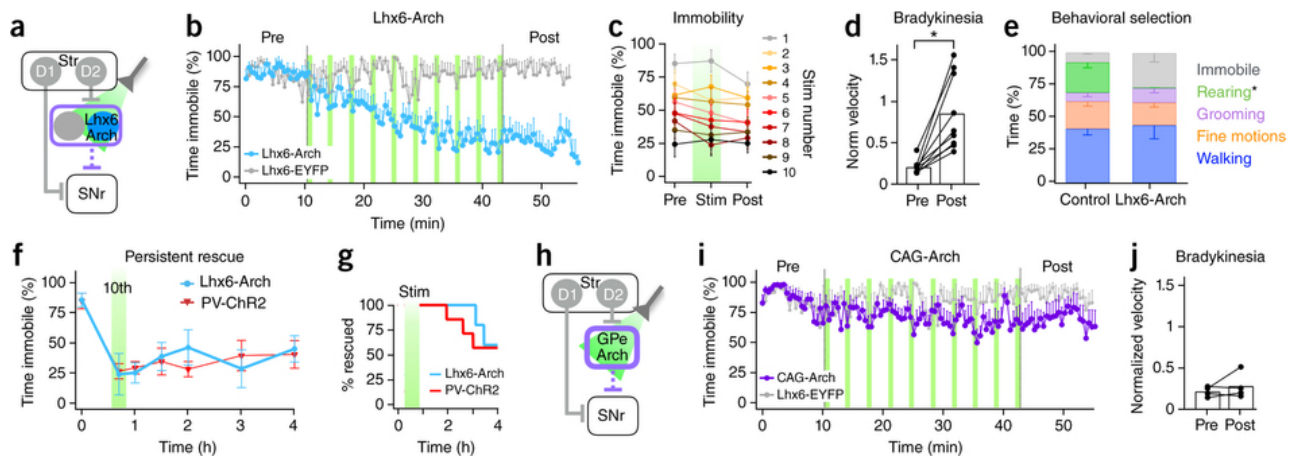


Figure 3-4 Selective suppression of Lhx6-GPe rescues movement persistently in DD mice.

(a) Schematic of optogenetic inhibition of Lhx6-GPe neurons. Str, striatum. (b) Percentage of time spent in the immobile state before (Pre), during and after (Post) Lhx6-Arch ($n = 9$) and Lhx6-EYFP ($n = 7$). (c) Overlay of immobility immediately before, during (Stim) and after each light pulse. (d) Movement velocities, normalized (Norm) to those in dopamine-intact controls, before and after stimulation in b ($*P = 0.002$, paired t -test). Bars denote population averages; connected circles show data for individual mice. (e) Comparison of behavioral patterns expressed by Lhx6-Arch ($n = 7$) mice during the post-stimulation period compared to those of dopamine-intact controls ($n = 6$). The average time engaged in each behavior is expressed as a percentage of total time. Only immobility and rearing ($P = 0.001$, Mann-Whitney U) were significantly different between conditions. (f) Duration of prokinetic effects of Lhx6-Arch ($n = 5$) and PV-ChR2 ($n = 7$), plotted for reference (main effect_{time}: $F(7,70) = 7.994$, $P < 0.0001$; main effect_{condition}: $F(1,10) = 0.5855$, $P = 0.462$; interaction effect_{time×condition}: $F(7,70) = 1.358$, $P = 0.2367$; two-way repeated-measures ANOVA). (g) Percentage of animals significantly more mobile than baseline (rescued) after Lhx6-Arch or PV-ChR2 over the post-stimulation period. Green bar (Stim) represents full optogenetic manipulation. (h) Schematic of optogenetic inhibition of all GPe neurons. (i) Percentage of time spent in the immobile state before, during and after CAG-Arch ($n = 4$) and Lhx6-EYFP ($n = 7$). (j) Movement velocities, normalized to those of dopamine-intact controls, before and after stimulation in i ($P = 0.393$, paired t -test). Error bars, s.e.m.

Behavioral patterns in Lhx6-Arch mice were similar to those of dopamine intact controls (Fig. 3-4e). Control (n = 6) and Lhx6-Arch mice (n = 7) spent similar percentages of time walking (Control: $42 \pm 12\%$ vs. Lhx6: $44 \pm 28\%$; $p = 0.886$, Mann Whitney U), grooming (Control: $6.9 \pm 7.7\%$ vs. Lhx6: $11.2 \pm 9.2\%$, $p = 0.568$, Mann Whitney U) and performing fine movements (Control: $21 \pm 9\%$ vs. Lhx6: $18 \pm 9\%$, $p = 0.445$, Mann Whitney U), but rearing behavior was not recovered (Control: $23 \pm 10\%$ vs. Lhx6: $0.3 \pm 0.3\%$, $p = 0.001$, Mann Whitney U). Lhx6-Arch mice spent a wide range (7-50%) of time in the immobile state (Control: $7.6 \pm 2.0\%$ vs. Lhx6: $26.5 \pm 18.3\%$, $p = 0.101$, Mann Whitney U). Walking bouts in Lhx6-Arch mice were significantly longer compared to control (Control: 2.7 ± 0.8 ms vs. Lhx6: 5.6 ± 2.4 ms, $p = 0.02$, Mann Whitney U) and they walked with a hunched posture and shuffling gait (Video B4). Combined, our behavioral results suggest that transiently dissociating the activity of GPe neurons with Lhx6-Arch induces a gradual, long-lasting recovery of movement that is qualitatively and quantitatively similar to that induced by PV-ChR2.

3.3.5 Persistent Behavioral Rescue Depends on the Ratio of Lhx6 and PV Activity

Thus far, our results have shown that movement can be persistently rescued by manipulations that dissociate the activity of PV-GPe neurons above that of Lhx6-GPe neurons. But because these subpopulations are partially overlapping at the molecular level (Fig. A6a-b), we wanted to determine whether their effects were truly segregated at the behavioral level. To test this, we assessed the prokinetic effects of inverse manipulations: Lhx6-ChR2 and PV-Arch. In mice stimulated with Lhx6-ChR2 (Fig. 3-5a, A3e), some relief from immobility was observed in 3 out of 5 mice during the stimulation period (Pre: $91 \pm 13\%$ vs. 10th Stim: $47 \pm 46\%$, $n = 5$, $p =$

0.067, Tukey's post hoc test), but this effect did not persist beyond 30 min. after stimulation (Pre: $91 \pm 13\%$ vs. Post30 min: $72 \pm 37\%$, $n = 5$, $p = 0.684$, Tukey's post hoc test) (Fig. 3-5b-c).

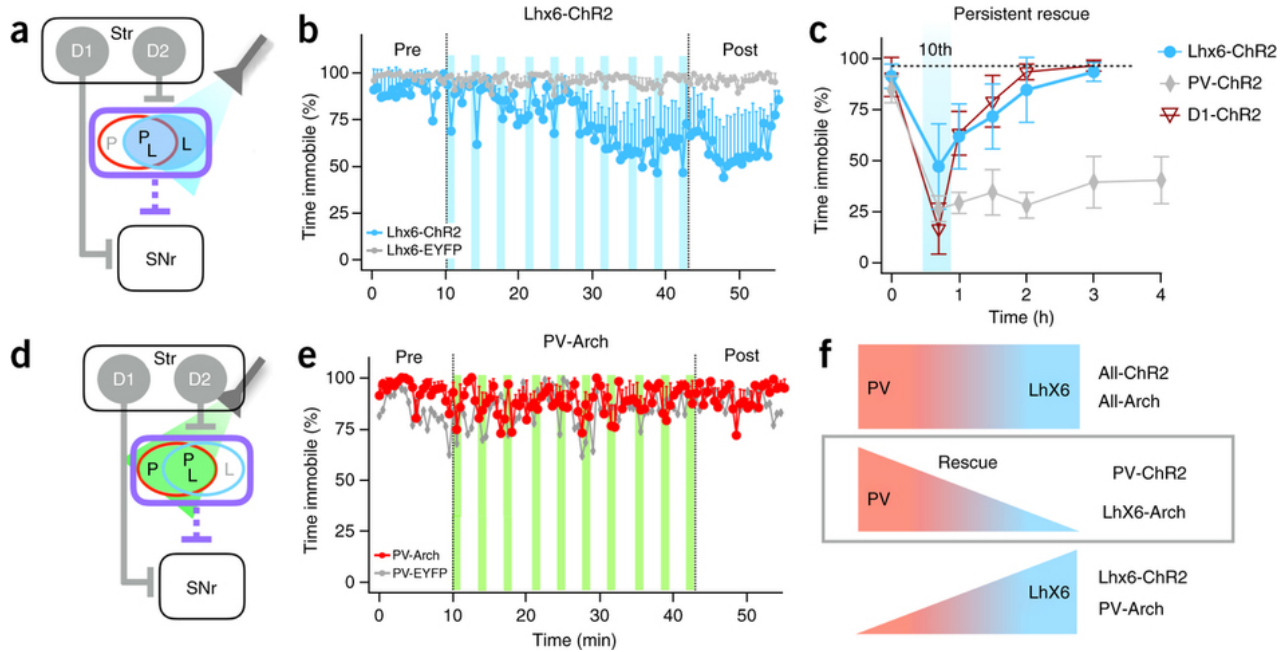


Figure 3-5 The induction of persistent behavioral rescue is cell-type specific.

(a) Schematic of optogenetic stimulation of Lhx6-GPe neurons. Str, striatum. (b) Percentage of time spent in the immobile state before, during and after Lhx6-ChR2 ($n = 5$) and Lhx6-EYFP ($n = 7$) stimulation. (c) Duration of prokinetic effects in Lhx6-ChR2 mice. Data from PV-ChR2 ($n = 10$) and D1-ChR2 ($n = 4$) are replotted for reference (main effect_{time}: $F(6,78) = 10.25$, $P < 0.0001$; main effect_{condition}: $F(2,13) = 7.177$, $P = 0.0079$; interaction effect_{time \times condition}: $F(12,78) = 3.947$, $P < 0.0001$, two-way repeated-measures ANOVA). (d) Schematic of optogenetic suppression of PV-GPe neurons. (e) Percentage of time spent in the immobile state before, during and after PV-Arch stimulation ($n = 4$). (f) Schematic of GPe manipulations that globally alter GPe physiology and those that shift the relative balance of PV and Lhx6 neurons to successfully induce behavioral rescue (PV-ChR2, Lhx6-Arch). Error bars, s.e.m.

In mice stimulated with PV-Arch (Fig. 3-5d, A3f), optogenetic suppression of PV-GPe neurons did not rescue movement (Fig. 3-5e). Immobility in PV-Arch mice was $94 \pm 4\%$ before the first stimulation and $92 \pm 8\%$ during the 10th stimulation ($n = 5$, $p = 0.448$, paired t-test) and no persistent effects were observed (Fig. 3-5e). Taken together, these results confirm that the induction of long-lasting behavioral recovery is cell-type specific, and is induced by

interventions that dissociate the firing rates of PV-GPe neurons above that of Lhx6-GPe neurons (Fig. 3-5f).

3.3.6 PV-ChR2 and Lhx6-Arch Reverse Pathological Burst Firing in SNr

How do transient imbalances between the firing rates of two subpopulations of GPe neurons produce a long-lasting effect on movement? To study the impact of GPe interventions on the basal ganglia circuit, we recorded neural activity in the substantia nigra reticulata (SNr), the major basal ganglia output nucleus in rodents.

A pathological hallmark of SNr dysfunction following dopamine depletion is an increase in burst firing and the percentage of bursting neurons (Soares et al., 2004, Rubin et al., 2012, Wang et al., 2016). Consistent with these findings, we observed a rightward shift in the proportion of bursting neurons in DD mice compared to dopamine intact controls ($p = 0.005$, K-S two sample test) (Fig. 3-6a-b). To test if optogenetic stimuli that rescue movement reduce the proportion of bursting neurons, we recorded from the SNr before, during, and after stimulation (Fig. 3-6c-d). PV-ChR2 induced a leftward shift in the distribution of bursting neurons in the SNr ($p = 0.005$, K-S two sample test) (Fig. 3-6e). This effect was most pronounced for 'highly bursty' units, as identified by burst frequencies that exceeded 1 median absolute deviation (MAD) above the median (Fig. 3-6f). The fraction of highly bursting neurons was reduced from 27% pre stimulation to 10% post stimulation (Pre: $n = 22/81$ vs. Post: $n = 6/58$ across 3 animals, $p = 0.044$, chi-squared test) (Fig. 3-6g). In contrast, hSyn-ChR2 did not shift the distribution of bursting neurons ($p = 0.188$, K-S two sample test) (Fig. 3-6h); 31% of units were classified as highly bursty pre stimulation compared to 20% post stimulation (Pre: $n = 17/55$ vs. Post: $n = 14/69$ across 3 animals, $p = 0.295$, chi-squared test) (Fig. 3-6i-j). In recordings stable enough to track

the activity of single units across all 10 light pulses, a reduction in the number of bursts was apparent at the level of individual neurons recorded in PV-ChR2 mice (Fig. 3-6k), but not in hSyn-ChR2 mice (Fig. 3-6l). Intriguingly, bursts diminished gradually over the first 2-4 stimuli, mirroring the kinetics of behavioral rescue in the open field.

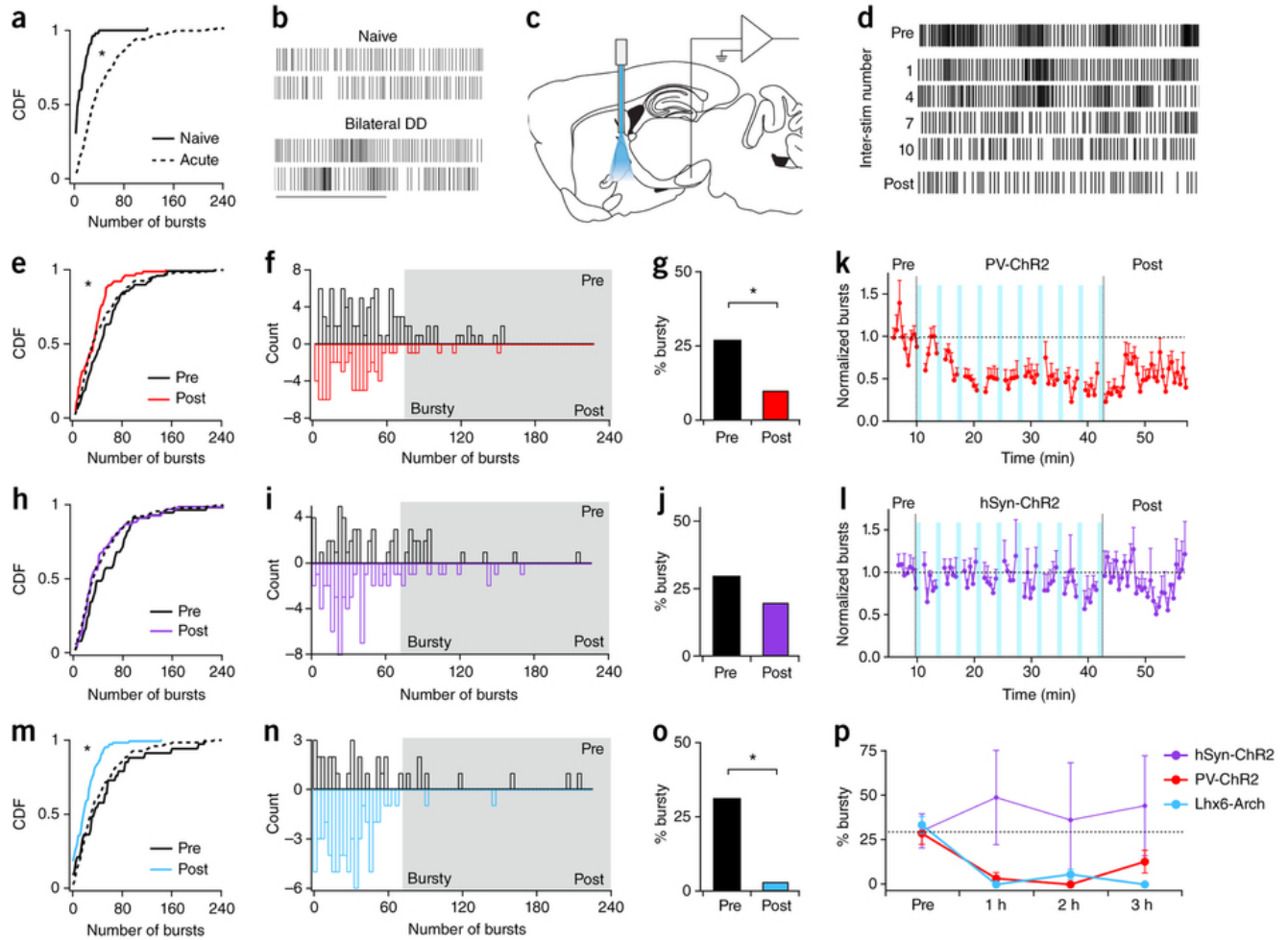


Figure 3-6 PV-ChR2 and Lhx6-Arch reverse pathological bursting activity persistently.

(a) Cumulative distribution function (CDF) plots of burst firing in the SNr of dopamine intact (naive; solid line) and bilaterally DD mice (acute; dotted line). $*P = 0.005$. (b) Representative raster of single-unit activity in naive and acute conditions. (c) Schematic of simultaneous GPe stimulation (bilateral, not depicted) and SNr recording. (d) Representative SNr single-unit activity before stimulation (Pre), between stimulations (Inter-stim) and after stimulation (Post) of the PV-GPe neurons. (e) Distribution of burst firing before and after PV-ChR2 stimulation. Acute distribution (dotted line) replotted for reference. $*P = 0.005$. (f) Histogram of burst firing before (top, 2 h) and after (bottom, 3 h) PV-ChR2 stimulation. (g) Fraction of bursty units before and after PV-ChR2 stimulation. $*P = 0.044$. (h) Distribution of burst firing before and after hSyn-ChR2 stimulation. (i) Histogram of burst firing before (top) and after (bottom) hSyn-ChR2 stimulation. (j) Fraction of bursty units before and after hSyn-ChR2 stimulation. (k,l) Single-unit burst activity normalized to the pre-stimulation baseline and plotted before, during and after PV-ChR2 (*n* = 7 across 3 animals) or hSyn-ChR2 (*n* = 3 across 2 animals). Error bars, s.e.m. (m) Distribution of burst firing before and after Lhx6-Arch inhibition. $*P = 0.005$. (n) Histogram of burst firing before (top) and after (bottom) Lhx6-Arch inhibition. (o) Fraction of bursty units before and after Lhx6-Arch inhibition. $*P = 0.0006$. (p) Fraction of bursty units over the course of the 3-h post-stimulation period across 3 animals per condition. Error bars, s.e.m.

To test whether Lhx6-Arch works through a similar mechanism, we repeated experiments in Lhx6-Arch mice. Consistent with the effects of PV-ChR2, Lhx6-Arch produced a leftward shift in the distribution of bursting neurons in the SNr ($p = 0.005$, K-S two sample test) (Fig. 3-6m) and the fraction of highly bursting neurons was reduced from 31% pre stimulation to 3% post stimulation (Pre: $n = 9/29$ vs. Post: $n = 2/69$ across 3 animals, $p = 0.0006$, chi-squared test) (Fig. 3-6n-o).

To determine how long burst attenuation persisted after stimulation, we separated the population activity into one hour time bins and calculated the fraction of bursty neurons over time. Consistent with the persistent effects on behavior, the fraction of bursty neurons across the population remained persistently reduced for hours after stimulation (Pre vs. Post2hr: PV-ChR2: $p = 0.007$, Lhx6-Arch: $p = 0.003$, Dunnett's multiple comparisons test), and only begins to drift back to pre-stimulation levels by ~3 hrs after stimulation (Pre vs. Post3hr: PV-ChR2: $p = 0.105$, Lhx6-Arch: $p = 0.001$, Dunnett's multiple comparisons test) (Fig. 3-6p). These data suggest a mechanism through which PV-ChR2 and Lhx6-Arch persistently rescue movement through a long-lasting normalization of basal ganglia output pattern. We also considered effects of stimulation on SNr firing rates, and although burst firing decreased, there was no change in the firing rate before and after PV-ChR2 and Lhx6-Arch (Fig. A7). In contrast, hSyn-ChR2 induced a pronounced decrease in the firing rate but no change to the overall proportion of highly bursty neurons (Pre vs. Post1-3hr: $p > 0.1$, Dunnett's multiple comparisons test).

Taken together, these results suggest that transient cell-specific interventions in the GPe induce long-lasting reductions in the pathological activity of basal ganglia output neurons in the SNr that persist for hours beyond stimulation.

3.4 DISCUSSION

Here, we demonstrate that cell-specific interventions in the GPe induce robust, long-lasting recovery of motor function in DD mice. Manipulations that transiently elevate the firing of PV-GPe neurons above that of Lhx6-Arch neurons reverse pathological burst firing in the SNr and ameliorate symptoms of immobility and bradykinesia for hours beyond stimulation. These results establish the behavioral significance of cell-type heterogeneity in the GPe, with potential implications for the treatment of PD.

Nearly thirty years ago, the discovery that striatal neurons can be molecularly divided into D1 and D2-subpopulations provided a cellular basis for the direct/indirect pathway model of the basal ganglia that has long dominated our conceptual framework(Gerfen et al., 1990). However, with the exception of neuronal diversity in the striatum, the classic direct/indirect pathway model treats all other downstream nuclei as relay structures, an oversimplification whose limits have become increasingly apparent as techniques to study circuit function become more sophisticated. The GPe contains different cell populations(Gittis et al., 2014, Hegeman et al., 2016), but this knowledge has been slow to translate into therapeutic strategies. Here, leveraging tools to optogenetically target subpopulations of GPe neurons, we can induce long-term recovery of motor function in DD mice.

Strategies that persistently restored movement shared a common mechanism of elevating the firing rates of PV-GPe neurons relative to that of Lhx6-GPe neurons (PV-ChR2, Lhx6-Arch). Interventions that activated or suppressed all GPe neurons were not effective (hSyn-ChR2, CAG-Arch), nor were interventions that elevated the firing rates of Lhx6-GPe neurons relative to PV-GPe neurons (Lhx6-ChR2, PV-Arch). Thus, despite some overlap between the Lhx6 and PV subpopulations at the molecular level(Abdi et al., 2015, Dodson et al., 2015, Hernandez et al.,

2015, Hegeman et al., 2016, Oh et al., 2016b), the behavioral effects produced by manipulating these populations are well segregated.

The GPe's impact on movement is thought to be mediated by its influence over basal ganglia output nuclei, predominantly the SNr in rodents (Albin et al., 1989, DeLong, 1990, Smith et al., 1998a). Under dopamine depleted conditions, neurons in the basal ganglia become more rhythmic and bursty, impairing basal ganglia output (Bevan et al., 2002, Rubin et al., 2012). Attenuation of pathological activity is well correlated with the therapeutic effects of DBS on bradykinesia and rigidity (Kuhn et al., 2006, Weinberger et al., 2006, Hammond et al., 2007, Vitek et al., 2012). The dissociation of pallidal subpopulations – elevating the activity of PV-GPe above Lhx6-GPe neurons – and the subsequent removal of pathological activity in the SNr, may be a possible mechanism for DBS. Although acute toxin models do not replicate all the features of a complex human disorder such as PD, they provide key insights into the function of neural circuits under conditions of low dopamine. The cardinal motor symptoms of PD such as immobility and bradykinesia do not arise until dopamine levels have decreased by ~70%, highlighting the need to discover strategies to restore motor function, even at advanced stages of dopamine loss (Bernheimer et al., 1973, Riederer and Wuketich, 1976, Betarbet et al., 2002, Deumens et al., 2002, Fahn, 2003).

It has long been assumed that the prokinetic effects of DBS are limited to the stimulation period, with symptoms (and pathological activity) rapidly returning within minutes after stimulation. However, a modified DBS protocol, called coordinated reset (CR-DBS), has been shown to provide some prokinetic benefits that persist for hours, or even days, after stimulation in both MPTP primate models (Tass et al., 2012, Wang et al., 2016) and human PD

patients(Adamchic et al., 2014). The ability to destabilize the network by shifting the balance of neuronal subpopulations may be sufficient to rescue motor function.

Although we do not know whether GPe stimulation engages similar mechanisms, the GPe is a central node for the amplification and propagation of pathological network oscillations in PD(Bergman et al., 1998, Bevan et al., 2002, Kita, 2007, Holgado et al., 2010, Vitek et al., 2012, Corbit et al., 2016). Our data identify PV and Lhx6-GPe neurons as critical nodes within the basal ganglia circuit for the induction of long-lasting attenuation of pathological activity in the SNr. The convergent effects of PV and Lhx6-GPe neurons on the SNr could be mediated via their direct projections to the nucleus, or via their indirect projections by way of the STN, a nucleus which is differentially innervated by Lhx6 vs. PV subpopulations(Mastro et al., 2014). Elucidating the circuit and synaptic mechanisms that give rise to pathological rhythmicity in disease, and discovering interventions to best counteract this rhythmicity, is an important area of research in the field.

3.4.1 Conclusions

In conclusion, our results demonstrate that cell-specific, but not global interventions in the GPe induce long-lasting behavioral rescue and physiological restoration of basal ganglia output in DD mice. These results establish important functional distinctions between subpopulations of GPe neurons, delineated in part by their expression of Lhx6 and PV. These results reconcile a number of conflicting reports in the literature: that successful DBS can either increase or decrease firing rates of GPe neurons(Bar-Gad et al., 2004, Chin and Hutchison, 2008, Erez et al., 2009, Bugaysen et al., 2011), that DBS directly in the GPe can reduce bradykinesia(Johnson et al., 2012, Vitek et al., 2012) but restoring autonomous firing after DD has no effect(Chan et al.,

2011). Finally, because the proportion of PV-GPe neurons in humans is similar to that in mice(Hardman and Halliday, 1999), our results suggest that interventions that preferentially increase their activity relative to other GPe neurons might provide more persistent prokinetic benefits than current treatments.

3.5 ACKNOWLEDGEMENTS

The authors thank V. Corbit and T. Whalen for Matlab analysis scripts and B. Rogowski for surgical support and behavioral video editing. We also thank N. Kessarlis and H. Zeng for their gifts of the Lhx6-iCre and Pvalb-2A-Cre mice, respectively. This work was supported by NIH grants F31 NS090745-01 (K.M.), F31 NS093944-01 (A.W.), R00 NS076524, NSF grant DMS 1516288, and grants from the Brain and Behavior Research Foundation (National Alliance for Research on Schizophrenia and Depression Young Investigator Grant), the Parkinson's Disease Foundation, and the NIH Intramural Research Program.

4.0 SUMMARY AND CONCLUSIONS

By understanding and interrogating cellular diversity, we gain clarity into the physiological and functional capabilities of neural circuits. As discussed in the introduction, the use of transgenic animals and bevy of emerging tools available to isolate, manipulate and control distinct populations of neurons have revolutionized neuroscience. We are gaining an incredible insight into the underlying structure of neural circuits that previously was inaccessible. Here, we defined cellular diversity within the GPe, a nucleus within the motor-suppressing pathway of the basal ganglia, and investigated its contributions to circuit function in health and disease.

In Chapter 2, we utilize transgenic animals to subdivide the GPe into two distinct populations of neurons based on their expression of parvalbumin (PV-GPe) or Lim homeobox 6 (Lhx6-GPe). These neurons differed across a range of topographic, physiological and anatomical factors. Most notably, PV-GPe neurons were more often found within the lateral GPe, had a greater response to current, and had a unique projection to the parafascicular nucleus of the thalamus. Lhx6-GPe neurons were more often found in the medial GPe, had lower spontaneous firing rates and sent a denser projection to both the striatum and dopamine neurons within the substantia nigra pars compacta. This study was the first to utilize transgenic mice to define distinct populations of GPe neurons and provided tools to understand their contributions to behavior in health and disease.

The GPe is highly implicated in the initiation, propagation and maintenance of dysfunction within basal ganglia (Lozano et al., 2000, Kita, 2007, Obeso et al., 2008). Therefore; we assessed the functional contribution of the GPe cell-types in a model of Parkinson's disease. By using targeted viral expression of optogenetics, we activated or inhibited GPe, globally or cell-type specifically, to determine whether GPe manipulation would provide a therapeutic benefit. As shown in Chapter 3, cell-type specific but not global manipulations rescues motor function in dopamine-depleted mice. Specifically, the PV-GPe population must be elevated above Lhx6-GPe neurons, for the successful induction of a persistent motor recovery. Consistent with the long-lasting motor recovery, the activation of PV-GPe or inhibition of Lhx6-GPe neurons attenuated burst firing within the basal ganglia output nucleus that persisted for hours and hours after the stimulation. These results demonstrate the distinct functional contributions of these two-partially overlapping populations and uncover a potential therapeutic intervention during disease.

Taken together, these results demonstrate the wide range of differences that exist within the GPe cell-types and its potential to disrupt pathological activity and behavior within the disease state. The main goal of this discussion is two-fold: 1) discuss the evolving and often-controversial field of cellular heterogeneity within the GPe and 2) provide potential mechanisms for which the GPe cell-types exert profound therapeutic benefit during disease. Though these cell-types have their shortcomings and limitations; they have provided a great opportunity to break open a critical node within the basal ganglia and continue to understand how it influences behavior.

4.1 SHIFTING CELLULAR LANDSCAPE OF THE GPE

Since the golden age of basal ganglia research, there has been evidence of neuronal heterogeneity within the GPe (see review by (Hegeman et al., 2016). Attempts have been made to classify GPe cell-types, but these criteria are often difficult to generalize across preparations (Nambu and Llinas, 1994, Cooper and Stanford, 2000, Kita, 2007, Deister et al., 2013), rely on postmortem cell-type identification (Hoover and Marshall, 1999, Sato et al., 2000, Hoover and Marshall, 2002), or rely on activity in disease states (Mallet et al., 2012). Over the last ten years, the field has capitalized on modern techniques to categorize GPe neurons and with it has brought a great deal of attention and some conflict to the GPe field. The goal of the following section is to highlight emerging GPe cell-type definitions and to identify areas that can be improved within future experiments.

From the seminal GPe recordings within awake behaving monkeys (DeLong, 1971), there were two physiological distinct populations of neurons based on their spontaneous firing rates: ‘high-frequency discharge with pause’ and ‘low-frequency discharge with bursts’. Subsequent studies have studied these two populations of neurons extensively and have provided new tools to access and further delineate functionally-relevant distinctions.

4.1.1 Low-Frequency Discharge with Bursts: Arkypallidal Population

The slowly firing population that tends to fire in bursts makes up approximately 15-20% of pallidal neurons and express the opioid precursor preproenkephalin and the transcription factor FoxP2 (Mallet et al., 2012, Abdi et al., 2015, Dodson et al., 2015). They were recently termed the arkypallidal population due to their extensive projections to the dorsal striatum. These

neurons send a massive net-like axonal projection synapses onto all cell-types within the striatum that was first described in non-human primates by Kita et al. (1999) and later confirmed within rodents (Mallet et al., 2012, Abdi et al., 2015, Dodson et al., 2015). Furthermore, the majority of arypallidal neurons originate from the lateral ganglion eminence (Dodson et al., 2015) and have been linked to the suppression of motor output (Glajch et al., 2016) by exerting a widespread ‘stop’ signal in the striatum (Mallet et al., 2016). Though not the focus of this dissertation, the presence of these neurons provide a diversity in function that is in stark contrast to the widespread connections made by the remaining ~80% of neurons. These neurons and their emerging role in terminating behavioral sequences will influence the function of all other pallidal neurons.

Future studies must unravel the relationship between the arypallidal and remaining neuronal populations in the GPe. For instance, do these neurons receive a distinct set of inputs from cortex, striatum or thalamus? Are these neurons critical or specifically wired into the ‘hyperdirect’ pathway (monosynaptic cortical input to STN)? How do GPe collaterals from distinct cell-types impact the function of these neurons in health and disease? By capitalizing on these distinct markers and physiological patterns, we are poised to capitalize on optical and physiological approaches to delineate their contributions in health and disease.

4.1.2 High-Frequency Discharge with Pause: Prototypic Population

Over the last five years, there has been a strong push to define the ‘high-frequency pausers’, or prototypic population utilizing currently available tools. The prototypic population is defined by dense projections to the subthalamic nucleus (STN) and the fast spontaneous firing rate exhibited in both *in vivo* (Mallet et al., 2012, Mallet et al., 2016, Mastro et al., 2017) and *ex vivo*

preparations (Nambu and Llinas, 1994, Cooper and Stanford, 2000, Mastro et al., 2014). The evidence strongly indicates that within the remaining 80% of neurons there exist multiple classes that may be separable based on molecular expression, anatomic connectivity or enhanced physiological parameters.

Our study highlighted one of the first molecularly distinct populations of neurons, parvalbumin (PV)-expressing GPe neurons. Utilization of PV-expression had been used in previous studies (Bevan et al., 1998, Kita et al., 1999, Mallet et al., 2012) but the confirmation of its selectivity in transgenic animals provided a toolset that could be transferrable across experimental manipulations (Mastro et al., 2014, Hernandez et al., 2015). Recently, Oh et al. (2016b) created transgenic rats that expressed cre-recombinase by way of the PV-promotor and confirmed many previously established results (Bevan et al., 1998, Kita et al., 1999, Mallet et al., 2012, Mastro et al., 2014, Abdi et al., 2015, Dodson et al., 2015). PV-GPe neurons make up approximately 35-55% of the total population which is similar to the amount reported within humans (Hardman and Halliday, 1999). Other studies have used a host of molecular markers with varying levels of distinction and overlap (Hegeman et al., 2016).

As noted in a recent review, there is overlap between many of the neuronal markers but these distinguishable populations provide a new investigative tool to better understand how the GPe processes information and shapes behavior (Hegeman et al., 2016). While the arkypallidal population has been linked to the hyperdirect ‘stop’ pathway (Dodson et al., 2015, Mallet et al., 2016), the role of other GPe neurons are still not well understood. Though it should be noted that even from the earliest recordings within the GPe, there has been brilliant work to understand how GPe neurons shape behavior. From in vivo recordings, GPe neurons have been shown to fire independently (Nini et al., 1995); with firing rates that are characterized by complex temporal

patterns and low correlation during movement (DeLong et al., 1985, Wichmann et al., 1994, Jaeger et al., 1995, Bergman et al., 1998) that are related to the movement kinematics (Turner and Anderson, 1997). Though some brain areas may be able to contribute distinct functions to distinct cell-types, it is obvious that interaction between pallidal neurons, through powerful collaterals, may play a critical role in how GPe influences behavior.

Dodson et al. (2015) observed no physiological and functional difference between their ‘prototypic’ subdivisions in response to movement (Dodson et al., 2015). Briefly, neurons were subdivided based on their expression of PV, Lhx6, and an additional transcription factor Nkx2.1 and recorded extracellularly in awake, head-restrained mice. All neuronal subdivisions had heterogeneous levels of responsivity to the onset and termination of spontaneous movements. Therefore, the molecular and genetic differences between the prototypic populations will not be the only subdivision necessary to delineate their functional contributions. Emerging evidence suggests that the connectivity of neurons within cell-types may provide unparalleled access into their functional ramifications (Lerner et al., 2016).

4.1.3 Probing Diversity in Axonal Projections

The ability to map the input/output relationship of neurons provides a great deal of information regarding their connectivity and potential for functional contribution (Lerner et al., 2016). Utilizing transgenic mice and viral expression of fluorescent probes, we confirmed the wide-spread connectivity of GPe neurons with targets within and outside of the basal ganglia (Mastro et al., 2014). Previously, single-cell tracing of GPe neurons showed that a single neuron is capable of sending collaterals to multiple brain regions (Bevan et al., 1998). But do some

pallidal neurons project to all basal ganglia targets while others selectively innervate one or two targets?

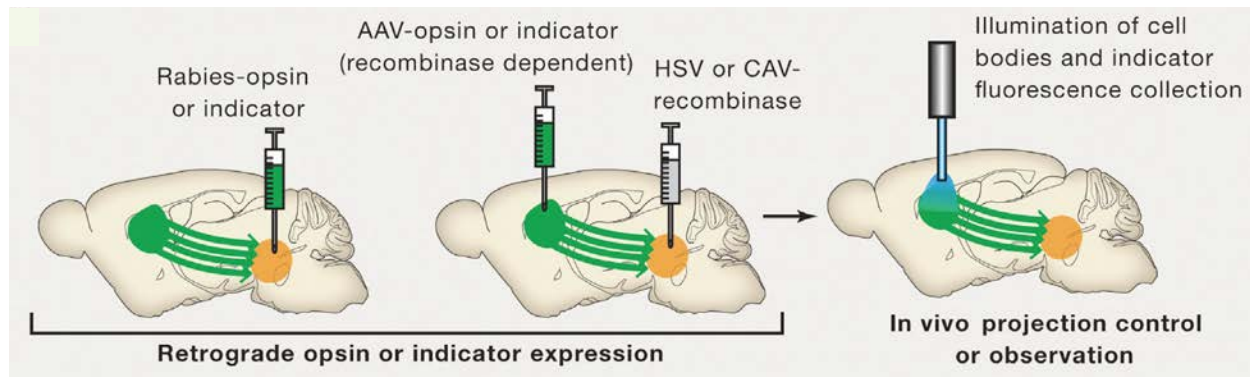


Figure 4-1 Retrograde opsin or indicator expression

Specific stimulation or observation of a projection can also be achieved by using a retrograde virus such as rabies, HSV, or CAV to express an opsin or activity indicator only in cells that have a specific efferent target. In this case, cell bodies may be illuminated directly. *Adapted from Lerner et al. (2016), with permission*

With recent advancements in retrograde expression of viral constructs (Figure 4-1), we have the capacity to break down current cell-types based on their projection targets and monitor or manipulate these projections selectively (Lerner et al., 2016).

The identification of projection specific populations will provide clarity in their physiological response during movement. Recently, there were no clear physiological differences observed in response to self-generated movements within any given prototypic delineation (Dodson et al., 2015), but as noted above, further delineations may occur within any given cell-type. In a recent study, cell-type diversity in the internal segment of the globus pallidus was shown to have an impact on the processing of limbic and sensorimotor output of the basal ganglia (Wallace et al., 2017). In this study, cell-types were defined within the GPi and found to have distinct projections to thalamic targets. Moreover, upon retrograde analysis of the inputs, Lhx6-GPe neurons projected to the limbic GPi territory while PV-GPe neurons projected to the sensorimotor GPi territory (Wallace et al., 2017). This pathway specificity is a prime example of

how diversification of neuronal cell-types can be used to organize the functional and anatomical segregation that leads, in theory, to more efficient neural processing.

Future studies can utilize these technologies to observe the dynamics of GPe neurons based on what and how many output targets they are connected to. How different does a PV to STN only neuronal population act in comparison to PV to SNr only? Moreover, exploration of their inputs will provide insights into how the GPe is tied into the circuit at large. These differences will shed light on the GPe's widespread inhibitory connections and their impact on circuit dynamics.

4.1.4 Cellular Controversy

There has been considerable controversy on the use of Lhx6 as a marker for pallidal neurons (Mastro et al., 2014, Abdi et al., 2015, Dodson et al., 2015, Hernandez et al., 2015, Hegeman et al., 2016). Lhx6 is a homeobox protein expressed in the medial ganglionic eminence (MGE) during development. The MGE is the origin of most forebrain GABAergic interneurons (Marin et al., 2000, Cobos et al., 2006) as well as GPe neurons (Flandin et al., 2010, Nobrega-Pereira et al., 2010). In the GPe, all prototypical neurons express Lhx6 early in development (Dodson et al., 2015) but it is unclear why there is a subset of neurons that express Lhx6 into adulthood. Therefore, all prototypical neurons, regardless of their expression of PV or Nkx2.1, will have expressed Lhx6 during development. This observation does not conflict with Lhx6 being a marker of a distinct population of neurons in adulthood (Mastro et al., 2014) but rather increases the need to understand the role of homeobox proteins after development. Previous work has indicated the expression of these proteins as critical for the specification and maintenance of cellular phenotypes (Thor et al., 1991).

The expression of Lhx6 in adulthood has been linked to distinct functions within other subcortical nuclei (Choi et al., 2005). Specifically, it was found to represent a population of neurons critical for reproductive behaviors in the amygdala-hypothalamic pathway (Choi et al., 2005). Though there is no evidence to support a similar functional relevance within the GPe, it clearly shows Lhx6 expression in adulthood as a marker for a functional distinct population of neurons. In Chapter 3, Lhx6 suppression is a necessary component for the induction of the motor rescue and therefore defines Lhx6 as a functional relevant population to investigate. Interestingly, the expression of PV and Nkx2.1 has not produced robust functional distinctions within the prototypic populations (Dodson et al., 2015) but their validity as cellular markers is not challenged. Together, the results highlight the complexity of GPe neural processing that will be the focus of many future studies on the interaction of these neural cell-types in health and disease.

Future studies can capitalize on intersection approaches that grant access to each distinct and overlapping subdivision. For example, to assess the differences between PV+/Lhx6-, PV+/Lhx6+ and PV-/Lhx6+, we can breed the newly developed PV-flp (flp-dependent system, in contrast to cre-recombinase) with the Lhx6-cre mouse lines. Utilizing the suite of new viral constructs, you can identify or manipulate each of these cellular divisions and delineate their anatomic and functional contributions. In the years to come, there will be greater opportunities to selectively label neurons across a range of factors and understand how each neuronal cell-type contributes to function.

4.2 MECHANISMS FOR LONG-LASTING THERAPEUTIC INTERVENTION

In Parkinson's disease, patients experience a range of symptoms including primary (bradykinesia, tremor and rigidity) and secondary (freezing and uncontrolled accelerations) motor impairments. Associated with these dysfunctions, firing rates of GPe neurons in Parkinson's patients are severely diminished and the synchrony across cortical and subcortical (especially GPe and STN) brain regions is amplified (Nini et al., 1995, Plenz and Kital, 1999, Raz et al., 2000, Bevan et al., 2002, Levy et al., 2002, Terman et al., 2002). The role of the GPe is unknown but due to anatomic connectivity with all major basal ganglia nuclei, detrimental relationship with the STN (Galvan and Wichmann, 2008, Mallet et al., 2008, Tachibana et al., 2011) and the success of stimulating the GPe during deep brain stimulation (Vitek et al., 1998, Yelnik et al., 2000, Vitek et al., 2004, Vitek et al., 2012), the GPe is believed to be a major player in basal ganglia dysfunction.

The induction of a long-lasting rescue in the motor function of dopamine-depleted mice was dependent on the elevation of the PV-GPe population relative to the Lhx6-GPe. After the successful optogenetic manipulations (PV-ChR2, Lhx6-Arch), pathological activity within the basal ganglia output nucleus was attenuated for hours and hours after stimulation. The following section will explore, in greater detail, the possible mechanisms of induction and how current treatments may be refined or developed to capitalize on the latest findings.

4.2.1 State-Dependent Shifts

Disruptions in the pathological activity are correlated with successful pharmacological and surgical interventions dependent on the continuous administration of selected treatment. As

discussed in the introduction, prolonged usage often lead to negative side effects that impede the treatment of Parkinson's patients. Therefore, identifying the characteristics of the optical manipulation that are necessary for the long-lasting recovery may produce novel therapies that extend well after their administration.

Recently, there have been advancements in the protocols of deep brain stimulation (DBS) that has provided relief not only during stimulation but for days and days afterward in both MPTP primate models (Tass et al., 2012, Wang et al., 2016) and a proof of concept for human PD patients (Adamchic et al., 2014). This new procedure is known as coordinated reset (CR) – DBS and utilizes the four contacts on the DBS electrode to destabilize the network (Figure 4-2A). In theory, traditional DBS, stimulating with all contacts simultaneously within target region, modulates the activity of neurons, astrocytes, and axonal projections that act to break pathological activity only transiently. As shown in Figure 4-2, CR-DBS posits that each lead comes into contact with a unique space in the brain and by electrically stimulating at each contact individually and at set intervals; you are modulating each of the areas independently (Popovich and Tass, 2012). This leads to a desynchronization of the underlying processes that kicks the circuit out of its detrimental rhythm and allows for relief of Parkinsonian deficits.

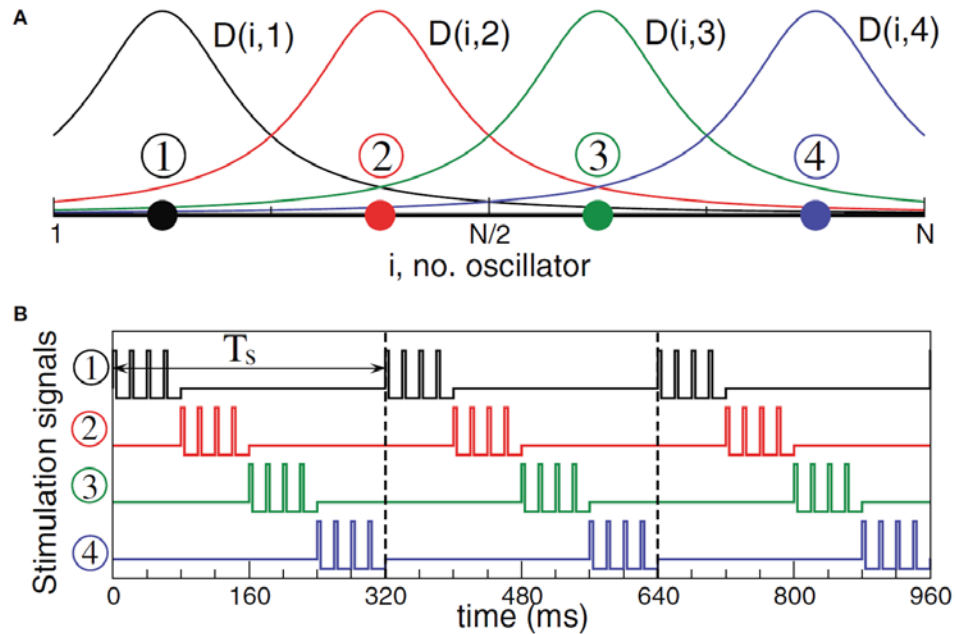


Figure 4-2 Stimulation setup for electrical stimulation.

(A) Schematic localization of four stimulation sites within the neuronal population and the corresponding spatial profiles of current decay in the neuronal tissue with the distance from the stimulation site. (B) Stimulation signals of electrical CR stimulation composed of short pulse trains of charge-balanced pulses. From (Popovych and Tass, 2012) Popovych and Tass (2012), with permission.

This model has many parallels to our recent discovery that cell-type specific but not global manipulations rescue motor function. Global manipulations, either activation or suppression, of GPe activity had no therapeutic benefit and may be due to the lack of desynchronization within the network. This was evident in the recordings of activity within the basal ganglia output nucleus where the percentage of highly ‘bursty’ neurons did not decrease after global GPe activation and in some cases increased shortly after. In contrast, the successful optogenetic manipulations (PV-ChR2, Lhx6-Arch) were able to transiently dissociate activity within the GPe and destabilize the network hours after. Unlike CR-DBS that relies heavily on the spatially distinct populations of neurons, the optogenetic GPe approach utilizes distinct population of neurons that are often interweaved spatially through the GPe.

To achieve dissociation of these neuronal populations without the aid of optogenetics, there are two avenues that are clinically beneficial to follow. Firstly, stereological evidence has

confirmed the presence of PV-GPe neurons in humans at roughly the same percentage as observed in mice and rodents (Hardman and Halliday, 1999). Utilizing drop-seq analysis of RNA expression, there are groups working to understand how these neurons differ from other GPe cell-types. In doing so, this analysis will provide a list of potential targets for drug development that would selectively modulate the activity of these neurons relative to other neuronal populations.

The second avenue may be the refinement of current DBS targeting strategies that capitalize on the potential gradient of PV-GPe neurons that may exist. We found that PV-GPe neurons are enriched within the lateral aspect of the GPe and therefore may contain functionally important differences than other areas. As discussed previously, previous studies have shown that focal activation with the GPe provide distinct alterations to behavior (Matsumura et al., 1995, Grabli et al., 2004). Furthermore, these territories receive distinct sets of inputs from the striatum and STN (Francois et al., 2004). Therefore, further analysis of cell-type specific roles within discrete GPe territories would provide clarity into their functional contributions in health and disease.

4.2.2 STN-Mediated Mechanisms

The STN-GPe complex is implicated in the onset and propagation of harmful synchrony within the Parkinsonian basal ganglia (Bevan et al., 2002). Due to the reciprocity and differences in neurotransmitter (STN: Glutamate, GPe: GABA), the relationship between GPe and STN form a critical node within the basal ganglia in health (Mirzaei et al., 2017) and disease (Bevan et al., 2002, Galvan and Wichmann, 2008, Mallet et al., 2008, Tachibana et al., 2011). Moreover, the synaptic weight and oscillatory tendencies of the GPe and STN are significantly altered in

disease (Plenz and Kital, 1999, Brown et al., 2001, Bevan et al., 2002, Rubin and Terman, 2004, Baufreton et al., 2005, Mallet et al., 2008, Fan et al., 2012, Fujita et al., 2012, Chu et al., 2015).

A recent study revealed a form of heterosynaptic plasticity that strengthens the GPe to STN synapses due to the recruitment of postsynaptic GABA receptors and the enhancement of presynaptic release (Fan et al., 2012, Chu et al., 2015). As discussed in Mastro and Gittis (2015), the heterosynaptic plasticity may act as a homeostatic mechanism that balances the contributions of inhibition and excitation in response to changes in internal (i.e. amount of dopamine, excessive cortical modulation) and external (i.e. learning, development) condition. The mechanism may be engaged over the course of dopamine loss and responsible for compensation that defers the onset of motor deficits until the majority of dopamine is lost. Moreover, upon significant changes pathophysiology, the mechanism is hijacked and becomes highly detrimental to circuit function. Therefore, changes in the GPe-STN relationship that shifts the balance of these two pathways may be responsible for the attenuation of pathological activity that was observed after the successful optogenetic manipulations.

The distinct pattern of STN innervation by PV- and Lhx6-GPe may be a contributing factor for successful induction of behavioral rescue (Mastro et al., 2014). As noted above, the basal ganglia contains parallel circuits that include ‘motor’, ‘limbic’ and ‘associative’ functions and are topographically segregated (Alexander et al., 1986, Middleton and Strick, 2000). While ~80% of GPe neurons project to the STN, subpopulations of GPe neurons innervate the STN differently. PV-GPe neurons project to the full extent of the STN while Lhx6-GPe neurons do not project to the central territory (see Fig. 2-4). This may correspond to the sensorimotor territory of the STN (Parent and Hazrati, 1995). Some evidence was provided indirectly by Chu et al. (2015) where virally-transfected axonal arborization from the motor cortex innervated the

central region of the STN. Baron et al. (2002) found that focal inactivation of the STN or GPi were sufficient to for the amelioration of Parkinsonian motor deficits. Moreover, the targeting of DBS electrodes is most effective within the sensorimotor region of either the STN or GPe (Wichmann and DeLong, 2016). Interestingly, optical activation of afferents to the STN provided a strong amelioration of PD deficits that was not observed upon direct activation of the STN neurons (Gradinaru et al., 2009). Together, these data indicate that modulation of the sensorimotor pathway, irrespective of STN neuronal activation, is sufficient to rescue motor function in animal models of PD.

To assess whether the behavioral induction is altering the GPe-STN network, future experiments should record simultaneously in the GPe and STN during and after the optogenetic manipulation. Secondly, if a form of plasticity is occurring, slices should be prepared shortly after the induction of the behavioral rescue and measured *ex vivo*. Together, these would provide the evidence necessary to implicate the GPe-STN as a critical node in the induction of the long-lasting recovery. If possible and with the advent of optical proteins capable of avoiding back-propagating action potentials, it would be interesting to ask if the excitation of PV-GPe or inhibition of Lhx6-GPe terminals within the STN is sufficient to induce the behavioral rescue.

4.3 FINAL REMARKS

In conclusion, the GPe is complex. It does, like most brain regions, contain a diverse set of cell-types that must be identified, appreciated and incorporated into models of circuit function. Our first contribution was the identification of distinct populations of GPe neurons utilizing transgenic mice. These mice provide an opportunity to exploit the proliferation of tools to

identify and manipulate across experimental conditions. These tools will be used in future studies to gain unparalleled access to GPe's complexity. From measuring the strength and influence of every connection, to identifying cell-type specific forms of plasticity, to perturbing brain and circuit dynamics as you image or record 1000s of identifiable neurons and learn how they respond and adapt; these cell-type delineations will alter the way we understand GPe function.

Our second contribution focused on harnessing these cell-types to treat neurological disorders. This study demonstrates the first evidence for cell-type specific intervention within the GPe that induces a robust and long-lasting recovery of movement. These results provide evidence for the utility of and the need for the development of GPe specific interventions. Although we do not know the mechanism of action, the GPe is a central node for pathological activity during PD (Bergman et al., 1998, Bevan et al., 2002, Kita, 2007, Holgado et al., 2010, Vitek et al., 2012, Corbit et al., 2016). Our data identify PV and Lhx6-GPe neurons as critical nodes within the basal ganglia circuit for the induction of long-lasting attenuation of pathological activity in the SNr. Moving forward, elucidating the cell-type specificity of GPe's influence on circuit function will provide a great benefit to both the basic understanding of basal ganglia function and the GPe's ability to treat neurological disorders.

APPENDIX A

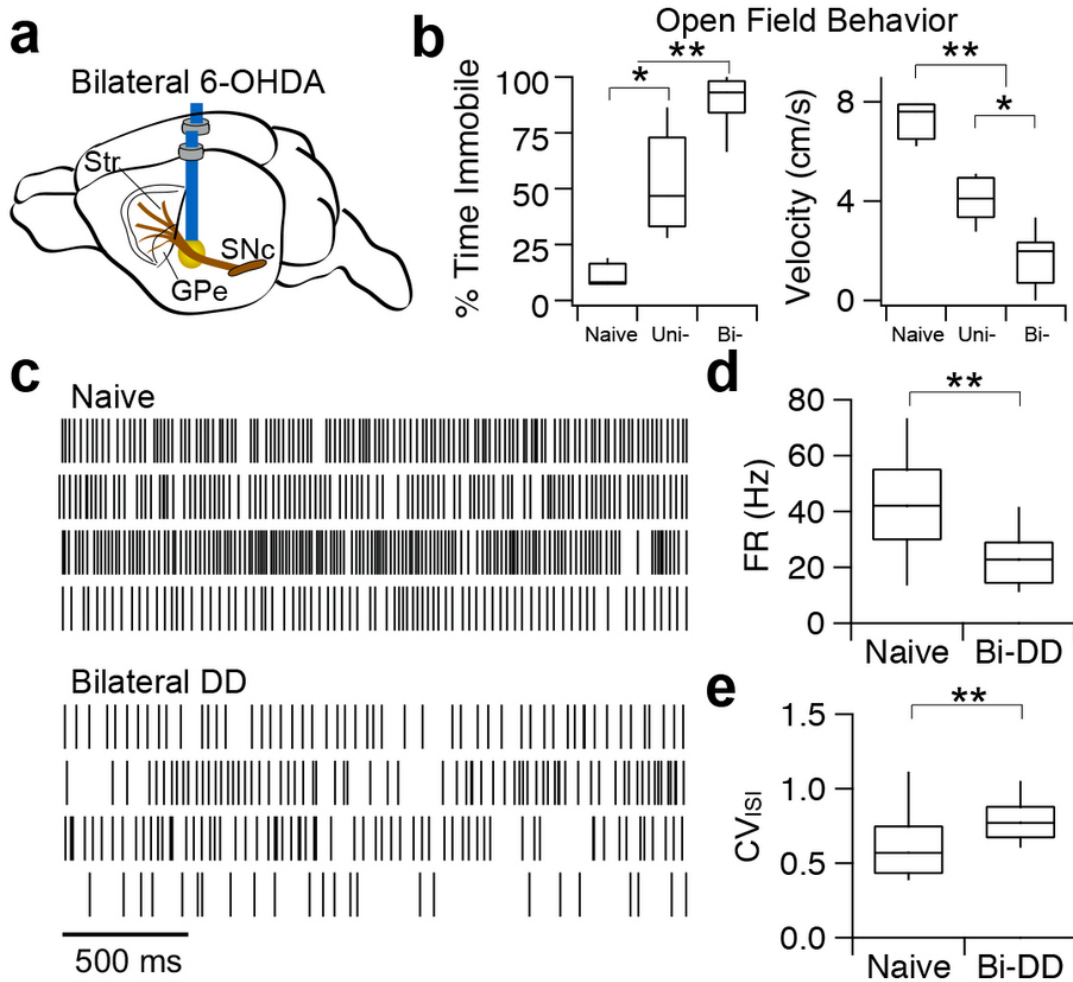


Figure A1 Behavioral and pathophysiological symptoms of bilateral DD are apparent within 3-5 d post-depletion

(a) Schematic of bilateral DD in the medial forebrain bundle (MFB). (b) Quantification of immobility and bradykinesia induced by unilateral (*Uni*, $n = 4$) and bilateral (*Bi*, $n = 51$) depletions, as compared to dopamine-intact controls (*Naive*, $n = 4$). (* $p < 0.02$, ** $p < 0.001$, Mann Whitney U). (c) Rasters of single units in the GPe of naïve vs. bilateral DD mice. Scale bar, 500 ms. (d) Box plots showing decreases in firing rates (Naive: 44.3 ± 2.6 Hz, $n = 73$ across 4 animals, versus Acute: 24.6 ± 1.6 Hz, $n = 62$ across 3 animals, $H(1) = 29.775$, ** $p < 0.001$, Kruskal-Wallis H test) and (e) increases in coefficients of variation of the interspike intervals (CV_{ISI}) (Naïve: 0.63 ± 0.03 versus Acute: 0.80 ± 0.03 , $H(1) = 22.615$, * $p < 0.001$, Kruskal-Wallis H test) following bilateral DD. Error bars, sem.

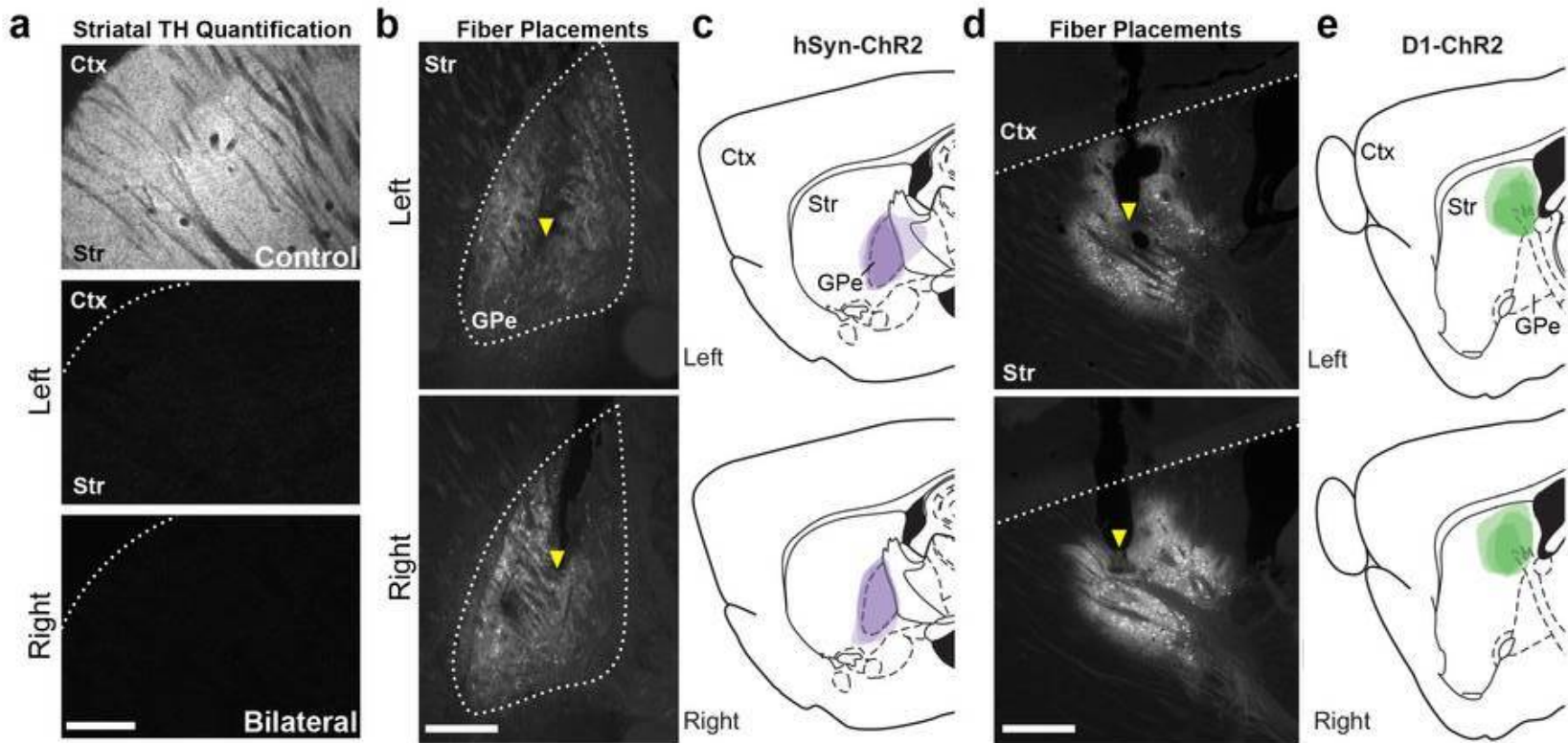


Figure A2 Histological verification of TH immunoreactivity, viral expression and fiber placements for behavioral optogenetics in global manipulations. (a) Representative images of striatal TH immunoreactivity in dorsal striatum of healthy dopamine intact tissue compared to a fully depleted bilateral animal. Scale Bar, 200 μm (b) Epifluorescent images of viral expression and fiber identification (yellow arrow) within the GPe. Scale Bar, 500 μm (c) Superimposed traces of viral expression across animals within hSyn-ChR2 (d) Epifluorescent images of viral expression and fiber identification (yellow arrow) with the dorsal striatum. Scale Bar, 500 μm (e) Superimposed traces of viral expression across animals within D1-ChR2 condition. Ctx = Cortex, Str = Striatum, GPe = globus pallidus externa.

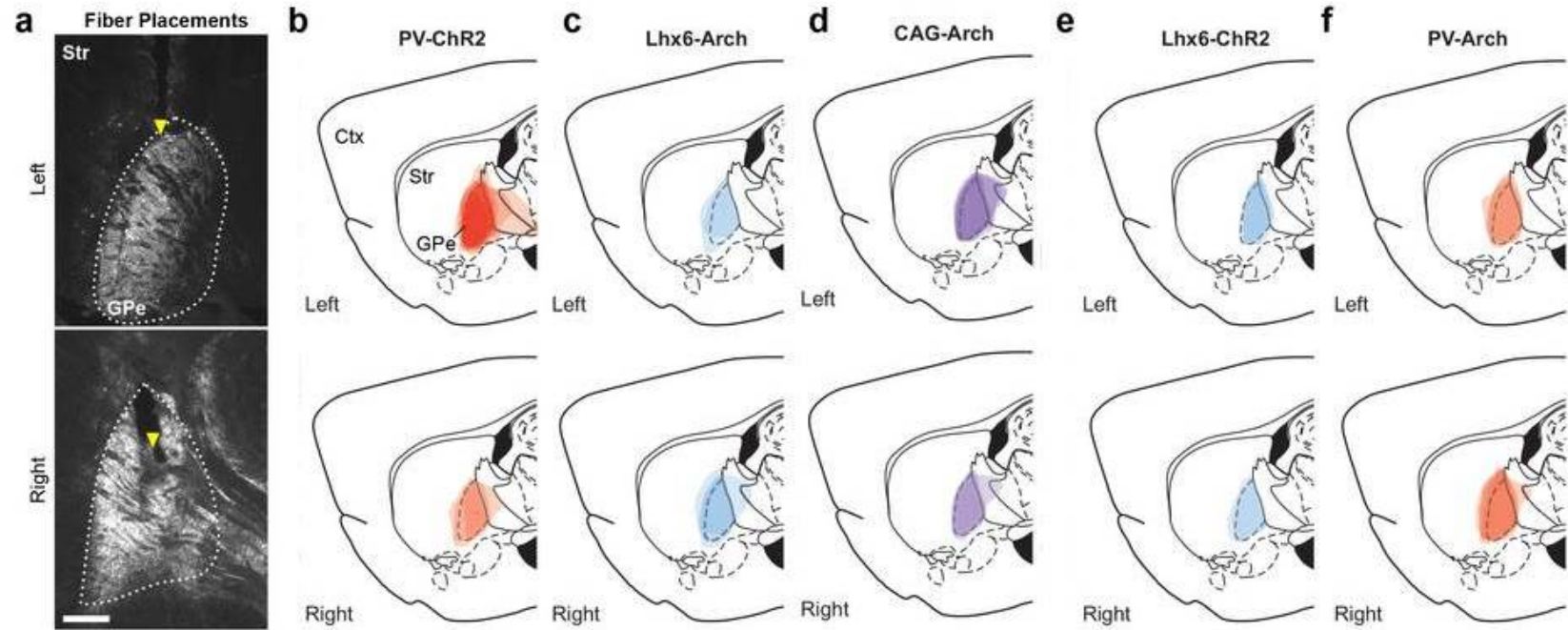


Figure A3 Histological verification of viral expression and fiber placements for behavioral optogenetics in cell-type manipulations.

(a) Epifluorescent images of viral expression and fiber identification (yellow arrow) within the GPe. Scale Bar, 500 μm (b-f) Superimposed traces of viral expression across animals within PV-ChR2, Lhx6-Arch, CAG-Arch, Lhx6-ChR2 and PV-Arch conditions.

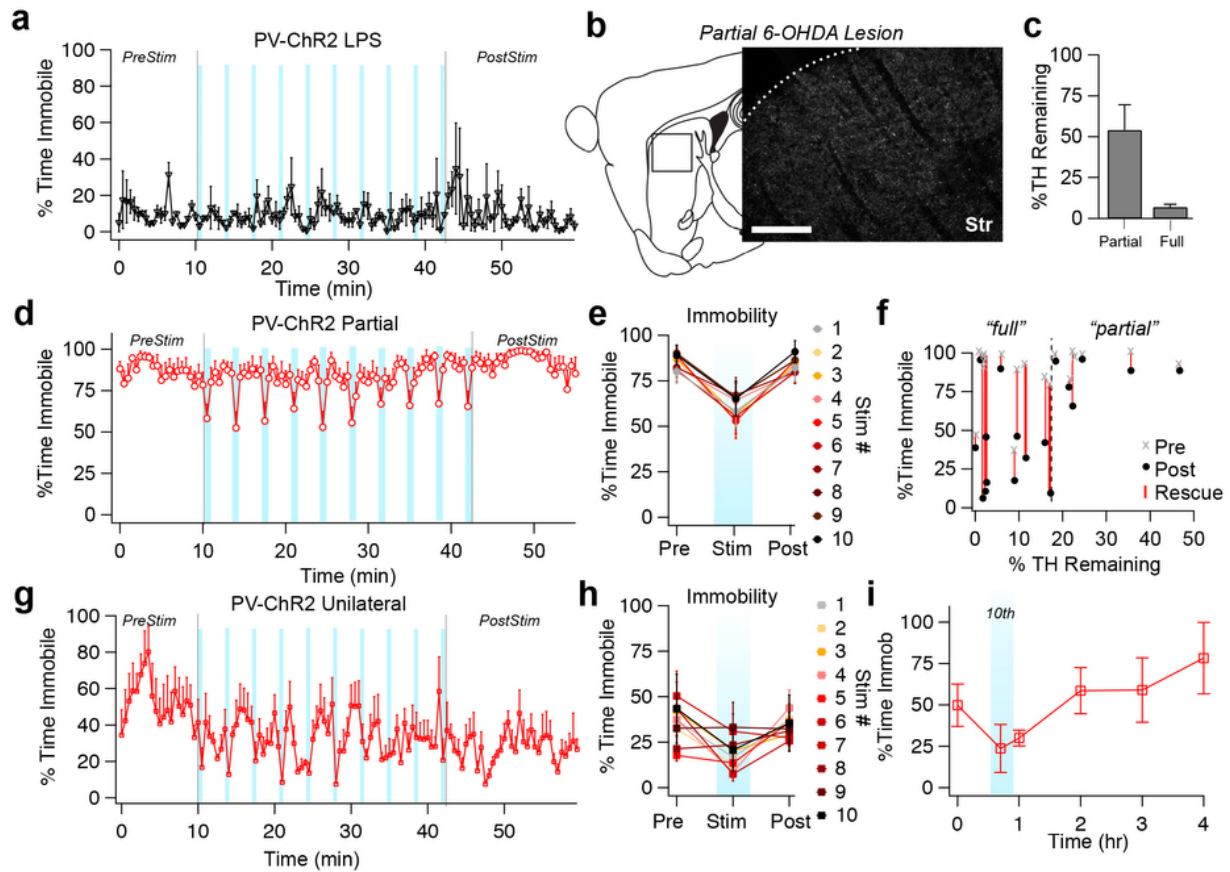


Figure A4 PV-ChR2 stimulation induces transient effects in partially and unilaterally depleted mice.

(a) Percentage of time spent in the immobile state before, during and after PV-ChR2 stimulation in lipopolysaccharide (LPS) injected mice. (b) Schematic representation of striatal location for TH analysis with epifluorescent image of a partial depletion of tyrosine hydroxylase. Scale Bar, 200 μ m. (c) Quantification of TH levels, normalized to dopamine intact littermate and subsequent categorization into partially and fully depleted animals. (d) Percentage of time spent in the immobile state before, during, and after PV-ChR2 stimulation in partially depleted mice. (e) Overlay of immobility immediately before (*pre*), during (*stim*), and after (*post*) each light pulse. (f) Percent time spent immobile for each animal (grey x = *pre*, black circle = *post*) and degree of rescue (red line) as a function of TH remaining. Note sharp cut-off for induction of behavioral rescue at \sim 20% dopamine remaining. (g) Percentage of time spent in the immobile state before, during, and after PV-ChR2 stimulation in unilaterally depleted mice. (h) Overlay of immobility immediately before (*pre*), during (*stim*), and after (*post*) each light pulse. (i) Percent time spent immobile over the course of the full experimental trial. Error bars, sem.

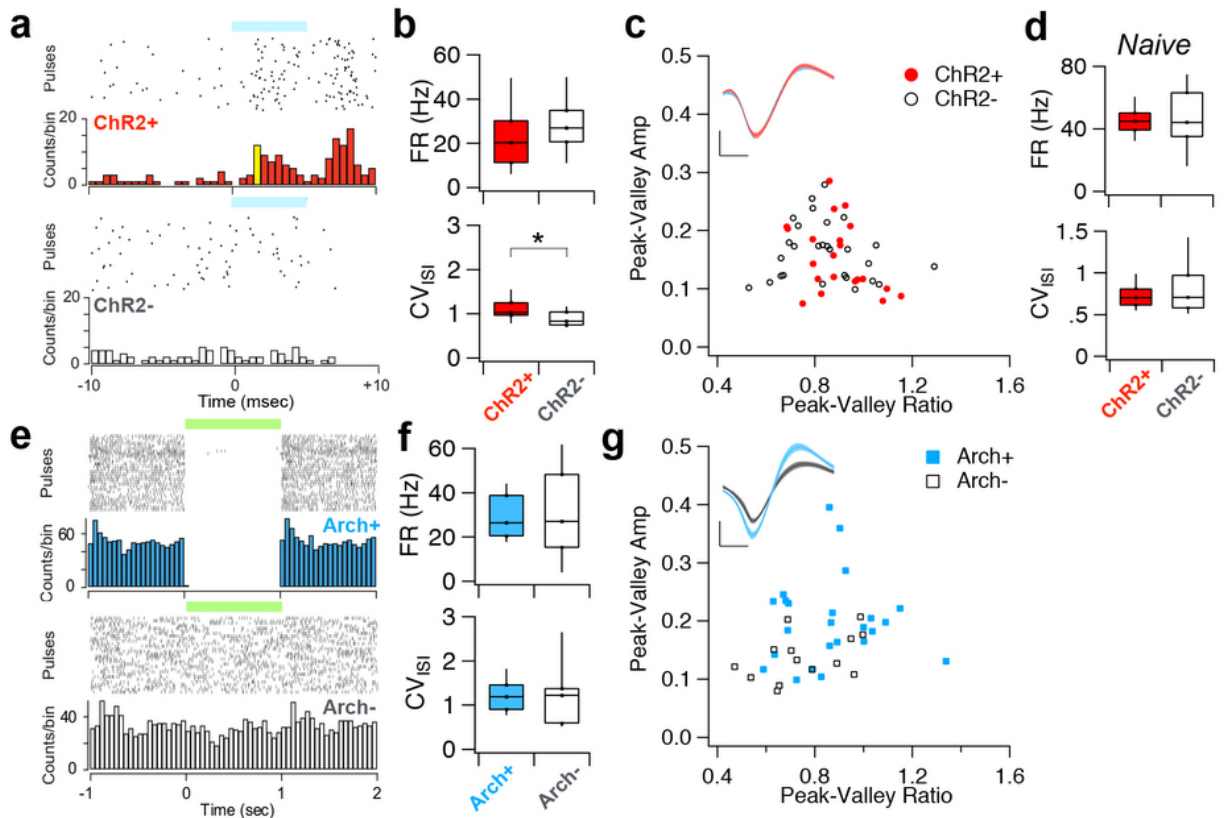


Figure A5 Optical identification using ChR2 and Arch and their corresponding firing properties and waveforms.

(a) Representative responses over 20 trials from a ChR2+ (putative PV) and ChR2- (putative non-PV) neuron responding to 5 ms optical pulses. Yellow bar denotes first significant bin as compared to baseline (b) Firing rate and coefficient of variation of the interspike interval (CV_{ISI}) for ChR2+ and ChR2- neurons in dopamine depleted (FR: $p = 0.128$, CV_{ISI} : $p = 0.005$, Mann Whitney U) (c) Extracellular waveform analysis of the peak-valley ratio and amplitude of individual units identified as ChR2+ (red, closed circles) and ChR2- (black, open circles). Inset: Average waveforms of ChR2+ and ChR2- (Note: nearly complete overlap). Scale bar: 50 μV (vertical), 220 μsec (horizontal) (d) Firing rate and coefficient of variation of the interspike interval (CV_{ISI}) for ChR2+ and ChR2- neurons in dopamine intact animals (Naïve) (e) Representative responses over 20 trials from a Arch+ (putative Lhx6) and Arch- (putative non-Lhx6) neuron responding to 1 s optical pulses. (f) Firing rate and CV_{ISI} for Arch+ and Arch- neurons (FR: $p = 0.990$, CV: $p = 0.454$, Mann Whitney U). (g) Extracellular waveform analysis of the peak-valley ratio and amplitude of individual units identified as Arch+ (blue, closed squares) and Arch- (black, open squares). Inset: Average waveforms of Arch+ and Arch-. Scale bar: 50 μV (vertical), 220 μsec (horizontal).

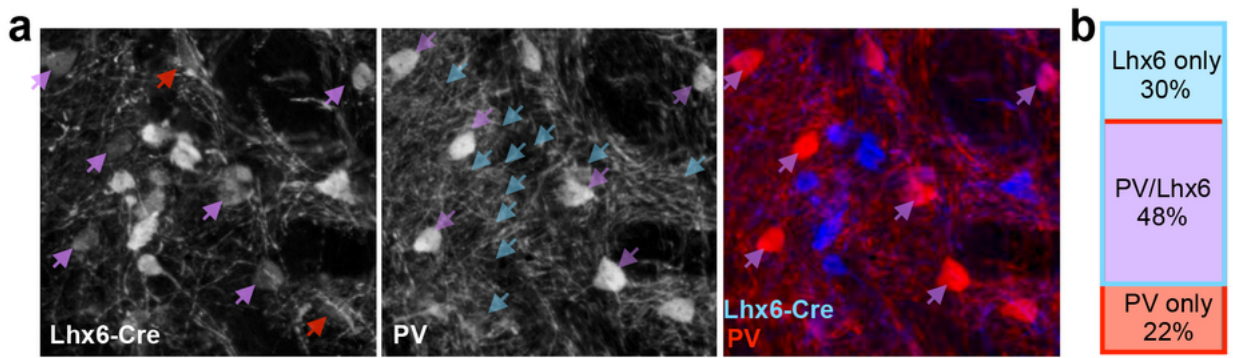


Figure A6 PV and Lhx6 overlap partially in the Lhx6-Cre transgenic mouse.

(a) Fluorescent images from the GPe showing overlap between Lhx6-iCre and PV. Left: Lhx6-EYFP neurons. Arrows denote position of PV+ neurons (Purple arrows: Lhx6/PV double labeled; Red arrows: PV-only neurons). Note weaker Lhx6-EYFP expression in Lhx6/PV neurons. Middle: PV+ neurons (Blue arrows: Lhx6-only neurons). Right: Overlay. (b) Box diagram summarizing the proportion of GPe neurons (n = 4194 total neurons across 5 animals) counted that expressed either PV, Lhx6, or both.

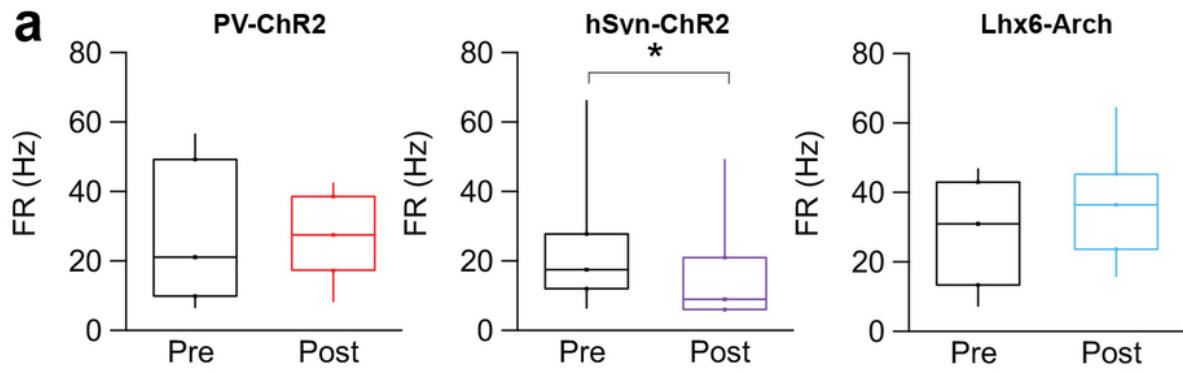


Figure A7 SNr firing rate is unaltered after PV-ChR2 and Lhx6-Arch, but decreased after hSyn-ChR2 manipulation.

(a) Firing rate of single units collected before (pre) and after (post) stimulation in PV-ChR2 ($n_{\text{Pre}} = 80$ vs $n_{\text{Post}} = 58$ units across 3 animals, $p = 0.976$, Mann Whitney U), hSYn-ChR2 ($n_{\text{Pre}} = 55$ vs $n_{\text{Post}} = 69$ unit across 3 animals, $p = 0.002$, Mann Whitney U) and Lhx6-Arch ($n_{\text{Pre}} = 30$ vs $n_{\text{Post}} = 69$ units across 3 animals, $p = 0.142$, Mann Whitney U).

APPENDIX B

Figure B1 Video 1: [PV-ChR2 fast speed](#)

Accelerated recording of a representative PV-ChR2 animal throughout the course of stimulation
http://www.nature.com/neuro/journal/v20/n6/fig_tab/nn.4559_SV1.html

Figure B2 Video 2: [PV-ChR2 HD](#)

High Definition recording of PV-ChR2 condition with representative clips from early stimulation, late stimulation and hours after stimulation.
http://www.nature.com/neuro/journal/v20/n6/fig_tab/nn.4559_SV2.html

Figure B3 Video 3: [Lhx6-Arch fast speed](#)

Accelerated recording of a representative Lhx6-Arch animal throughout the course of stimulation
http://www.nature.com/neuro/journal/v20/n6/fig_tab/nn.4559_SV3.html

Figure B4 Video 4: [Lhx6-Arch HD](#)

High Definition recording of Lhx6-Arch condition with representative clips from early stimulation, late stimulation and hours after stimulation.
http://www.nature.com/neuro/journal/v20/n6/fig_tab/nn.4559_SV4.html

BIBLIOGRAPHY

- Abdi A, Mallet N, Mohamed FY, Sharott A, Dodson PD, Nakamura KC, Suri S, Avery SV, Larvin JT, Garas FN, Garas SN, Vinciati F, Morin S, Bezard E, Baufreton J, Magill PJ (2015) Prototypic and arkypallidal neurons in the dopamine-intact external globus pallidus. *J Neurosci* 35:6667-6688.
- Adamchic I, Hauptmann C, Barnikol UB, Pawelczyk N, Popovych O, Barnikol TT, Silchenko A, Volkmann J, Deuschl G, Meissner WG, Maarouf M, Sturm V, Freund HJ, Tass PA (2014) Coordinated reset neuromodulation for Parkinson's disease: proof-of-concept study. *Movement disorders : official journal of the Movement Disorder Society* 29:1679-1684.
- Albin RL, Young AB, Penney JB (1989) The functional anatomy of basal ganglia disorders. *Trends Neurosci* 12:366-375.
- Alexander GE, Crutcher MD (1990) Functional architecture of basal ganglia circuits: neural substrates of parallel processing. *Trends Neurosci* 13:266-271.
- Alexander GE, DeLong MR, Strick PL (1986) Parallel organization of functionally segregated circuits linking basal ganglia and cortex. *Annual review of neuroscience* 9:357-381.
- Bar-Gad I, Elias S, Vaadia E, Bergman H (2004) Complex locking rather than complete cessation of neuronal activity in the globus pallidus of a 1-methyl-4-phenyl-1,2,3,6-tetrahydropyridine-treated primate in response to pallidal microstimulation. *J Neurosci* 24:7410-7419.
- Baron MS, Wichmann T, Ma D, DeLong MR (2002) Effects of transient focal inactivation of the basal ganglia in parkinsonian primates. *J Neurosci* 22:592-599.
- Baufreton J, Atherton JF, Surmeier DJ, Bevan MD (2005) Enhancement of excitatory synaptic integration by GABAergic inhibition in the subthalamic nucleus. *J Neurosci* 25:8505-8517.
- Beckstead R (1988) Association of dopamine d₁ and d₂ receptors with specific cellular elements in the basal ganglia of the cat: The uneven topography of dopamine receptors in the striatum is determined by intrinsic striatal cells, not nigrostriatal axons. *Neuroscience* 27:851-863.
- Beier KT, Steinberg EE, DeLoach KE, Xie S, Miyamichi K, Schwarz L, Gao XJ, Kremer EJ, Malenka RC, Luo L (2015) Circuit Architecture of VTA Dopamine Neurons Revealed by Systematic Input-Output Mapping. *Cell* 162:622-634.

- Benhamou L, Bronfeld M, Bar-Gad I, Cohen D (2012) Globus Pallidus external segment neuron classification in freely moving rats: a comparison to primates. *PLoS one* 7:e45421.
- Bergman H, Feingold A, Nini A, Raz A, Slovin H, Abeles M, Vaadia E (1998) Physiological aspects of information processing in the basal ganglia of normal and parkinsonian primates. *Trends Neurosci* 21:32-38.
- Bergman H, Wichmann T, Karmon B, DeLong MR (1994) The primate subthalamic nucleus. II. Neuronal activity in the MPTP model of parkinsonism. *Journal of neurophysiology* 72:507-520.
- Bernheimer H, Birkmayer W, Hornykiewicz O, Jellinger K, Seitelberger F (1973) Brain dopamine and the syndromes of Parkinson and Huntington. Clinical, morphological and neurochemical correlations. *J Neurol Sci* 20:415-455.
- Betarbet R, Sherer TB, Greenamyre JT (2002) Animal models of Parkinson's disease. *Bioessays* 24:308-318.
- Bevan MD, Booth PA, Eaton SA, Bolam JP (1998) Selective innervation of neostriatal interneurons by a subclass of neuron in the globus pallidus of the rat. *The Journal of neuroscience* 18:9438-9452.
- Bevan MD, Magill PJ, Terman D, Bolam JP, Wilson CJ (2002) Move to the rhythm: oscillations in the subthalamic nucleus-external globus pallidus network. *Trends Neurosci* 25:525-531.
- Bjorklund A, Dunnett SB (2007) Dopamine neuron systems in the brain: an update. *Trends Neurosci* 30:194-202.
- Brown P, Oliviero A, Mazzone P, Insola A, Tonali P, Di Lazzaro V (2001) Dopamine dependency of oscillations between subthalamic nucleus and pallidum in Parkinson's disease. *J Neurosci* 21:1033-1038.
- Brownstein MJ, Mroz EA, Tappaz ML, Leeman SE (1977) On the origin of substance P and glutamic acid decarboxylase (GAD) in the substantia nigra. *Brain research* 135:315-323.
- Bugaysen J, Bar-Gad I, Korngreen A (2011) The impact of stimulation induced short-term synaptic plasticity on firing patterns in the globus pallidus of the rat. *Frontiers in systems neuroscience* 5:16.
- Calabresi P, Picconi B, Tozzi A, Ghiglieri V, Di Filippo M (2014) Direct and indirect pathways of basal ganglia: a critical reappraisal. *Nature neuroscience* 17:1022-1030.
- Cayal Ry (1888) Estructura de los centros nerviosos de las aves. *Rev Trim Histol Norm* 1:1-10.
- Cepeda C, Andre VM, Yamazaki I, Wu N, Kleiman-Weiner M, Levine MS (2008) Differential electrophysiological properties of dopamine D1 and D2 receptor-containing striatal medium-sized spiny neurons. *Eur J Neurosci* 27:671-682.
- Chan CS, Glajch KE, Gertler TS, Guzman JN, Mercer JN, Lewis AS, Goldberg AB, Tkatch T, Shigemoto R, Fleming SM, Chetkovich DM, Osten P, Kita H, Surmeier DJ (2011) HCN channelopathy in external globus pallidus neurons in models of Parkinson's disease. *Nature neuroscience* 14:85-92.
- Chan CS, Shigemoto R, Mercer JN, Surmeier DJ (2004) HCN2 and HCN1 channels govern the regularity of autonomous pacemaking and synaptic resetting in globus pallidus neurons. *The Journal of neuroscience* 24:9921-9932.
- Chattopadhyaya B, Di Cristo G, Higashiyama H, Knott GW, Kuhlman SJ, Welker E, Huang ZJ (2004) Experience and activity-dependent maturation of perisomatic GABAergic innervation in primary visual cortex during a postnatal critical period. *J Neurosci* 24:9598-9611.

- Chin GD, Hutchison WD (2008) Effects of cobalt and bicuculline on focal microstimulation of rat pallidal neurons in vivo. *Brain stimulation* 1:134-150.
- Choi GB, Dong H-w, Murphy AJ, Valenzuela DM, Yancopoulos GD, Swanson LW, Anderson DJ (2005) Lhx6 delineates a pathway mediating innate reproductive behaviors from the amygdala to the hypothalamus. *Neuron* 46:647-660.
- Chu HY, Atherton JF, Wokosin D, Surmeier DJ, Bevan MD (2015) Heterosynaptic regulation of external globus pallidus inputs to the subthalamic nucleus by the motor cortex. *Neuron* 85:364-376.
- Cobos I, Long JE, Thwin MT, Rubenstein JL (2006) Cellular patterns of transcription factor expression in developing cortical interneurons. *Cereb Cortex* 16 Suppl 1:i82-88.
- Cooper AJ, Stanford IM (2000) Electrophysiological and morphological characteristics of three subtypes of rat globus pallidus neurone in vitro. *The Journal of physiology* 527 Pt 2:291-304.
- Corbit VL, Whalen TC, Zitelli KT, Crilly SY, Rubin JE, Gittis AH (2016) Pallidostriatal Projections Promote beta Oscillations in a Dopamine-Depleted Biophysical Network Model. *J Neurosci* 36:5556-5571.
- Cui G, Jun SB, Jin X, Pham MD, Vogel SS, Lovinger DM, Costa RM (2013) Concurrent activation of striatal direct and indirect pathways during action initiation. *Nature* 494:238-242.
- Day M, Wokosin D, Plotkin JL, Tian X, Surmeier DJ (2008) Differential excitability and modulation of striatal medium spiny neuron dendrites. *J Neurosci* 28:11603-11614.
- Deister CA, Chan CS, Surmeier DJ, Wilson CJ (2009) Calcium-activated SK channels influence voltage-gated ion channels to determine the precision of firing in globus pallidus neurons. *J Neurosci* 29:8452-8461.
- Deister CA, Dodla R, Barraza D, Kita H, Wilson CJ (2013) Firing rate and pattern heterogeneity in the globus pallidus arise from a single neuronal population. *Journal of neurophysiology* 109:497-506.
- DeLong MR (1971) Activity of pallidal neurons during movement. *Journal of neurophysiology* 34:414-427.
- DeLong MR (1983) The neurophysiologic basis of abnormal movements in basal ganglia disorders. *Neurobehav Toxicol Teratol* 5:611-616.
- DeLong MR (1990) Primate models of movement disorders of basal ganglia origin. *Trends Neurosci* 13:281-285.
- DeLong MR, Crutcher MD, Georgopoulos AP (1985) Primate Globus Pallidus and Subthalamic Nucleus - Functional-Organization. *J Neurophysiol* 53:530-543.
- Deumens R, Blokland A, Prickaerts J (2002) Modeling Parkinson's disease in rats: an evaluation of 6-OHDA lesions of the nigrostriatal pathway. *Experimental neurology* 175:303-317.
- Dodson PD, Larvin JT, Duffell JM, Garas FN, Doig NM, Kessar N, Duguid IC, Bogacz R, Butt SJ, Magill PJ (2015) Distinct developmental origins manifest in the specialized encoding of movement by adult neurons of the external globus pallidus. *Neuron* 86:501-513.
- Erez Y, Czitron H, McCairn K, Belevsky K, Bar-Gad I (2009) Short-term depression of synaptic transmission during stimulation in the globus pallidus of 1-methyl-4-phenyl-1,2,3,6-tetrahydropyridine-treated primates. *J Neurosci* 29:7797-7802.
- Eshel N, Tian J, Bukwich M, Uchida N (2016) Dopamine neurons share common response function for reward prediction error. *Nature neuroscience* 19:479-486.

- Fahn S (2003) Description of Parkinson's disease as a clinical syndrome. *Annals of the New York Academy of Sciences* 991:1-14.
- Fan KY, Baufreton J, Surmeier DJ, Chan CS, Bevan MD (2012) Proliferation of external globus pallidus-subthalamic nucleus synapses following degeneration of midbrain dopamine neurons. *The Journal of Neuroscience* 32:13718-13728.
- Flandin P, Kimura S, Rubenstein JL (2010) The progenitor zone of the ventral medial ganglionic eminence requires Nkx2-1 to generate most of the globus pallidus but few neocortical interneurons. *J Neurosci* 30:2812-2823.
- Fogarty M, Grist M, Gelman D, Marin O, Pachnis V, Kessar N (2007) Spatial genetic patterning of the embryonic neuroepithelium generates GABAergic interneuron diversity in the adult cortex. *J Neurosci* 27:10935-10946.
- Francois C, Grabli D, McCairn K, Jan C, Karachi C, Hirsch EC, Feger J, Tremblay L (2004) Behavioural disorders induced by external globus pallidus dysfunction in primates II. Anatomical study. *Brain : a journal of neurology* 127:2055-2070.
- Fujita T, Fukai T, Kitano K (2012) Influences of membrane properties on phase response curve and synchronization stability in a model globus pallidus neuron. *J Comput Neurosci* 32:539-553.
- Gage GJ, Stoetzer CR, Wiltschko AB, Berke JD (2010) Selective activation of striatal fast-spiking interneurons during choice execution. *Neuron* 67:466-479.
- Galvan A, Devergnas A, Pittard D, Masilamoni G, Vuong J, Daniels JS, Morrison RD, Lindsley CW, Wichmann T (2016) Lack of Antiparkinsonian Effects of Systemic Injections of the Specific T-Type Calcium Channel Blocker ML218 in MPTP-Treated Monkeys. *ACS chemical neuroscience* 7:1543-1551.
- Galvan A, Wichmann T (2008) Pathophysiology of parkinsonism. *Clin Neurophysiol* 119:1459-1474.
- Gerfen CR, Engber TM, Mahan LC, Susel Z, Chase TN, Monsma FJ, Jr., Sibley DR (1990) D1 and D2 dopamine receptor-regulated gene expression of striatonigral and striatopallidal neurons. *Science* 250:1429-1432.
- Gerfen CR, Surmeier DJ (2011) Modulation of striatal projection systems by dopamine. *Annual review of neuroscience* 34:441-466.
- Gertler TS, Chan CS, Surmeier DJ (2008) Dichotomous anatomical properties of adult striatal medium spiny neurons. *J Neurosci* 28:10814-10824.
- Gittis AH, Berke JD, Bevan MD, Chan CS, Mallet N, Morrow MM, Schmidt R (2014) New roles for the external globus pallidus in basal ganglia circuits and behavior. *J Neurosci* 34:15178-15183.
- Glajch KE, Kelder DA, Hegeman DJ, Cui Q, Xenias HS, Augustine EC, Hernandez VM, Verma N, Huang TY, Luo M, Justice NJ, Chan CS (2016) Npas1+ Pallidal Neurons Target Striatal Projection Neurons. *J Neurosci* 36:5472-5488.
- Goff LK, Jouve L, Melon C, Salin P (2009) Rationale for targeting the thalamic centre-median parafascicular complex in the surgical treatment of Parkinson's disease. *Parkinsonism & related disorders* 15 Suppl 3:S167-170.
- Gong S, Doughty M, Harbaugh CR, Cummins A, Hatten ME, Heintz N, Gerfen CR (2007) Targeting Cre recombinase to specific neuron populations with bacterial artificial chromosome constructs. *J Neurosci* 27:9817-9823.

- Grabli D, McCairn K, Hirsch EC, Agid Y, Feger J, Francois C, Tremblay L (2004) Behavioural disorders induced by external globus pallidus dysfunction in primates: I. Behavioural study. *Brain : a journal of neurology* 127:2039-2054.
- Gradinaru V, Mogri M, Thompson KR, Henderson JM, Deisseroth K (2009) Optical deconstruction of parkinsonian neural circuitry. *Science* 324:354-359.
- Gunay C, Edgerton JR, Jaeger D (2008) Channel density distributions explain spiking variability in the globus pallidus: a combined physiology and computer simulation database approach. *J Neurosci* 28:7476-7491.
- Haber SN, Fudge JL, McFarland NR (2000) Striatonigrostriatal pathways in primates form an ascending spiral from the shell to the dorsolateral striatum. *J Neurosci* 20:2369-2382.
- Hammond C, Bergman H, Brown P (2007) Pathological synchronization in Parkinson's disease: networks, models and treatments. *Trends Neurosci* 30:357-364.
- Hardman CD, Halliday GM (1999) The external globus pallidus in patients with Parkinson's disease and progressive supranuclear palsy. *Movement disorders : official journal of the Movement Disorder Society* 14:626-633.
- Hausser MA, Yung WH (1994) Inhibitory synaptic potentials in guinea-pig substantia nigra dopamine neurones in vitro. *The Journal of physiology* 479 (Pt 3):401-422.
- Hazrati LN, Parent A (1991) Projection from the external pallidum to the reticular thalamic nucleus in the squirrel monkey. *Brain research* 550:142-146.
- He Z, Han D, Efimova O, Guijarro P, Yu Q, Oleksiak A, Jiang S, Anokhin K, Velichkovsky B, Grunewald S, Khaitovich P (2017) Comprehensive transcriptome analysis of neocortical layers in humans, chimpanzees and macaques. *Nature neuroscience*.
- Hegeman DJ, Hong ES, Hernandez VM, Chan CS (2016) The external globus pallidus: progress and perspectives. *Eur J Neurosci* 43:1239-1265.
- Hernandez VM, Hegeman DJ, Cui Q, Kelver DA, Fiske MP, Glajch KE, Pitt JE, Huang TY, Justice NJ, Chan CS (2015) Parvalbumin+ Neurons and Npas1+ Neurons Are Distinct Neuron Classes in the Mouse External Globus Pallidus. *J Neurosci* 35:11830-11847.
- Herrera AJ, Castano A, Venero JL, Cano J, Machado A (2000) The single intranigral injection of LPS as a new model for studying the selective effects of inflammatory reactions on dopaminergic system. *Neurobiology of disease* 7:429-447.
- Holgado AJ, Terry JR, Bogacz R (2010) Conditions for the generation of beta oscillations in the subthalamic nucleus-globus pallidus network. *J Neurosci* 30:12340-12352.
- Hoover BR, Marshall JF (1999) Population characteristics of preproenkephalin mRNA-containing neurons in the globus pallidus of the rat. *Neuroscience letters* 265:199-202.
- Hoover BR, Marshall JF (2002) Further characterization of preproenkephalin mRNA-containing cells in the rodent globus pallidus. *Neuroscience* 111:111-125.
- Houser CR, Vaughn JE, Barber RP, Roberts E (1980) GABA neurons are the major cell type of the nucleus reticularis thalami. *Brain research* 200:341-354.
- Jaeger D, Gilman S, Aldridge JW (1995) Neuronal activity in the striatum and pallidum of primates related to the execution of externally cued reaching movements. *Brain research* 694:111-127.
- Johnson MD, Zhang J, Ghosh D, McIntyre CC, Vitek JL (2012) Neural targets for relieving parkinsonian rigidity and bradykinesia with pallidal deep brain stimulation. *Journal of neurophysiology* 108:567-577.
- Jorgenson LA, Newsome WT, Anderson DJ, Bargmann CI, Brown EN, Deisseroth K, Donoghue JP, Hudson KL, Ling GS, MacLeish PR, Marder E, Normann RA, Sanes JR, Schnitzer

- MJ, Sejnowski TJ, Tank DW, Tsien RY, Ugurbil K, Wingfield JC (2015) The BRAIN Initiative: developing technology to catalyse neuroscience discovery. *Philos Trans R Soc Lond B Biol Sci* 370.
- Kelland MD, Soltis RP, Anderson LA, Bergstrom DA, Walters JR (1995) In vivo characterization of two cell types in the rat globus pallidus which have opposite responses to dopamine receptor stimulation: comparison of electrophysiological properties and responses to apomorphine, dizocilpine, and ketamine anesthesia. *Synapse* 20:338-350.
- Kelley AE (2004) Ventral striatal control of appetitive motivation: role in ingestive behavior and reward-related learning. *Neurosci Biobehav R* 27:765-776.
- Kincaid AE, Penney JB, Young AB, Newman SW (1991) The Globus-Pallidus Receives a Projection from the Parafascicular Nucleus in the Rat. *Brain Res* 553:18-26.
- Kita H (1994) Parvalbumin-immunopositive neurons in rat globus pallidus: a light and electron microscopic study. *Brain Res* 657:31-41.
- Kita H (2007) Globus pallidus external segment. *Progress in brain research* 160:111-133.
- Kita H, Kitai ST (1991) Intracellular Study of Rat Globus-Pallidus Neurons - Membrane-Properties and Responses to Neostriatal, Subthalamic and Nigral Stimulation. *Brain Res* 564:296-305.
- Kita H, Kitai ST (1994) The Morphology of Globus-Pallidus Projection Neurons in the Rat - an Intracellular Staining Study. *Brain Res* 636:308-319.
- Kita H, Tokuno H, Nambu A (1999) Monkey globus pallidus external segment neurons projecting to the neostriatum. *Neuroreport* 10:1467-1472.
- Kodama T, Guerrero S, Shin M, Moghadam S, Faulstich M, du Lac S (2012) Neuronal classification and marker gene identification via single-cell expression profiling of brainstem vestibular neurons subserving cerebellar learning. *J Neurosci* 32:7819-7831.
- Krauss JK, Pohle T, Weigel R, Burgunder JM (2002) Deep brain stimulation of the centre median-parafascicular complex in patients with movement disorders. *Journal of neurology, neurosurgery, and psychiatry* 72:546-548.
- Kravitz AV, Freeze BS, Parker PR, Kay K, Thwin MT, Deisseroth K, Kreitzer AC (2010) Regulation of parkinsonian motor behaviours by optogenetic control of basal ganglia circuitry. *Nature* 466:622-626.
- Kravitz AV, Kreitzer AC (2011) Optogenetic manipulation of neural circuitry in vivo. *Current opinion in neurobiology* 21:433-439.
- Kravitz AV, Owen SF, Kreitzer AC (2013) Optogenetic identification of striatal projection neuron subtypes during in vivo recordings. *Brain research* 1511:21-32.
- Kreitzer AC, Malenka RC (2007) Endocannabinoid-mediated rescue of striatal LTD and motor deficits in Parkinson's disease models. *Nature* 445:643-647.
- Kreitzer AC, Malenka RC (2008) Striatal plasticity and basal ganglia circuit function. *Neuron* 60:543-554.
- Kuhn AA, Kupsch A, Schneider GH, Brown P (2006) Reduction in subthalamic 8-35 Hz oscillatory activity correlates with clinical improvement in Parkinson's disease. *Eur J Neurosci* 23:1956-1960.
- Lammel S, Ion DI, Roeper J, Malenka RC (2011) Projection-specific modulation of dopamine neuron synapses by aversive and rewarding stimuli. *Neuron* 70:855-862.

- Lavoie B, Smith Y, Parent A (1989) Dopaminergic innervation of the basal ganglia in the squirrel monkey as revealed by tyrosine hydroxylase immunohistochemistry. *The Journal of comparative neurology* 289:36-52.
- Lerner TN, Shilyansky C, Davidson TJ, Evans KE, Beier KT, Zalocusky KA, Crow AK, Malenka RC, Luo L, Tomer R, Deisseroth K (2015) Intact-Brain Analyses Reveal Distinct Information Carried by SNc Dopamine Subcircuits. *Cell* 162:635-647.
- Lerner TN, Ye L, Deisseroth K (2016) Communication in Neural Circuits: Tools, Opportunities, and Challenges. *Cell* 164:1136-1150.
- Levy R, Hutchison WD, Lozano AM, Dostrovsky JO (2002) Synchronized neuronal discharge in the basal ganglia of parkinsonian patients is limited to oscillatory activity. *J Neurosci* 22:2855-2861.
- Lopez-Munoz F, Boya J, Alamo C (2006) Neuron theory, the cornerstone of neuroscience, on the centenary of the Nobel Prize award to Santiago Ramon y Cajal. *Brain research bulletin* 70:391-405.
- Lozano AM, Lang AE, Levy R, Hutchison W, Dostrovsky J (2000) Neuronal recordings in Parkinson's disease patients with dyskinesias induced by apomorphine. *Annals of neurology* 47:S141-146.
- Macosko EZ, Basu A, Satija R, Nemesh J, Shekhar K, Goldman M, Tirosh I, Bialas AR, Kamitaki N, Martersteck EM, Trombetta JJ, Weitz DA, Sanes JR, Shalek AK, Regev A, McCarroll SA (2015) Highly Parallel Genome-wide Expression Profiling of Individual Cells Using Nanoliter Droplets. *Cell* 161:1202-1214.
- Madisen L, Zwingman TA, Sunkin SM, Oh SW, Zariwala HA, Gu H, Ng LL, Palmiter RD, Hawrylycz MJ, Jones AR, Lein ES, Zeng H (2010) A robust and high-throughput Cre reporting and characterization system for the whole mouse brain. *Nature neuroscience* 13:133-140.
- Magill PJ, Bolam JP, Bevan MD (2001) Dopamine regulates the impact of the cerebral cortex on the subthalamic nucleus-globus pallidus network. *Neuroscience* 106:313-330.
- Mallet N, Micklem BR, Henny P, Brown MT, Williams C, Bolam JP, Nakamura KC, Magill PJ (2012) Dichotomous organization of the external globus pallidus. *Neuron* 74:1075-1086.
- Mallet N, Pogosyan A, Marton LF, Bolam JP, Brown P, Magill PJ (2008) Parkinsonian beta oscillations in the external globus pallidus and their relationship with subthalamic nucleus activity. *J Neurosci* 28:14245-14258.
- Mallet N, Schmidt R, Leventhal D, Chen F, Amer N, Boraud T, Berke JD (2016) Arkypallidal Cells Send a Stop Signal to Striatum. *Neuron* 89:308-316.
- Marin O, Anderson SA, Rubenstein JL (2000) Origin and molecular specification of striatal interneurons. *J Neurosci* 20:6063-6076.
- Mastro KJ, Bouchard RS, Holt HA, Gittis AH (2014) Transgenic mouse lines subdivide external segment of the globus pallidus (GPe) neurons and reveal distinct GPe output pathways. *J Neurosci* 34:2087-2099.
- Mastro KJ, Gittis AH (2015) Striking the right balance: cortical modulation of the subthalamic nucleus-globus pallidus circuit. *Neuron* 85:233-235.
- Mastro KJ, Zitelli KT, Willard AM, Leblanc KH, Kravitz AV, Gittis AH (2017) Cell-specific pallidal intervention induces long-lasting motor recovery in dopamine-depleted mice. *Nature neuroscience*.

- Matsumoto N, Minamimoto T, Graybiel AM, Kimura M (2001) Neurons in the thalamic CM-Pf complex supply striatal neurons with information about behaviorally significant sensory events. *Journal of neurophysiology* 85:960-976.
- Matsumura M, Tremblay L, Richard H, Filion M (1995) Activity of pallidal neurons in the monkey during dyskinesia induced by injection of bicuculline in the external pallidum. *Neuroscience* 65:59-70.
- Menegas W, Bergan JF, Ogawa SK, Isogai Y, Umadevi Venkataraju K, Osten P, Uchida N, Watabe-Uchida M (2015) Dopamine neurons projecting to the posterior striatum form an anatomically distinct subclass. *Elife* 4:e10032.
- Mercer JN, Chan CS, Tkatch T, Held J, Surmeier DJ (2007) Nav1.6 sodium channels are critical to pacemaking and fast spiking in globus pallidus neurons. *J Neurosci* 27:13552-13566.
- Middleton FA, Strick PL (2000) Basal ganglia and cerebellar loops: motor and cognitive circuits. *Brain Res Rev* 31:236-250.
- Minamimoto T, Kimura M (2002) Participation of the thalamic CM-Pf complex in attentional orienting. *J Neurophysiol* 87:3090-3101.
- Mirzaei A, Kumar A, Leventhal D, Mallet N, Aertsen A, Berke J, Schmidt R (2017) Sensorimotor Processing In The Basal Ganglia Leads To Transient Beta Oscillations During Behavior. *bioRxiv* 136879.
- Mroz EA, Brownstein MJ, Leeman SE (1977) Evidence for substance P in the striato-nigral tract. *Brain research* 125:305-311.
- Nambu A, Llinas R (1994) Electrophysiology of globus pallidus neurons in vitro. *Journal of neurophysiology* 72:1127-1139.
- Nelson AB, Kreitzer AC (2014) Reassessing models of basal ganglia function and dysfunction. *Annual review of neuroscience* 37:117-135.
- Nini A, Feingold A, Sloviter H, Bergman H (1995) Neurons in the globus pallidus do not show correlated activity in the normal monkey, but phase-locked oscillations appear in the MPTP model of parkinsonism. *Journal of neurophysiology* 74:1800-1805.
- Nobrega-Pereira S, Gelman D, Bartolini G, Pla R, Pierani A, Marin O (2010) Origin and molecular specification of globus pallidus neurons. *J Neurosci* 30:2824-2834.
- O'doherty J, Dayan P, Schultz J, Deichmann R, Friston K, Dolan RJ (2004) Dissociable roles of ventral and dorsal striatum in instrumental conditioning. *Science* 304:452-454.
- Obeso JA, Rodriguez-Oroz MC, Benitez-Temino B, Blesa FJ, Guridi J, Marin C, Rodriguez M (2008) Functional organization of the basal ganglia: therapeutic implications for Parkinson's disease. *Movement disorders : official journal of the Movement Disorder Society* 23 Suppl 3:S548-559.
- Obeso JA, Rodriguez-Oroz MC, Rodriguez M, Lanciego JL, Artieda J, Gonzalo N, Olanow CW (2000) Pathophysiology of the basal ganglia in Parkinson's disease. *Trends Neurosci* 23:S8-19.
- Oh Y-M, Karube F, Takahashi S, Kobayashi K, Takada M, Uchigashima M, Watanabe M, Nishizawa K, Kobayashi K, Fujiyama F (2016a) Using a novel PV-Cre rat model to characterize pallidonigral cells and their terminations. *Brain Structure and Function* 1-20.
- Oh YM, Karube F, Takahashi S, Kobayashi K, Takada M, Uchigashima M, Watanabe M, Nishizawa K, Kobayashi K, Fujiyama F (2016b) Using a novel PV-Cre rat model to characterize pallidonigral cells and their terminations. *Brain structure & function*.
- Ohara PT (1988) Synaptic organization of the thalamic reticular nucleus. *Journal of electron microscopy technique* 10:283-292.

- Packard MG, Knowlton BJ (2002) Learning and memory functions of the basal ganglia. *Annu Rev Neurosci* 25:563-593.
- Paladini CA, Celada P, Tepper JM (1999) Striatal, pallidal, and pars reticulata evoked inhibition of nigrostriatal dopaminergic neurons is mediated by GABA(A) receptors in vivo. *Neuroscience* 89:799-812.
- Parent A, Hazrati LN (1995) Functional-Anatomy of the Basal Ganglia .2. The Place of Subthalamic Nucleus and External Pallidum in Basal Ganglia Circuitry. *Brain Res Rev* 20:128-154.
- Parent A, Mackey A, Debellefeuille L (1983) The Subcortical Afferents to Caudate-Nucleus and Putamen in Primate - a Fluorescence Retrograde Double Labeling Study. *Neuroscience* 10:1137-&.
- Parent A, Smith Y (1987) Differential dopaminergic innervation of the two pallidal segments in the squirrel monkey (*Saimiri sciureus*). *Brain research* 426:397-400.
- Paxinos G (2004) *The mouse brain in stereotaxic coordinates*: Academic press.
- Penney JB, Jr., Young AB (1983) Speculations on the functional anatomy of basal ganglia disorders. *Annual review of neuroscience* 6:73-94.
- Pinault D, Deschenes M (1998) Projection and innervation patterns of individual thalamic reticular axons in the thalamus of the adult rat: a three-dimensional, graphic, and morphometric analysis. *The Journal of comparative neurology* 391:180-203.
- Plenz D, Kital ST (1999) A basal ganglia pacemaker formed by the subthalamic nucleus and external globus pallidus. *Nature* 400:677-682.
- Popovych OV, Tass PA (2012) Desynchronizing electrical and sensory coordinated reset neuromodulation. *Frontiers in human neuroscience* 6:58.
- Ragozzino ME, Ragozzino KE, Mizumori SJ, Kesner RP (2002) Role of the dorsomedial striatum in behavioral flexibility for response and visual cue discrimination learning. *Behavioral neuroscience* 116:105-115.
- Ragsdale CW, Jr., Graybiel AM (1991) Compartmental organization of the thalamostriatal connection in the cat. *The Journal of comparative neurology* 311:134-167.
- Rajasethupathy P, Ferenczi E, Deisseroth K (2016) Targeting Neural Circuits. *Cell* 165:524-534.
- Raz A, Vaadia E, Bergman H (2000) Firing patterns and correlations of spontaneous discharge of pallidal neurons in the normal and the tremulous 1-methyl-4-phenyl-1,2,3,6-tetrahydropyridine vervet model of parkinsonism. *J Neurosci* 20:8559-8571.
- Riederer P, Wuketich S (1976) Time course of nigrostriatal degeneration in parkinson's disease. A detailed study of influential factors in human brain amine analysis. *J Neural Transm* 38:277-301.
- Robledo P, Feger J (1990) Excitatory Influence of Rat Subthalamic Nucleus to Substantia-Nigra Pars Reticulata and the Pallidal Complex - Electrophysiological Data. *Brain Res* 518:47-54.
- Rommelfanger KS, Wichmann T (2010) Extrastriatal dopaminergic circuits of the Basal Ganglia. *Frontiers in neuroanatomy* 4:139.
- Rubin JE, McIntyre CC, Turner RS, Wichmann T (2012) Basal ganglia activity patterns in parkinsonism and computational modeling of their downstream effects. *Eur J Neurosci* 36:2213-2228.
- Rubin JE, Terman D (2004) High frequency stimulation of the subthalamic nucleus eliminates pathological thalamic rhythmicity in a computational model. *J Comput Neurosci* 16:211-235.

- Sato F, Lavallee P, Levesque M, Parent A (2000) Single-axon tracing study of neurons of the external segment of the globus pallidus in primate. *The Journal of comparative neurology* 417:17-31.
- Saunders A, Oldenburg IA, Berezovskii VK, Johnson CA, Kingery ND, Elliott HL, Xie T, Gerfen CR, Sabatini BL (2015) A direct GABAergic output from the basal ganglia to frontal cortex. *Nature* 521:85-89.
- Schultheiss NW, Edgerton JR, Jaeger D (2010) Phase response curve analysis of a full morphological globus pallidus neuron model reveals distinct perisomatic and dendritic modes of synaptic integration. *J Neurosci* 30:2767-2782.
- Schultz W (1998) Predictive reward signal of dopamine neurons. *Journal of neurophysiology* 80:1-27.
- Shen W, Flajolet M, Greengard P, Surmeier DJ (2008) Dichotomous dopaminergic control of striatal synaptic plasticity. *Science* 321:848-851.
- Smith Y, Bevan MD, Shink E, Bolam JP (1998a) Microcircuitry of the direct and indirect pathways of the basal ganglia. *Neuroscience* 86:353-387.
- Smith Y, Bolam JP (1989) Neurons of the Substantia Nigra Reticulata Receive a Dense Gaba-Containing Input from the Globus Pallidus in the Rat. *Brain Res* 493:160-167.
- Smith Y, Parent A (1986) Differential connections of caudate nucleus and putamen in the squirrel monkey (*Saimiri sciureus*). *Neuroscience* 18:347-371.
- Smith Y, Raju DV, Pare JF, Sidibe M (2004) The thalamostriatal system: a highly specific network of the basal ganglia circuitry. *Trends Neurosci* 27:520-527.
- Smith Y, Shink E, Sidibe M (1998b) Neuronal circuitry and synaptic connectivity of the basal ganglia. *Neurosurg Clin N Am* 9:203-+.
- Smith Y, Surmeier DJ, Redgrave P, Kimura M (2011) Thalamic contributions to Basal Ganglia-related behavioral switching and reinforcement. *J Neurosci* 31:16102-16106.
- Soares J, Kliem MA, Betarbet R, Greenamyre JT, Yamamoto B, Wichmann T (2004) Role of external pallidal segment in primate parkinsonism: comparison of the effects of 1-methyl-4-phenyl-1,2,3,6-tetrahydropyridine-induced parkinsonism and lesions of the external pallidal segment. *J Neurosci* 24:6417-6426.
- Stefani A, Peppe A, Pierantozzi M, Galati S, Moschella V, Stanzione P, Mazzone P (2009) Multi-target strategy for Parkinsonian patients: the role of deep brain stimulation in the centromedian-parafascicularis complex. *Brain research bulletin* 78:113-118.
- Surmeier DJ, Carrillo-Reid L,argas J (2011) Dopaminergic modulation of striatal neurons, circuits, and assemblies. *Neuroscience* 198:3-18.
- Tachibana Y, Iwamuro H, Kita H, Takada M, Nambu A (2011) Subthalamo-pallidal interactions underlying parkinsonian neuronal oscillations in the primate basal ganglia. *Eur J Neurosci* 34:1470-1484.
- Tass PA, Qin L, Hauptmann C, Dovero S, Bezard E, Boraud T, Meissner WG (2012) Coordinated reset has sustained aftereffects in Parkinsonian monkeys. *Annals of neurology* 72:816-820.
- Terman D, Rubin JE, Yew AC, Wilson CJ (2002) Activity patterns in a model for the subthalamopallidal network of the basal ganglia. *J Neurosci* 22:2963-2976.
- Thor S, Ericson J, Brannstrom T, Edlund T (1991) The homeodomain LIM protein Isl-1 is expressed in subsets of neurons and endocrine cells in the adult rat. *Neuron* 7:881-889.
- Turner RS, Anderson ME (1997) Pallidal discharge related to the kinematics of reaching movements in two dimensions. *Journal of neurophysiology* 77:1051-1074.

- Tye KM, Deisseroth K (2012) Optogenetic investigation of neural circuits underlying brain disease in animal models. *Nat Rev Neurosci* 13:251-266.
- Udupa K, Bahl N, Ni Z, Gunraj C, Mazzella F, Moro E, Hodaie M, Lozano AM, Lang AE, Chen R (2016) Cortical Plasticity Induction by Pairing Subthalamic Nucleus Deep-Brain Stimulation and Primary Motor Cortical Transcranial Magnetic Stimulation in Parkinson's Disease. *J Neurosci* 36:396-404.
- Vitek JL, Bakay RA, Hashimoto T, Kaneoke Y, Mewes K, Zhang JY, Rye D, Starr P, Baron M, Turner R, DeLong MR (1998) Microelectrode-guided pallidotomy: technical approach and its application in medically intractable Parkinson's disease. *Journal of neurosurgery* 88:1027-1043.
- Vitek JL, Hashimoto T, Peoples J, DeLong MR, Bakay RA (2004) Acute stimulation in the external segment of the globus pallidus improves parkinsonian motor signs. *Movement disorders : official journal of the Movement Disorder Society* 19:907-915.
- Vitek JL, Zhang J, Hashimoto T, Russo GS, Baker KB (2012) External pallidal stimulation improves parkinsonian motor signs and modulates neuronal activity throughout the basal ganglia thalamic network. *Experimental neurology* 233:581-586.
- Wallace ML, Saunders A, Huang KW, Philson AC, Goldman M, Macosko EZ, McCarroll SA, Sabatini BL (2017) Genetically distinct parallel pathways in the entopeduncular nucleus for limbic and sensorimotor output of the basal ganglia. *Neuron* 94:138-152. e135.
- Wang J, Nebeck S, Muralidharan A, Johnson MD, Vitek JL, Baker KB (2016) Coordinated Reset Deep Brain Stimulation of Subthalamic Nucleus Produces Long-Lasting, Dose-Dependent Motor Improvements in the 1-Methyl-4-phenyl-1,2,3,6-tetrahydropyridine Non-Human Primate Model of Parkinsonism. *Brain stimulation* 9:609-617.
- Watabe-Uchida M, Zhu L, Ogawa SK, Vamanrao A, Uchida N (2012) Whole-brain mapping of direct inputs to midbrain dopamine neurons. *Neuron* 74:858-873.
- Weinberger M, Mahant N, Hutchison WD, Lozano AM, Moro E, Hodaie M, Lang AE, Dostrovsky JO (2006) Beta oscillatory activity in the subthalamic nucleus and its relation to dopaminergic response in Parkinson's disease. *Journal of neurophysiology* 96:3248-3256.
- Wichmann T, Bergman H, DeLong MR (1994) The primate subthalamic nucleus. III. Changes in motor behavior and neuronal activity in the internal pallidum induced by subthalamic inactivation in the MPTP model of parkinsonism. *Journal of neurophysiology* 72:521-530.
- Wichmann T, DeLong MR (1996) Functional and pathophysiological models of the basal ganglia. *Curr Opin Neurobiol* 6:751-758.
- Wichmann T, DeLong MR (2016) Deep Brain Stimulation for Movement Disorders of Basal Ganglia Origin: Restoring Function or Functionality? *Neurotherapeutics : the journal of the American Society for Experimental NeuroTherapeutics* 13:264-283.
- Willis T (1973) *Cerebri anatome: cui accessit nervorum descriptio & usus: apud Joannem Maximilianum Lucas.*
- Wilson CJ (2009) What Controls the Timing of Striatal Spiny Cell Action Potentials in the Up State? *Proceedings of the 9th Triennial Meeting of the International Basal Ganglia Society.*
- Yelnik J, Damier P, Bejjani BP, Francois C, Gervais D, Dormont D, Arnulf I, A MB, Cornu P, Pidoux B, Agid Y (2000) Functional mapping of the human globus pallidus: contrasting

- effect of stimulation in the internal and external pallidum in Parkinson's disease. *Neuroscience* 101:77-87.
- Yin HH, Ostlund SB, Knowlton BJ, Balleine BW (2005) The role of the dorsomedial striatum in instrumental conditioning. *Eur J Neurosci* 22:513-523.
- Yuste R (2015) From the neuron doctrine to neural networks. *Nat Rev Neurosci* 16:487-497.
- Zeisel A, Munoz-Manchado AB, Codeluppi S, Lonnerberg P, La Manno G, Jureus A, Marques S, Munguba H, He L, Betsholtz C, Rolny C, Castelo-Branco G, Hjerling-Leffler J, Linnarsson S (2015) Brain structure. Cell types in the mouse cortex and hippocampus revealed by single-cell RNA-seq. *Science* 347:1138-1142.